



The
University
Of
Sheffield.

Modelling and EMG based Control of Upper Limb Exoskeletons for Hand Impairments

A thesis submitted to the University of Sheffield for the degree of

Doctor of Philosophy

By:

Norafizah binti Abas

Department of Automatic Control and Systems Engineering

The University of Sheffield

October 2019

Abstract

Functional losses associated with hand impairments have led to the growing development of hand exoskeletons. The main challenges are to develop the exoskeletons that work according to the user's motion intention, which can be done by utilizing the electromyogram signals generated by forearm muscles contributed from the movement and/or grasping abilities of the hand. In this research, modelling and EMG based control of hand exoskeletons with the aim to assist stroke survivors in regaining their hand strength and functionality, and improve their quality of life is presented.

The exoskeleton model was developed within the virtual environment; a software platform where design and control performances can be evaluated prior to expensive experimental trials that can save the resources and cost-effective. Besides, it can also simplify the modelling process for the exoskeleton hand that is complex and highly articulated. Its inverse kinematic task is complex to solve analytically, and its numerical calculation often entails difficulties. The conceptual design was done in Solidworks tool and was imported to the SimMechanics program scheme that enables interconnection between physical components with geometric and kinematic relationships of the robot in the form of interconnected blocks. This integration allows verification of the model and facilitates the design process of the controller that was executed in MATLAB environment.

A hierarchical controller was employed to control the exoskeleton hand which comprises of three-level controllers; the perception layer (high-level control), the transition layer (mid-level control), and the execution layer (low-level control). In the highest level, the kinematic estimation of the hand was computed based on the established relationship between forearm electromyogram signals with various finger pinches, handgrip forces, and wrist positions. A feed-forward artificial neural network (ANN) and adaptive neuro-fuzzy inference system (ANFIS) with subtractive clustering were used to establish the relationship and compute the hand kinematics estimations. All methods were trained and tested using EMG data collected non-invasively using multi-channel

EMG sensors from eight healthy subjects. The contractions of the muscles were detected from several forearm (flexion and extensor) muscles, and the data were processed through several pattern recognition steps, before being mapped to various pinching forces and angular joints. Time-domain features; root mean square (RMS), integrated EMG (IEMG), mean absolute value (MAV), and waveform length (WL) was chosen to extract useful information hidden in the EMG signals collected.

The experimental results show separable classes of features with WL features produced a more significant result. Additionally, the feed-forward ANN provides better joint angles estimation with a correlation coefficient of 0.95 ± 0.04 and root mean square error lesser than 3%, when compared to the ANFIS model. This result suggests that ANN with WL features provides a viable and effective myoelectric control and demonstrates a potential control input, which was then applied to the finite state controller in the mid-level control and the PID controller in the low-level control for continuous control of the hand exoskeleton.

Declaration

The work in this thesis is based on the research work conducted at the Automatic Control and Systems Engineering, The University of Sheffield. The EMG datasets utilized were collected after obtaining research ethical approval from The University of Sheffield for this research.

Acknowledgments

Many people have contributed to this dissertation in ways great and small. I wish to acknowledge some of them here. My deep thanks and gratitude go to my dissertation supervisor, Professor Osman Tokhi and Professor Mahdi Mahfouf, for their patience, encouragement, continuous, consistent and generous guidance and invaluable support throughout the years of my doctoral studies.

My great appreciation goes to Wan Bukhari who helped me in collecting the data and advised me on the analysis itself. My thanks also go to my colleagues, Dr. Daniela, Dr. Ghasaaq, Dr. Siti Khadijah, Dr. Ruzaini, Dr. Ahmad Firdaus, Dr. Abdolha Benomair and Abdullah Al-shatti, who shared their knowledge with me and allowed me to learn from their expertise.

I also thank my parents, Abas and Jamaliah, my siblings, Norazlin, Mohd Azman, and Nursiah, for being supportive, encouraging and stimulating people over the last few years who helped me to survive this long and challenging journey. Finally, my deepest gratitude goes to my husband, Zulkifli and our adorable twin, Zahin Noah and Nuha Zulaikha, who continually encouraged and supported me throughout the studies, who always believed in me and who made this journey possible.

Table of Content

Abstract	ii
Declaration	iii
Acknowledgments.....	iv
Table of Content	v
List of Table.....	x
List of Figure.....	xii
Nomenclatures	xvii
CHAPTER 1 INTRODUCTION	1
1.1 Background and Motivation	1
1.2 A Solution for Hand Impairment: Exoskeletons.....	3
1.3 Main Challenges	6
1.4 Aim and Objectives.....	8
1.5 Research Contributions and Publications	8
1.6 Thesis Outline	11
CHAPTER 2 LITERATURE REVIEW	13
2.1 Introduction.....	13
2.2 Exoskeleton Hand.....	13

2.3 Forearm Electromyogram Signals	25
2.4 Dynamic Modeling based on Forearm EMG Signals for Exoskeleton Hand Control.....	28
2.5 Issues of Control Design for Exoskeleton Hand.....	31
2.6 Issues of Performance Analysis for Exoskeleton Hand.....	32
2.7 Summary.....	33
CHAPTER 3 SYSTEM MODELLING AND DESIGN	35
3.1 Introduction.....	35
3.2 Hand Anatomy and Biomechanics.....	36
3.3 Anthropometric Hand Measurements for Women.....	37
3.4 Design of the Exoskeleton Hand using Solidwork	41
3.5 Modelling of the Exoskeleton Hand using SimMechanics.....	44
3.5.1 Body and Joint Specifications.....	46
3.5.2 Physical Model Visualization and Motion Analysis.....	50
3.6 Summary.....	51
CHAPTER 4 FOREARM ELECTROMYOGRAPHY SIGNALS ANALYSIS.....	52
4.1 Introduction	52
4.2 EMG Data Collection	53
4.2.1 Muscle Selection Procedures	54
4.2.2 Experiment Set-up.....	58
4.2.3 Experimental Procedures for Data Collection.....	60

4.3	Processing Techniques for the Forearm Electromyogram Signals.....	62
4.4	Results and Analysis.....	66
4.4.1	Samples for Raw and Normalised EMG Signals	66
4.4.2	Features for Finger Movement.....	68
4.4.3	Features for Wrist Movement	71
4.4.4	Performance Analysis for Feature Selections	74
4.5	Summary.....	79
CHAPTER 5 MODELLING FRAMEWORK FOR JOINT ANGLE ESTIMATION.....		80
5.1	Introduction.....	80
5.2	Artificial Neural Network Model.....	81
5.2.1	Feed-forward Neural Network with Backpropagation Algorithm.....	83
5.2.2	Modelling for the Finger Joint Angle	85
5.2.3	Modelling for the Wrist Joint Angle.....	89
5.3	Artificial Neural Fuzzy Inference System Models	91
5.3.1	ANFIS with Hybrid Learning and Subtractive Clustering	93
5.3.2	Modelling of the Finger Joint Angle.....	95
5.3.3	Modelling of the Wrist Joint Angle	97
5.4	Validation of the Joint Angle Estimations	99
5.4.1	Validation for the Finger Joint Angle	99
5.4.2	Validation for the Wrist Joint Angle.....	101

5.5 Summary	102
CHAPTER 6 DESIGN AND CONTROL FRAMEWORK FOR EXOSKELETON HAND....	103
6.1 Introduction.....	103
6.2 Exoskeleton Hand Control Framework	104
6.3 Hierarchical Control of the Exoskeleton Hand.....	105
6.3.1 Finite State Machine Controller.....	106
6.3.2 PID controller.....	112
6.4 Summary	114
CHAPTER 7 CONCLUSION AND RECOMMENDATION FOR FUTURE WORK.....	115
7.1 Conclusions.....	115
7.2 Recommendations for Future Work.....	118
References.....	116
Appendix A: The Commercially Available Exoskeleton Hand.....	131
Appendix B: Documentation for EMG Data Collection	134
Appendix C: Time Domain Features without Normalisation for Finger Movements.....	136
Appendix D: Time Domain Features with Normalisation for Finger Movements.....	139
Appendix E: The Standard Deviation Computed for the Features Contributed to the Finger Movements.....	143
Appendix F: Time Domain Features without Normalisation for Wrist Movements.....	145
Appendix G: Time Domain Features with Normalisation for Wrist Movements	148

Appendix H: Validation of Finger Joint Angle Estimations based on ANN Model150

Appendix I: Validation of Finger Joint Angle Estimations based on ANFIS Model154

List of Table

Table 2.1: Previous work related to the development of the exoskeleton hand	14
Table 2.2: Previous work done related to the dynamic modelling of the hand	30
Table 3.1: Hand dimension and biomechanics measurement definition	39
Table 3.2: Comparison of selected hand dimensions.....	40
Table 3.3: Dimensions and specifications of the hand exoskeleton	43
Table 3.4: Description of the block parameters and their functions employed in the exoskeleton hand model.....	47
Table 4.1: Muscles under consideration with their characteristics	55
Table 4.2: Muscles identification test and location for electrode placement.....	56
Table 4.3: List of research equipment and material.....	60
Table 4.4: The standard deviation computed for the	75
Table 4.5: The summary of data used in the ANOVA test.....	76
Table 4.6: The results for ANOVA test.....	76
Table 4.6: Tukey-Kramer significance test.....	76
Table 5.1: Performance index for the four medial finger joint models of a single subject	87
Table 5.2: Performance index for the four medial finger joint models of multi-subjects	88
Table 5.3: Performance index for the wrist angle model of single and multi-subjects	87

Table 6.1: The state with input set and output function for finger pinches 108

List of Figure

Figure 1.1: Commercially available assistive exoskeleton hands; (a) MyoPro, (b) Power Assist Glove, (c) Carbonhand.....	4
Figure 2.1: The exoskeleton hand systems: (a) Assisting wrist movement, (b) Assisting finger(s) movement, and (c) Assisting wrist and finger(s) movement	20
Figure 2.2: The sEMG based controlled exoskeleton hand (a) from Carnegie Mellon University (b) from Technische University of Berlin.....	24
Figure 2.3: EMG pattern recognition process; adopted and modified from Lalitharatne et al, (2014)	26
Figure 3.1: Sketch for bones and joints of a human hand.....	37
Figure 3.2: Hand measurement diagram (unit is in cm unless otherwise specified)	38
Figure 3.3: The exoskeleton hand in SolidWorks.....	42
Figure 3.4: The exoskeleton fingers: (a) Design for the index, middle, ring and little fingers, (b) Design for the thumb	42
Figure 3.5: Transformation process; from conceptual design in Solidworks into the exoskeleton hand model computed in the Simulink environment	45
Figure 3.6: The SimMechanics block diagram for four medial fingers (index, middle, ring, and pinky fingers) that are mapped to the respective Solidworks-based assembly parts and constraints	48
Figure 3.7: The SimMechanics scheme for the exoskeleton hand.....	49
Figure 3.8: The SimMechanics visualization window displaying the exoskeleton hand model ..	50

Figure 4.1: Block diagram for the experimental set-up	53
Figure 4.2 Sketch for anterior compartment of a human forearm with location of muscles under consideration: FDS, FDP, FPL and FCR.	54
Figure 4.3: Sketch for posterior view of a human forearm with location of muscles under consideration: ED, EPB and ECRL.	55
Figure 4.4: Experimental set-up for EMG and hand grip force measurement.....	59
Figure 4.5: Fingers pinch muscle contractions of forearm with 4 groups of movement and angles: (a) index to thumb finger pinch, (b) middle to thumb finger pinch, (c) ring to thumb finger pinch and (d) pinky to thumb finger pinch.	61
Figure 4.6: The raw EMG collected at different handgrip strength (20, 40, 60, and 80% of MVC) for FDS muscle at neutral wrist position.	66
Figure 4.7: The raw EMG signals contributed to the movement of four medial finger without normalisation.....	67
Figure 4.8: The raw EMG signals contributed to the movement of four medial finger with normalisation.....	68
Figure 4.9: Features extracted (from FDS, FDP and EDC muscles) at 20% of MVC finger pinch strength for four medial fingers (a) RMS (b) MAV (c) IEMG (d) WL.....	69
Figure 4.10: Features extracted (from FPL and EPB muscles) at 20% of MVC finger pinch strength for a thumb (a) RMS (b) MAV (c) IEMG (d) WL	69
Figure 4.11: Features extracted (from FDS, FDP and EDC muscles) at 40% of MVC finger pinch strength for four medial fingers (a) RMS (b) MAV (c) IEMG (d) WL.....	70
Figure 4.12: Features extracted (from FPL and EPB muscles) at 40% of MVC finger pinch strength for a thumb (a) RMS (b) MAV (c) IEMG (d) WL	70

Figure 4.13: Features extracted from flexion-extension muscles (ECRL and FCR muscles) at 20% of MVC for handgrip strength at wrist positions with prismatic power grip (adducted thumb). . 72

Figure 4.14: Features extracted from flexion muscles (FDS and FCR muscles) at 20% of MVC for handgrip strength at wrist positions with prismatic power grip (adducted thumb). **Error! Bookmark not defined.**73

Figure 4.15: Features extracted from extension muscles (EDC and ECRL muscles) at 20% of MVC for handgrip strength at wrist positions with prismatic power grip (adducted thumb)..... **Error! Bookmark not defined.**74

Figure 5.1: The example of a feed-forward neural network with 3 input neurons, 3 hidden neurons and one output neuron..... 82

Figure 5.2: The proposed feed-forward neural network with Levenberg-Marquardt backpropagation algorithm for the finger/wrist joint angle estimations. The number of input changes depending on the respective output estimation (either finger or wrist joint angles). 84

Figure 5.3: Prediction results for the DIP joint angle model (a) modelling dataset (b) validation datasets 86

Figure 5.4: Prediction results for the PIP joint angle model (a) modelling dataset (b) validation datasets 86

Figure 5.5: Prediction results for the MCP joint angle model (a) modelling dataset (b) validation datasets 86

Figure 5.6: Prediction results for the DIP, PIP and MCP joint angle model for multi-subjects (a) modelling dataset (b) validation datasets 88

Figure 5.7: Prediction results for the wrist joint angle model for single subject (a) modelling dataset (b) validation datasets 89

Figure 5.8: Prediction results for the wrist joint angle model for multi-subject (a) modelling dataset (b) validation datasets 90

Figure 5.9: The fuzzy inference system.....	91
Figure 5.10: (a) Type-3 fuzzy reasoning and (b) Equivalent ANFIS (Jang, 1993)	92
Figure 5.11: The prediction results for DIP joint estimations using ANFIS subtractive clustering model.....	96
Figure 5.12: The prediction results for PIP joint estimations using ANFIS subtractive clustering model.....	96
Figure 5.13: The prediction results for MCP joint estimations using ANFIS subtractive clustering model.....	97
Figure 5.14: The prediction results for wrist joint estimations using ANFIS subtractive clustering model.....	99
Figure 5.15: The DIP joint angle estimated from the ANN model for four medial fingers based on wavelength features at 20% MVC for different finger pinches (FR, FP1, FP2, FP3, & FP4). ..	100
Figure 5.16: The PIP joint angle estimated from the ANN model for four medial fingers based on wavelength features at 20% MVC for different finger pinches (FR, FP1, FP2, FP3, & FP4). ..	100
Figure 5.17: The MCP joint angle estimated from the ANN model for four medial fingers based on wavelength features at 20% MVC for different finger pinches (FR, FP1, FP2, FP3, & FP4).	101
Figure 5.18: The grasping and wrist angles estimated from the ANN model based on wavelength features at 20% MVC using target data for a single subject.....	101
Figure 5.19: The grasping and wrist angles estimated from the ANN model based on wavelength features at 20% MVC using target data for multi-subject.	102
Figure 6.1: Hierarchical control framework for the Exoskeleton Hand	104
Figure 6.2: The block diagram of the activity mode intent recogniser.....	105

Figure 6.3: Block diagram for overall system controller that shows the integration of the proposed hierarchical control framework for the exoskeleton hand; the perception level, the transition level and the execution level.....	106
Figure 6.4: Finite state controller for finger pinches	102
Figure 6.4: Finite state controller for wrist movements.....	105
Figure 6.6: The reference trajectories divided by states based on the estimated DIP, PIP and MCP joint angles.	111
Figure 6.7: The angle references computed by the FSM controller.	112
Figure 6.8: The joint angle and torque computed for index finger with control parameter of $K_p=0.5$, $K_d=0.02$, $K_i=1.5$	113
Figure 6.9: The joint angle and torque computed for index finger with adjusted control of $K_p=0.5$, $K_d=0.01$, $K_i=1$	113

Nomenclatures

EMG	Electromyogram
RMS	Root Mean Square
MAV	Mean Absolute Value
EMG	Integrated EMG
WL	Wave Length
ANN	Artificial Neural Network
ANFIS	Artificial Neural Fuzzy Inference System
MSE	Mean Square Error
PID	Proportional-Integral-Differential

Chapter 1

INTRODUCTION

'Stroke can be a hopeless experience for a while.'

Mark Flood, a 14-years old stroke survivor

1.1 Background and Motivation

Hand plays a vital role in a human's life by offering physical interaction and grasping capabilities. The design of a human hand is indeed a miraculous creation. It comprises a palm with five fingers and is connected to the forearm by a wrist joint. Its movement and sleight are unique and cannot be found in any other creature on the planet making the hand a valuable body part for the human. A deficit in hand function due to hand impairment will significantly affect and degrade one's life, not only financially but also in living a quality life. Hand impairment is referred to any loss or deviation in hand function, which includes amputation, sensory and motion impairment (Swanson et al., 1987) that can occur due to several factors such as birth defect, ageing factors, disease (Poole et al., 2013), injury (Barr et al., 2004; Farzad et al., 2015; Trybus et al., 2006), and stroke (Armagan et al., 2003; Pretti Raghavan, 2007; Xu et al., 2015). Stroke is a sudden illness that happens when there is a disruption to the flow of blood to the brain. There are two types of stroke; Ischaemic stroke occurs when a blockage cuts the blood supply to the brain, and Haemorrhagic stroke that is caused when a blood vessel is set off within or on the surface of the brain (NHS Healthcare Trust, 2014).

Worldwide, stroke is the third leading cause of disability with 15 million people experiencing stroke every year (Johnson et al., 2016) and it is the most common neurological disease in Western countries (Carolei et al., 2002). According to the UK Stroke Association released statistics in

February 2018, there are more than 100, 000 strokes happen every year (approximately one stroke every 5 minutes) with over 1.2 million stroke survivors living in the UK. In the next 20 years (between 2015 to 2035), the rate of people aged 45 years old and over experiencing first-time stroke are expected to increase by 59% causing a rise in the estimation on the number of stroke survivors to increase by 123% (The Stroke Association, 2018b). The commonly effects of stroke are physical; the survivors of stroke can experience muscle weakness, muscle tightness, or difficult movement coordination, usually on one side of their body (hemiparesis). These effects may be incorporated with memory problems making it difficult to move some parts of the body and causing the survivors to struggle in performing Activities of Daily Living (ADL). In most stroke cases, the hand is one of the vulnerable members of the body that has a high chance of suffering; over 75% of stroke survivors experience upper limb weakness that includes limited hand and wrist movement (The Stroke Association, 2018a).

The hand impairment following stroke can be cured through treatment and rehabilitation, but the amount of recovery varies among individuals, depending on many factors; the type of impairment, the amount of damage to the brain cells, etc (Franck et al., 2017). Most survivors make a significant improvement in the first few months, but the recovery usually slows down and can continue for a long time. The treatment and rehabilitation can be challenging especially in determining which impairment needs to be treated and how it can be treated. According to Raghavan (2015), the impairment is commonly not static causing the nature of the impairment to change as the motor recovery proceeds. Moreover, the impairment can multiply by time, i.e., hand weakness may occur immediately after the stroke, and remain unresolved when spasticity sets in a few weeks or months later. In some cases, the hand function is not fully restored even after an intensive rehabilitation. According to Heo et al., (2012) only 5% to 20% of hemiplegic stroke survivors complete functional recovery after the intensive rehabilitation, meanwhile 66% have not regained the hand functions when measured 6 months after stroke. The prolonged recovery process restricts survivors' daily activities, affects social integration, decreases productivity, and leads to economic burdens (Bertani et al., 2017). This has led to the emergence of technology-assisted devices such as exoskeletons as a solution to assist the survivors to regain the functionality of their hands and to restore their quality of life.

1.2 A Solution for Hand Impairment: Exoskeletons

The innovative advances in the field of robotic technologies alongside the challenging hand impairment recovery process and its enormous impact on the survivors have steered to a rapid increase in the interest for development of assistive robotics: the exoskeletons. An exoskeleton is a novel man-machine intelligent system that is wearable and powered by a system of motors with corresponding joints and links that allow limb movement, increase in strength and endurance. It can be classified into three groups; empowering exoskeleton which extends the strength of human beyond its natural ability while maintaining human control of the robot, orthotic exoskeleton whose mechanical structure maps onto the anatomy of the human limb with a purpose to restore lost or weak functions, and prosthetic exoskeleton which substitutes the lost limb after amputation (Pons et al., 2008).

Depending on its purpose, the orthotic exoskeleton can be further divided into three subclasses: augmentative, rehabilitative or assistive systems that can be mapped into human limb functionality such as upper-limb, lower-limb, and full body exoskeleton. The augmentative exoskeletons are explicitly designed to enhance the ability of the human hand for professional use and work as muscle strengthening systems that can help to reduce fatigue and injury due to repetitive tasks. On the other hand, the rehabilitation exoskeletons are proposed to provide guided movement, repetitive training and support to the wearer in restoring the lost function of limbs while assistive exoskeletons are intended to provide physical support to activities of daily living for the physically weak wearer (Viteckova et al., 2018). In the context of this research, an upper-limb orthotic exoskeleton is designed and developed as an assistive device that can provide practical assistance to the hand that is not fully paralyzed (weak).

Exoskeletons have been studied since the 1960s for industrial and medical applications. The first whole-body exoskeleton robot; Hardiman, was built during 1965 and 1971 by General Electric in conjunction with the United State military, actuated and supposed to be driven by a human operator from the inside of the robot. The Hardiman I arm system consists of eight powered joints, where six joints are bilateral servo-controlled while two joints are rate controlled using velocity valve. The operator makes contact with the system at three points; the hand, the wrist, and the upper forearm. The system, however, is not overall successful due to several limitations and

stability issues (General Electric Company, 1969; Gopura et al., 2011). Since then, research on upper-limb exoskeletons for restoring and improving deficit in hand functions have continued.

Recently, several commercially available hand exoskeletons have been designed, such as, the MyoPro, Power Assist Glove, Carbonhand, AMADEO, Hand of Hope, InMotion HAND, InMotion WRIST, Exohand, Ironhand and RoboGlove (Exoskeleton Report, 2018). Amongst these, the MyoPro, the Power Assist Glove and the Carbonhand (Figure 1.1) work as assistive devices, while the others are designed to work as rehabilitative and augmentative devices. Appendix A presents a comparison table between devices; their functions, basic features, supported movement and cost.



Figure 1.1: Commercially available assistive exoskeleton hands; (a) MyoPro, (b) Power Assist Glove, (c) Carbonhand from Exoskeleton Report (2018)

MyoPro is a powered orthosis originally designed by MIT with Harvard Medical School to restore arms and hand functions for upper-limb impairment survivors (Myomo Inc, 2015). It is a portable and lightweight arm brace that enables elbow flexion/extension with grasping function and works based on user motion intention. The user initiates the movement through their muscles that generate myoelectric signals, which are amplified by the brace and converted into desired motion. It is currently the only marketed device that can restore the individual's ability to perform activities of daily living. The MyoPro is available in three models using the same brace design with different functionality; Motion E for the powered elbow with static wrist support, Motion W for the powered elbow with multi-articulating wrist and Motion G for powered elbow with multi-articulating wrist and a powered 3-jaw-chuck grasp (MyoMo Inc and Compliance Solutions Ltd, 2017). The only drawback of the device is on its brace structure that provides significant support

only for the arm and elbow movements with limited wrist and hand function. Even though there are three models offered to match patient-specific needs, none of the models offers the full range of motion and degrees of freedom for the fingers that are crucial to fully regain the hand function and mobility.

The other assistive orthosis devices are the Power Assist Glove and Carbonhand that are designed to compensate for weak grasping by employing the soft exoskeletons technology; made from soft materials, light in weight, inflatable membrane, etc. The Power Assist Glove is developed by Daiya Industry to facilitate people who experience reduced hand functionality. It consists of a glove with three fingers compartment (with the middle, ring and pinky fingers merged together), sensors, pneumatic artificial muscles and a controller that is linked to the compressed gas canister. The glove is inflated to provide grasping assistant to the user (Kadowaki et al., 2011; Marinov, 2015; Noritsugu et al., 2008).

Similarly, the carbonhand is designed to work as an assistive device to counteract weak grasping. It was developed and launched in 2017 by Bioservo Technologies using soft extra muscle (SEM) technology; comprises of soft extra muscle glove and a control unit with touch sensors mounted at the fingertip of the gloves. Artificial tendons are sewed into the glove alongside the length of the fingers (for the thumb, middle and ring fingers). The glove mimics human hand anatomy and strengthens the handgrip by adding extra force and endurance through the application of artificial tendons. When the weak hand grasps the object, the touch sensor will signal the control unit to pull the tendon and increase the gripping force in proportion to the strength supplied by the user making it easy for the user to control it.

Both devices have been clinically tested and proved useful in providing assistant for the physically weak users. The main limitation of inflatable technology, however, is lacking of structural support as the components that are used to provide movement forces are also responsible for supporting the weakened body parts. Despite its advantages in providing comfort, and customizable to wear longer, the inflatable membrane has no external rigid frame causing the excessive force to be absorbed by the user and adds more strain to the weak muscles.

1.3 Main Challenges

The significance of this research lies in the assistive hand exoskeletons over the past decade. Despite many types of research that have been carried out on exoskeletons, both in academic and industrial settings with various levels of success, there are still issues that prevent them from being widely commercialized. The existing hand exoskeletons face numerous challenges concerning both hardware and software, which include but are not limited to safety and efficacy, mechanical system, human-machine interface/control, device performance evaluation, and cost-effectiveness.

Ideally, the exoskeleton hand should be designed to provide safe and seamless integration with the user without restricting motion. It is crucial to consider the user's motion capabilities as a range of motion of their hand might reduce with stiffening joints depending on their type of impairments. Over-restricting movement provides limited hand functions while under-restricting movement can cause hyperextension joints with potential injuries. Moreover, the biomechanics and anatomy of human hand should be carefully studied and followed in designing the exoskeleton frame as misalignment between human and exoskeleton joints can generate motions that may be harmful to the user, especially for the joints. There are several techniques used to minimize the effect of joint misalignment; hyperstaticity was formulated to prevent undesired forces (Jarrasse and Morel, 2012), self-adjusted joints (Cempini et al., 2013), optimal joint offset (Esmaeili et al., 2011), minimal attachment points (Lambercy et al., 2013), and complex mechanisms (Li et al., 2017).

The exoskeleton hand should also be designed to be portable, light in weight and power independent. The recent technological advances in robotic hardware have enabled and offered much smaller and more powerful mechanical components; the sensors, actuators, power transmission, and power supply, etc. According to Gopura et al. (2016), analysis of mechanical design is essential in developing an exoskeleton and it plays a significant role to achieve the efficacy function of the robot and provides comfort to the user. To make the portable design feasible, small actuators with efficient power transmission and lighter materials for the frame should be considered as it can reduce the power consumption to overcome the power supply limitation.

Aside from the safety, efficacy, and hardware development issues, human-machine interface/control that considers intelligence in controlling the exoskeleton appears to be the additional challenge. Comparing the control design of an exoskeleton with traditional robot shows a whole diversity as the human operator is not only the commander of the system but also as part of the control loop itself. This is known as ‘human-in-the-loop.’ The human operator mainly makes the decisions, and the exoskeleton implements the tasks. In controlling the exoskeleton robot, the principal criterion is to work according to the user’s motion intention. The robot should be able to adequately recognize the wearer actions and intentions to assist them properly. Novak and Riener (2015), have surveyed sensor fusion methods in wearable robots and have reported a drawback in exoskeletons in obtaining the information related to the wearer’s intentions. Numerous sensors and inference methods have been used with more advanced sensor fusion algorithms to provide optimal assistance and robust reaction to the changes in the user’s motion intention such as sensor fusion based on EMG signals or electrical brain activity, mechanical sensor fusion and EMG-mechanical sensor fusion.

Another major challenge is device performance evaluation, due to limited accessibility to exoskeletons in clinical settings, partly because of the cost and high level of training that is required to supervise the users. Alternatively, the device performance is evaluated either in physical labs using prototype with able-bodied users or using software simulation that is cost effective as it can provide effective integration between the exoskeleton and human and eliminates the design flaws without actual prototypes.

Finally, the elevated cost in developing exoskeletons cause a significant challenge to commercialize the robots. Technically, advanced technology is always associated with high price as it involves specialized hardware and materials, complex testing and performance validation. This process would increase the efficacy of the function making the device more reliable but often sacrifice the target market for the exoskeletons.

1.4 Aim and Objectives

This research embarks on the modelling and control of upper limb exoskeletons for hand impairments based on forearm EMG signals. Hierarchical control with user motion intention is proposed to help individuals with hand impairments to perform finger pinching and hand grasping at various wrist positions. It involves experimental work (for EMG data collection) and simulations (for the theoretical works, control design, and performance validation). The objectives of the research are as follows:

- i. To design and model an exoskeleton hand that includes fingers and wrist movements in simulated environment.
- ii. To establish the relationships between forearm EMG signals, finger pinches and handgrip forces and various wrist positions and use these relationships to predict handgrip forces exerted and joint angles computed when forearm EMG signals are used as input.
- iii. To design a hierarchical controller for the exoskeleton hand based on the established relationships.
- iv. To evaluate and validate overall system performance.

1.5 Research Contributions and Publications

The research contributions can be highlighted as follows:

Fully actuated fingers and wrist design of the exoskeleton hand. The physical design of the exoskeleton hand is done in Simulink environment before conversion to SimMechanics. The hand comprises of five fully actuated fingers following the bony segment of human fingers and a one-degree of freedom wrist. Often, the exoskeleton hand is designed as underactuated system, which makes it difficult to resemble the actual human movement in terms of system mechanics and controllability. Moreover, the virtual hand design simplifies the modelling and mathematical representation of the real system and facilitates the verification of a controller designed for the exoskeleton hand. Furthermore, it is more accessible as it integrates all components; the hierarchical controller and the testbed/plant, in the same simulation environment.

Design of experimental set-up for EMG data collection. A new experimental set-up is designed for EMG data collection to study inter-relation between EMG signals, various finger pinch/hand grasps, and different wrist movements. The experimental procedure considers a broad data collection process; skin preparation, muscle selection, and extraction of EMG signals on forearm muscles contributing to the finger pinching and hand grasping forces at various wrist movements. To the author's knowledge, there is no experimental procedure found in the literature that studies such inter-relation and used establish the relationship as a control input to control the exoskeleton hand.

Myoelectric control of the exoskeleton hand. The myoelectric control approach is introduced to establish the inter-relation between EMG signals, various finger pinches/handgrip forces, and wrist movements. It involves several sensor fusion stages to extract useful information from forearm EMG signals; data segmentation, filtration, normalization, and feature extraction process. This approach plays a vital role in decision making pertaining to the interpretation of the user's intentions that are useful for effective human-machine interaction.

Finger and wrist joints position estimation based on forearm EMG signals and finger pinches/grasping forces. The proposed myoelectric control approaches have successfully established the inter-relation between EMG signals at various finger pinches/handgrip forces and wrist movements. Over the years, many have successfully studied and performed a pattern recognition scheme for the classification of hand gestures with decoding accuracies of above 95%. However, the applicability of this scheme is limited to be used in controlled laboratory condition only. Moreover, the human hand is highly articulated with a wide range of degree of freedom. Therefore, its movements are not limited only to discrete gestures but more to continuous and coordinated gestures allowing various and complex movements. Artificial neural network (ANN) and adaptive neural fuzzy inference system (ANFIS) are employed to map the EMG signals and finger pinch/grasping forces with various finger and wrist joints positions. It is crucial in providing accurate control input to the controller so that when muscles are flexed/extended, the hand moves predictably and resembles movement and/or grasping abilities of the real human hand.

Novel control design for finger pinching, hand grasping and wrist motion of the exoskeleton hand. Hierarchical control framework that incorporates the environment in which the human and exoskeleton move as part of its control design considerations is proposed. It comprises a three-level control scheme with specific control functions; high-level, mid-level and low-level control. The high-level recognises the user's intention based on the established inter-relation while the mid-level is the transition layer that interprets the directions from user defined the input to the specific actuation/movement that activates low-level control, which contains the feedback loop that computes the error for each particular control action. The transitions layer utilises a finite state controller to switch between finger pinching and hand grasping controller with specific wrist motions depending on the user-defined input send from the high-level controller. To the author's knowledge, there is no control design found in the literature to accomplish the control tasks of exoskeleton hand using the same methods.

The research publications are:

- i. Assessment strategy of human upper forearm inter-relation and muscle fatigue. Proceedings of CLAWAR 2017: 20th International Conference on Climbing and Walking Robots and the Support Technologies for Mobile Machines, Porto, Portugal, 11-13 September 2017.
- ii. Electromyography assessment of forearm muscles: towards the control of exoskeleton hand. Proceedings of 5th International Conference on Control, Decision, and Information Technologies, Thessaloniki, Greece, April 2018.
- iii. Study on effect of two adjacent muscles of flexor & extensor of finger pinch & handgrip force. Proceedings of 5th International Conference on Control, Decision, and Information Technologies, Thessaloniki, Greece, April 2018.

1.6 Thesis Outline

The thesis is arranged and structured as follows:

Chapter 1: This chapter presents an overview of the research focus on the myoelectric modelling and control of an exoskeleton hand as an assistive device for individuals that suffered from hand impairment; specifically, stroke survivors. An exoskeleton is expected to assist survivors to regain their abilities in performing necessary daily activities and indirectly restore their quality of life. It started with a brief discussion about research background and motivation, followed by the solution to hand impairments and its design challenges. Based on the challenges, aim and objectives of the research are formulated. The chapter also highlights the research contributions together with the list of research publications.

Chapter 2: This chapter presents literature review conducted covering the broad aspects of design considerations for the exoskeleton hand; design of exoskeleton hand, issues related to myoelectric control, myoelectric modelling, control design and performance evaluation for the exoskeleton hand. It also summarizes the key research questions and the approaches adopted in this research.

Chapter 3: In this chapter, the design of the exoskeleton hand is presented in two design environments, namely Solidworks and SimMechanics. It provides details of the conceptual model of the exoskeleton hand in Solidworks and the steps for importing the model to SimMechanics program scheme. The results from this chapter, which are illustrated in the form of interconnected blocks, are then used in Simulink to represent the test bed of this research for testing the performance of the controller designed for the whole system.

Chapter 4: This chapter presents the data collection and pattern recognition process of forearm electromyography signals. It covers the muscles selection and experimental procedure for EMG data collection. Moreover, it discusses the pattern recognition process which involves several steps; signal conditioning, data segmentation, and features extraction. The features considered are time domain features such as root mean square, mean absolute value, integrated EMG and wavelength. The chapter explains the process carried out for EMG signal collection so as to be fully utilized for the next steps; finger and wrist joints estimations and control design.

Chapter 5: In this chapter, myoelectric modelling for the exoskeleton hand is presented. It starts with an introduction of possible method to establish inter-relation between the forearm EMG signals with various handgrip strengths and joint/wrist positions. The focus is on machine learning methods; ANN and ANFIS modelling. The structure and simulation results for each method are discussed.

Chapter 6: This chapter presents the design and control framework for the exoskeleton hand. The control framework is divided into three main levels; high-level, mid-level and low level control. Moreover, it discusses the integration process between each level and how the control is switched between finger movement to wrist movement and vice versa. This chapter presents and discusses the performance analysis of the developed controller.

Chapter 7: This chapter present the main conclusions drawn from the research carried out. The overall research contributions that have been successfully achieved are hihglighted. The chapter further provides recommendations for future work.

Chapter 2

LITERATURE REVIEW

It is the absence of facts that frightens people: the gap you open, into which they pour their fears, fantasies, and desires.'

2.1 Introduction

In this research, hand exoskeleton is designed, modelled and controlled based on user motion intention incorporated in forearm EMG signals. A literature review has been conducted to examine the previous design approaches and associated issues. Each of the design decisions and requirements provides challenges that need to be considered to design more reliable and efficient hand exoskeleton. The review is divided into few sub-sections; the hand exoskeletons, forearm electromyogram signals, dynamic modelling (fingers and wrist kinematics estimations), and control design, validation and performance evaluation for the exoskeleton hand. Based on the strengths and limitations discussed, several key research questions are formulated, and appropriate approaches/methodologies are selected to provide holistic design considerations and implementations.

2.2 Exoskeleton Hand

A considerable amount of literature has been published on the design and development of orthotic exoskeleton hand for assistive and rehabilitation purposes. Table 2.1 presented the previous research work related to this development. Each of the research work is evaluated, synthesised and analysed based on various criteria; supported movements, degrees of freedom, modelling, control methods, type of applications and special features.

Table 2.1: Previous work related to the development of the exoskeleton hand

References, System Name	Supported Movements	DOF	Modelling	Main Control Input, Control Method	Type; Field of Application	Stage of development; Special Feature
Systems assisting wrist movements						
Gopura and Kiguchi (2008)	Wrist – flexion/extension, ulnar/radial, pronation/supination,	3 DOF	Muscle modelling	EMG signal and forearm torque, a fuzzy controller	Wearable orthosis; Assistive device	Three muscles; healthy subject
Sasaki et al., (2005), ASSIST	Wrist – flexion	1 DOF	Not specified	Joint angle, EMG signal, Pressure control system.	Wearable orthosis; power assistance	One muscle; flexor carpi ulnaris. healthy subject
Hu et al., (2009)	Wrist – flexion and extension	1 DOF	Not specified	Surface EMG,	Stationary system; rehabilitation device	Four muscles; (BIC), (TRI), (FCR), and (ECR). Post-stroke subjects
Song et al., (2007), PolyJbot.	Wrist – flexion and extension	1 DOF	Muscle modelling	Surface EMG, joint angle and torque, PID controller	Stationary system; rehabilitation device	Two muscles. Post-stroke subjects
Systems assisting finger(s) movements						
Cesqui et al., (2013)	1 finger	3 DOF	Dynamics modeling	Emg, pattern recognition and learning	Wearable orthosis;	Not specified
Yamada et al., (2001), SkilMate	Glove-type hand	3 DOF	Not specified	Position control mode	Portable system (orthosis)	Not specified

References, System Name	Supported Movements	DOF	Modelling	Main Control Input, Control Method	Type; Field of Application	Stage of development; Special Feature
Shields et al., (1997)	Active flexion for thumb, index and middle fingers	3 DOF	Not specified	Programmable microcontroller (PWM driven)	Portable system (orthosis)	Not specified
Martinez et al., (2009) and (2010)	Flexion and extension for thumb, index and middle fingers	3 DOF	Not specified	Digital control system (under development)	Portable system (orthosis)	Not specified
Ho et al., (2011), <i>Hand of Hope, Rehab-Robotics</i>	Flexion for each fingers	5 DOF	Not specified	sEMG	Portable system (orthosis); physical therapy	Commercial system
Baker et al., (2011), OHAE	Extension for thumb, index and middle fingers	3 DOF	Not specified	C-Stamp (coded in C)	Portable system (orthosis)	Finger tracking for back-drivability
Kline et al., (2005)	Extension for all fingers	1 DOF	Not specified	Joint angles, sEMG	Wearable glove; physical therapy	Stroke subjects
Chen et al., (2009)	Independent linear movement of each finger	5 DOF	Not specified	Fingers positions and forces, sEMG	Stationary system; physical therapy	Not specified

References, System Name	Supported Movements	DOF	Modelling	Main Control Input, Control Method	Type; Field of Application	Stage of development; Special Feature
Broaden Horizons, Inc. (2010), <i>Power Grip</i> ,	Grasping using thumb with index and middle fingers (joined together)	2 DOF	Not specified	Switches or sEMG	Wearable orthosis; grasp assistance	Commercial system
Lucas et al., (2004)	Flexion and passive extension of an index finger	1 DOF	Not specified	sEMG	Wearable orthosis; grasp assistance	Not specified
Mulas et al., (2005)	Flexion and extension for thumb and flexion for other fingers	2 DOF	Not specified	sEMG, pulleys position	Wearable orthosis; physical therapy	Not specified
Tong et al., (2010)	Flexion for each finger	10 DOF	Not specified	sEMG	Wearable orthosis; physical therapy	Not specified
Fleischer et al., (2009) <i>TU Berlin Hand Exoskeleton</i> ,	flexion and abduction of all major joints of each finger	20 DOF	Joint angles, end-point force, sEMG	Joint angles, end-point force, sEMG	Wearable orthosis; physical therapy	Not specified
Brokaw et al., (2011) <i>HandSome</i>	4 bar linkage for thumb and fingers	4 DOF	Kinematics trajectory	Not specified	Wearable orthosis; rehabilitation device	Not specified

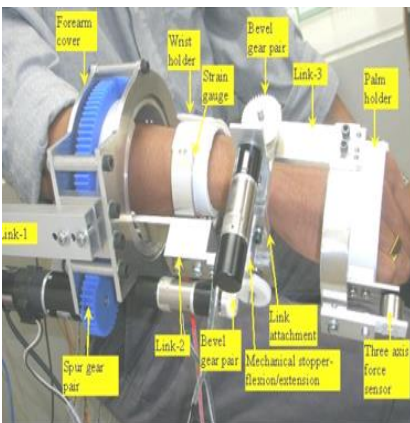
References, System Name	Supported Movements	DOF	Modelling	Main Control Input, Control Method	Type; Field of Application	Stage of development; Special Feature
Engeberg et al., (2013)	4 fingers	12 DOF	Dynamics modeling	Human model reference adaptive controller (HMRAC) compared with Sliding mode control; force and position control	Prosthetic hand;	EMG data collected from amputee and nonamputee
Wang et al., (2011), ATX exoskeleton	1 finger	5 active, 3 passive DOF	Kinematics trajectory	Real time control	Wearable orthosis; rehabilitation device	Not specified
Worsnopp et al., (2007) AFX exoskeleton	1 finger	3DOF	Kinematics trajectory	Force and position input, PID controller	Wearable orthosis; rehabilitation device	Not specified
Wei et al., (2013)	5 fingers	14 DOF	Force simulation analysis	Motor controller	Wearable orthosis; rehabilitation device	Haptic device (phantom premium)
Iqbal et al., (2010; 2014), HEXOSYS	2 finger; thumb and index finger.	6DOF	Kinematic and dynamic modeling	Minimum jerk trajectory generation, DSP (56F807) based controller; position control	Wearable orthosis; rehabilitation device	Multi-objective optimisation strategy
Peerdeman et al., (2010)	5 fingers - flexion	14 DOF	Ellipsoidal representation of the phalanges.	EMG input, state machine to describe the hand behaviour	Prosthesis; amputee, simulation	Pre-shaping

References, System Name	Supported Movements	DOF	Modelling	Main Control Input, Control Method	Type; Field of Application	Stage of development; Special Feature
Yang et al., (2016)	5 fingers	14 DOF	Kinematic and dynamic modeling	Microcontroller as a pulse generator; forward, reverse, fast forward and fast reverse pulse signals.	Wearable orthosis; rehabilitation device	New jointless tendon-driven exoskeleton
Wang et al., (2010)	1 finger; index finger	3DOF	Dynamic modeling	A resistance compensation control; real time controller that sample the angle and force data in real-time	Wearable orthosis; rehabilitation device	Not specified
Yu et al., (2011)	1 finger	3 DOF	Kinematics and dynamics modeling	Position and force input, force compensation algorithm (active) (Passive mode) using PID	Wearable orthosis; rehabilitation device	Not specified
Gilardi et al., (2009; 2010)	1 artificial finger	4 DOF;	Kinematic and dynamic modelling	Microcontroller (PWM-PD) feedback controller and a minimum jerk trajectory feedforward controller	Prosthesis;	new biomimetic tendon-driven actuation system
J. Iqbal et al., (2010; 2011)	1 index finger	3DOF	Kinematics and dynamic modelling	Grasping force as input, optimization using Monte Carlo method	Wearable orthosis; rehabilitation device	Not specified

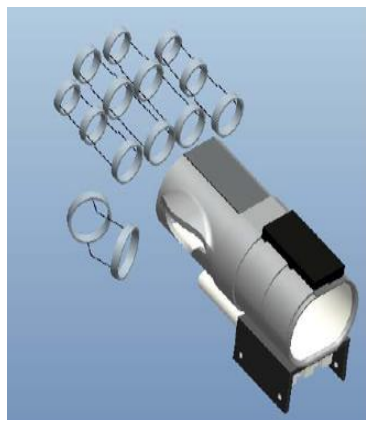
References, System Name	Supported Movements	DOF	Modelling	Main Control Input, Control Method	Type; Field of Application	Stage of development; Special Feature
Systems assisting wrist and finger(s) movements						
Hasegawa et al., (2011; 2008)	5 fingers with a wrist, flexion and extension, adduction and abduction	11 DOF	Surface EMG	bioelectric potential-based switching control	Portable system (orthosis)	Not specified
Koeneman et al., (2004) <i>Hand Mentor™</i> , Kinematic Muscles, Inc.;	Extension for wrist and 4 fingers (except the thumb)	1 DOF	Not stated	Wrist angle, flexion torque	Wearable orthosis; physical therapy	Commercial system
Takahashi et al., (2008), <i>HWARD</i> ,	Flexion and extension for wrist, thumb, and joined four medial finger	3 DOF	Not stated	Joint angles and torques	Stationary system (with desktop mounted orthosis); physical therapy	Not specified
S. Ates et al., (2014; 2013, 2014, 2015, 2017)	Extension assistance for wrist and fingers, abduction and adduction for the thumb	6 DOF	Dynamics modelling; estimation of the angle based on readings from bending sensors attached at each finger	Microcontroller to interface sensors with the dedicated PC to guide the user to play the therapeutic game	Wearable orthosis; rehabilitation device	Working prototype; Interactive game

References, System Name	Supported Movements	DOF	Modelling	Main Control Input, Control Method	Type; Field of Application	Stage of development; Special Feature
Rose et al., (2015) and Pezent et al., (2017) READAPT	Flexion, extension, radial, and ulnar movements for wrist attached to Maestro hand exoskeleton	12 DOF	Kinematic coupling analysis	Critically damped PD controller	Wearable orthosis; rehabilitation device	Donning and doffing for impaired subject; OpenWrist features

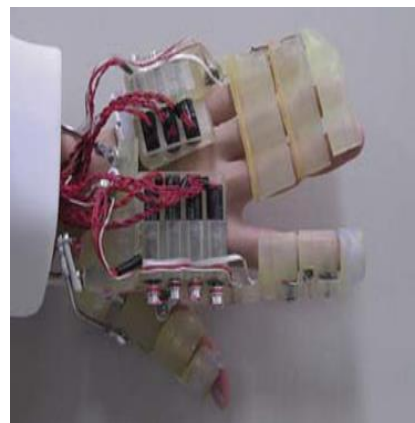
Based on the literature review conducted, the orthotic exoskeleton hand generally comprises a rigid molded basic structure with actuators and sensors that support specific movements. Table 2.1 categorises the exoskeleton hand into three classes; system assisting wrist movement, system assisting finger(s) movement and system assisting wrist and finger(s) movement. Gopura et al. (2008) have proposed 3 DOF EMG based controlled exoskeleton robot that permits wrist ulnar/radial, flexion/extension and forearm pronation/supination motions (Figure 2.1(a)).



(a) Gopura et al. (2008)



(b) Baker et al. (2011)



(c) Hasegawa et al. (2011)

Figure 2.1: The exoskeleton hand systems: (a) Assisting wrist movement, (b) Assisting finger(s) movement, and (c) Assisting wrist and finger(s) movement

The hardware of the exoskeleton is adaptable to the human wrist regarding segmental lengths, number of DOF, the range of motion and its centre of rotation. Surface EMG and hand force/forearm torque are used as the input control parameters for the fuzzy controller. The fuzzy-neuro controller managed to implement a smooth natural and flexible wrist motion assistance.

Baker et al. (2011) developed an orthotic hand assistive exoskeleton (OHAE) that reduces the muscular force needed to pinch or grasp (Figure 2.1 (b)). It has three actuated fingers: the thumb, middle, and index fingers, that are driven by cables attached to a glove. The device is portable, easily manufactured and consists of four major sub-systems. FSR sensor is installed at the corresponding fingertip to trigger the actuating motors to retract or extend, reducing the amount of muscular energy utilized. Peerdeman et al. (2010) have presented a model of myoelectric hand prosthesis based on the biomechanical structure of human hand that is served as a testbed for the development of control systems based on electromyography (EMG) input. The grasp selection and execution is control based on the myoelectric signals that are acquired and classified before being fed to the model to control the motions that virtually represent the prosthetic hand. The model is validated using two different grasping types on a simple object, demonstrating reshaping of the hand and flexion of the fingers and thumb. The results show the exact finger movement. However, the dynamic analysis for the finger extension is not included in this research and is left as future work. Iqbal et al. (2010) proposed a novel design of a thumb exoskeleton system for rehabilitation. The optimisation of the device was achieved through natural finger workspace and capabilities. The procedure includes analysis of daily hand life common activities. The optimization results show adequate functionality of thumb exoskeleton with adequate ergonomics.

Hasegawa et al. (2011; 2008) have introduced a five-fingered assistive hand that supports human hand and wrist activities (Figure 2.1 (c)). It has 11 DOF: eight active joints and three passive joints. A cable-driven mechanism mimicking human finger motion has been adopted with each of the joints controlled independently. The movement of the device is controlled based on the user's bioelectric potential. The grasping force is estimated from the bioelectric potential measured by surface electrodes on the lumbrical muscles. The performance of the device has been validated through experiments and show that the exoskeleton allows pinch of a small object and augments grasping force for heavy work.

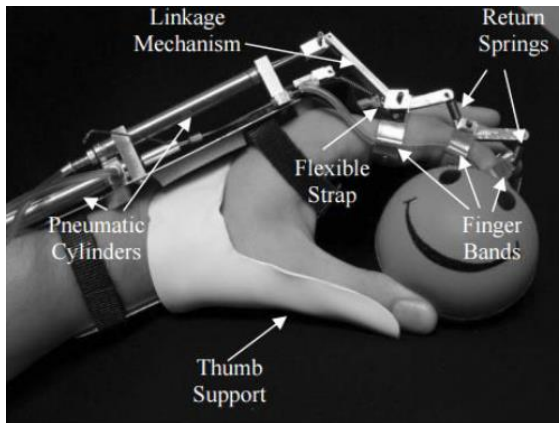
In 2013, Supervised Care and Rehabilitation Involving Personal Tele-robotics (SCRIPT) project conducted by research collaboration (between researchers from Netherland, USA, UK, Italy and Germany) has introduced a new hand and wrist exoskeleton design named as SCRIPT Passive Orthosis (SPO). The SPO is an interactive hand and wrist orthosis that provides adaptable extension assistance, interfaced with motivational games for post-stroke rehabilitation. It comprises of an off-the-shelf mobile arm support with hand plate and digit caps, wrist-torque transfer mechanism, torque generation mechanism, and is equipped with various sensors; IMU, flex sensor, and potentiometer (Amirabdollahian et al., 2014; Ates et al., 2013, 2015). The prototype has been evaluated in many clinical setting (three clinical sites; United Kingdom, Netherlands, and Italy) by therapists and has been extensively used by post-stroke patients at home (Amirabdollahian et al., 2014; Ates et al., 2017). The main limitation of the developed exoskeleton, however, is the absence of controller that can actively generate or control the movements to provide automatic assistance orthosis for stroke survivors.

Considering the strengths and limitations, it can be concluded that in developing competent assistive device, seamless integration with the user by considering intelligent control as part of the human machine interface; specifically, the user motion intention is a primary concern. Advanced hands-free human machine interface with intention-driven control approach is favorable when compared to traditional user interfaces (ie joysticks, keyboards, GUI etc) because it can control the exoskeleton hand naturally in predictable way, making it more reliable and efficient in communicating with the user and in providing assistance. It is important to improve the quality of support for basic ADL to avoid dissatisfaction among the users that may lead to the discontinuation of the device shortly after use. The realization of user motion intention can be achieved by employing mechanical sensor or biomechanical sensing method like EMG signals. Huo et al. (2010, 2015) proposed intentional reaching direction (IRD) method to quantitatively describe the user motion intention for a 3 DOF power-assist upper-limb exoskeleton. The device was embedded with multiple force sensing resistors with two modeling modes; static force model for the relaxed state and hybrid model for motion state. The motion intention of the user was estimated online using Kalman Filter and a mode transition detector with admittance control strategy. The method was tested on healthy subjects and offered satisfactory results. However, according to Kiguchi et al. (2007) to activate the exoskeleton robot according to the user motion intention, a force sensor based control can be employed for user without limb problem while for those who are not strong

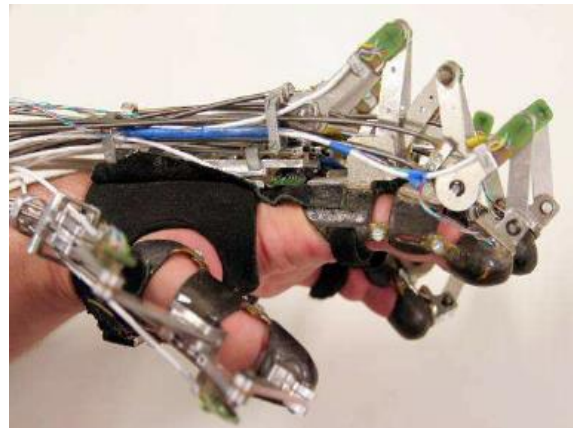
enough to move their limb, EMG-based control with the EMG signals from certain muscles can be adopted to activate the system accordingly.

Meng et al. (2017) conducted a survey on the existing surface EMG control strategies employed in controlling wearable hand exoskeleton for rehabilitation and categorized the control methods according to control input, control architecture and algorithm, and control output. Based on the survey, it can be concluded that different exoskeletons would have different surface EMG control methods depending on their operating principles. DiCocco et al. (2004) developed a lightweight orthotic (Figure 2.2(a)) control based on EMG signals and compared several control strategies for the device. Natural reaching and pinching sequence control strategies were designed using binary control (a simple on/off control states), continuous variable control (a proportional controller based on filtered EMG signals) and natural reaching algorithm (tested only on contralateral arm), with conclusion that binary control provides faster interaction with objects while variable control provides more controlled interactions. They concluded that the system is effective in enabling pinching movements to those who suffered from hand mobility. However, only index-thumb finger pinch was studied in the research.

Wege and Zimmermann (2007) had developed an exoskeleton hand comprised of four fingers (with four joints for each finger) for rehabilitation following hand injuries or stroke. The device (Figure 2.2(b)) was controlled using sliding mode position control integrated with several sensors; hall sensors to measure the joint angles, optical encoders to measure angles of the motor axes, force sensor to measure the force between the user and the device, and EMG sensor to measure the muscle contractions. According to them, the user intention recognition via force sensors is often impossible to distinguish between the forces exerted by the user or environment, and human-machine interaction is less efficient. Thus, EMG signals were acquired and blind source separation was applied to avoid signals overlapping and variations in the different muscles. However, due to several limitations of the experimental setup, the results yielded were not accurate. Non-distinguishable overlapping movements were detected due to the natural effect of two adjacent muscles (flexor and extensor) and the co-activation of neighboring muscles.



(a) DiCicco et al., (2004)



(b) Wege and Zimmerman, (2007)

Figure 2.2: The sEMG based controlled exoskeleton hand (a) from Carnegie Mellon University (b) from Technische University of Berlin

Besides seamless human machine interaction, another significant challenge is to develop an exoskeleton hand that can emulate the function and movement of actual human hand. Design optimization in virtual environments that consider the biomechanical conditions and human factors in a systematic manner can benefit the device development process not only in terms of safety and efficacy measures, but also in terms of cost effectiveness and mechanical/hardware system selection for the exoskeleton hand. Virtual environment such as SimMechanics, Visual Nastran and AnyBody software provide useful design and significant testing platform for complex systems like exoskeleton hand where researchers can simulate the conceptual and detailed design, test their controllers and validate their functionality without constructing the actual prototype. Miranda-Linares et al. (2015) developed a humanoid and lower-limb exoskeleton model, tested the finite state controller and tested the functionality of the exoskeleton in SimWise, virtual environment platform. The model was assembled and coupled with appropriate kinematics characteristics, which was then computed and integrated with the controller to validate the overall system performance. The visualization of motion for both (the humanoid and exoskeleton) interacting with external forces and disturbances yielded satisfactory and realistic results.

2.3 Forearm Electromyogram Signals

The electromyogram signal (or also known as myoelectric signal) is a summation of Motor Unit Action Potential (MUAP), a tiny voltage generated from the contraction of activated muscle fibres by motor neurons. There are many muscle fibres within human forearm muscles, which acts individually and add up to a larger unit each time the hand flexes or extends. During hand gripping, when the person intends to exert more hand grip force, the strength of muscle contraction is increased by central nervous system in two ways; increasing the number of motor units activated (spatial recruitment) and increasing the firing rate (frequency) at which individual motor units' fire (temporal recruitment). The electrical signals obtained from muscle are displayed on oscilloscope as common practice since 1922. However due to the random and stochastic nature of the EMG signals, there is limited information that could be extracted from the oscilloscope readings. According to De Luca, (1979) the EMG signal is an exceedingly complicated signal which is affected by the anatomical and physiological properties of muscles. Thus, it is crucial to process the signal before utilizing in the research. Konrad (2006), defined EMG as an experimental technique concerned with the development, recording and analysis of myoelectric signals. The structure of the EMG can be identified and analysed in few processes named as pattern recognition process. According to Lalitharatne et al, (2014) there are four steps to recognize the pattern of EMG signals: acquiring the data, segmenting the data, extracting the features from the recorded data and mapping the data into classes. Each steps involves several methods or techniques (Figure 2.3). The pattern recognition step has been employed by other researchers with several modifications on the methods or techniques used to improve the efficiency of the myoelectric control scheme.

According to Khushaba et al. (2010, 2011), it is crucial to produce a highly discriminative feature set that can well recognise different finger movements to facilitate the implementation of myoelectric control scheme for the hand prosthesis. They have investigated forearm sEMG signals from nine subjects performing 10 classes of individual and combined fingers movements, and extracted and projected various feature sets using several time domain methods; waveform length, zero crossing, slope-sign changes, skewness, root-mean-square, mean absolute value, integral absolute value, and autoregression features. They have proposed an accurate and efficient feature

projection method based on Fuzzy Neighborhood Preserving Analysis (FNPA) showing practical results indicating a significant classification with average accuracy of 91%. In 2012, they have further studied and proposed a combined feature selection and projection method denoted as Mutual Components Analysis (MCA). They have compared the performance of the MCA with traditional Principle Components Analysis (PCA), Linear Discriminant Analysis (LDA) and Uncorrelated Linear Discriminant Analysis (ULDA). Later in the same year, they have extended the research and proposed Bayesian data fusion post-processing approach as part of the classification method and managed to maximise the probability of correct classification with average accuracy of 90% (Khushaba et al., 2012; Khushaba and Kodagoda, 2012). The approaches used are similar to that used by other researchers but with extensive explanation on the selection of features.

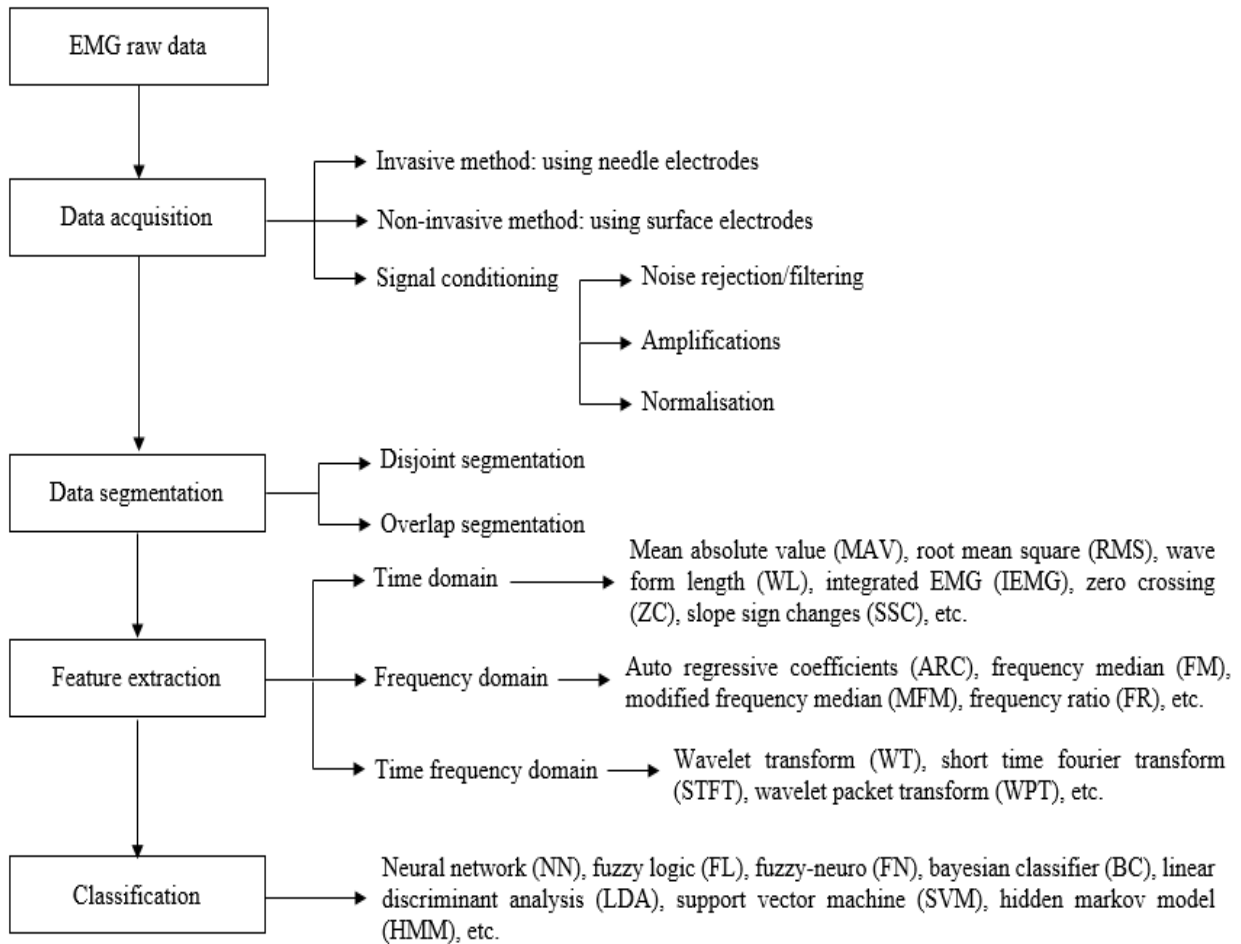


Figure 2.3: EMG pattern recognition process; adopted and modified from Lalitharatne et al, (2014)

Phinyomark et al. (2012) suggested that careful selection of features is important for successful analysis of the EMG signals and their classification to avoid producing feature sets that contain a number of redundant features. They have studied most complete and up-to-date thirty-seven time-domain and frequency-domain features and indicated that some of the time-domain features are redundant while the frequency-domain features performance in class separability is not suitable for EMG signal recognition. Based on mathematical properties, the time-domain features can be grouped into 4 main types; energy and complexity information method, frequency information method, prediction model method and time-dependence method. They have further extended the research and investigated the behavior of fifty time-domain and frequency-domain features to classify 10 upper limb motions using forearm EMG signals. The result shows that the sample entropy (SampEn) outperformed other features when compared using LDA classifier. (Phinyomark et al., 2013, 2014).

Khezri and Jahed (2011) have designed a multistep-based sEMG pattern-recognition system for identifying the hand motion commands for rehabilitation purposes. They adopted an adaptive neuro-fuzzy inference system (ANFIS) to classify and recognize six classes of hand movements. A hybrid back propagation and least-mean-square algorithm was used to train the fuzzy system while a subtractive-clustering algorithm was utilized to optimise the number of fuzzy rule. The proposed recognition scheme yields satisfactory result in identifying complex hand movements.

Mohideen et al. (2012; 2011) have constructed an EMG circuit to pre-process the EMG signals extracted from forearm muscle to study the relationship between EMG from forearm muscle and hand grip strength. It amplified, filtered, and rectified the raw signals to acquire linear enveloped signals through electronic instrumentation. They also included feature extraction and mapping for the extracted signals in their research. The developed circuit yielded satisfactory result. There are several research works conducted similar to this work. Cesqui et al. (2013) have investigated the use of EMG signals in robot-based stroke neuro-rehabilitation to enhance functional recovery. The classical approach for EMG based pattern recognition is explored to study its relevance in predicting patients' intention while attempting to generate goal-directed movement. Nine right-handed healthy subjects and seven right-handed stroke survivors were used as the test subjects. The results were satisfactory for the EMG detection but showed that the EMG pattern recognition might not be practical to interpret the normal and abnormal muscle patterns.

2.4 Dynamic Modeling based on Forearm EMG Signals for Exoskeleton Hand Control

In biomechanics, the use of surface EMG has dominated three applications, one of which is its relationship to the force produced by a muscle. Thus, this section will explore the recent developments in establishing the relationship between EMG signal, generated by muscles at different hand grip forces and wrist joint angles. The results of forearm muscle activity include the finger(s) and wrist flexion or extension. In controlling the movements of the exoskeleton hand, information relating handgrip force and wrist joint angles to forearm muscle activity is useful to be used as part of the control algorithm. There are several research works that have been conducted to investigate these relationships. Sidek et al. (2012) has studied the relationship between muscular effort of the flexor muscles in the forearm and hand grip strength. EMG signals were measured using constructed electronic circuit from the subject while applying minimum, intermediate and maximum hand grips on a hand gripper. The results have shown that EMG frequency from the Flexor Digitorum Superficialis (FDS) increases with increased handgrip strength. This information relating EMG from flexor muscles to hand grip strength is useful for use in hand rehabilitation devices to estimate suitable resistance to be provided to patients during rehabilitation routines. Similarly, Haarlal et al. (2016), Khushaba et al. (2012), Suresh et al. (2011), Lucas et al. (2004), and Zardoshti-Kermani (1995) have investigated the same inter-relation between EMG and hand grip force.

Gopura et al. (2008) has studied the relationship between muscle activation levels with wrist position. They have implemented natural and flexible wrist motion assistance by employing fuzzy-neuro control based on EMG signals measured from various flexor, extensor, supinator and pronator muscles. Change in muscle activation levels in accordance with the angles of wrist motions is analysed and this information is used to formulate fuzzy rules of the fuzzy controller. The authors pointed out the difficulty of discriminating wrist motions based on the EMG activity of the subject's forearms as some muscles are used not only for one type of motion but also for multiple motions. Similarly, Sasaki et al. (2005) have developed an active support splint driven by pneumatic soft actuator (ASSIST) for bending motion assist at a wrist. The effectiveness of the device is evaluated by measuring the bending angle of the wrist without human muscular force. EMG signal is measured at a flexor carpi ulnaris; one of the muscles used in bending a wrist. The

amplitude of the EMG signal decreases significantly in the cases with or without ASSIST showing that the burden for the muscle can be decreased by the generated torque from ASSIST. This relationship is important in proving that with proper analysis of EMG, the bending motion of the wrist can be realized even without human muscular force.

Hu et al. (2009) also investigated the motor functional recovery process in chronic stroke during robot-assisted wrist training. 20 training sessions that involved wrist tracking using an interactive rehabilitation robot have been conducted utilizing EMG activation levels from four muscles: biceps brachii (BIC), triceps brachii (TRI, lateral head), flexor carpiradialis (FCR), and extensor carpiradialis (ECR) to monitor the neuromuscular changes during the training course. The quantitative changes in EMG activation level for individual subjects suggested that most of the subjects had decreased EMG activity and reduced muscle co-contraction in the related muscles by simple pre- and post-training tests. On the other hand, Song et al. (2007) designed a horizontal robotic system that is myoelectrically control to assist wrist movement for the post-stroke patient. The subject's intention measured based on the EMG signals collected from the FCR and ECR muscles are used to control the wrist flexion or extension. The neuromuscular changes during the wrist training course from BIC, TRI, FCR and ECR muscles are monitored where most of the muscles had decreased EMG activity and reduced muscle co-contraction with the increase of assistance, which reflected that less effort was needed for the subject to flex or extend the wrist.

All the aforementioned studies that have attempted to establish the relationship between EMG signals, various hand grip strength, and finger and wrist position, have not dealt with the intricate dynamics modelling of the hand. Researchers have not treated the transformation process between muscle activation dynamics into forces and joint movement estimations in much detail. According to Buchanan et al. (2004) the biomechanics of human movement can be fundamentally studied using two approaches; forward dynamics and inverse dynamics, and can be used to estimate the joint moments during movements. In forward dynamics approach, neural command that specifies magnitude of muscle activation based on forearm EMG signals is used as the control input. The magnitudes of EMG signals change with respect to the neural command and vary depending on many factors; e.g. the muscle itself, the gain of amplifiers, the types of electrode used etc. Thus, the EMG signals need to transform into a parameter called as muscle activation, which will produce an output in terms of time varying value with a magnitude between 0 and 1. This can be

done by normalising the raw data. The muscle activation can then be mapped into joint angle for wrist and respective fingers. To better understand the continuous kinematics estimation and dynamic modelling of the hand, extensive literature review was conducted covering a range of statistical approaches that can be used in estimating the relationships among the aforesaid variables. Table 2.2 presents the related work found in the literature for joint angle estimation of the hand based on EMG signals.

Table 2.2: Previous work done related to the dynamic modelling of the hand

References	Subjects, number of electrodes	Movement, DOF/, muscles	Features extraction method	Estimation method	Performance Indicator
Ngeo et al., (2012, 2013; 2014)	10 able bodied subject, 8 bipolar electrodes	Multiple finger flexion and extension, muscles; APL, FCR, FDS, FDP, ED, EI, ECU,	EMG-to-muscle activation, time domain features; MAV, WL, WA and VAR	ANN and Gaussian Process (GP) for joint angle estimation	RMS error and mean correlation coefficient
Shrirao et al., (2009)	15 able bodied subject, 2 electrodes	Flexion and extension of an index finger; EDS muscle	Normalised RMS value	ANN for finger joint angle estimation	RMS error
Worden et al., (2018)	NinaPro database, 40 subjects, 12 electrodes	Flexion of the fingers and thumb, extensor, flexor, triceps and biceps muscles	MAV, WL, RMS, FILT	Multivariate Bayesian mixture of expert for finger force regression	Normalised RMS error
Hahne et al., (2014)	10 able bodied subject, 192 electrodes	Flexion, extension, radial, ulnar of the wrist.	Variance	LR, ME, MLP, KRR	RMS and standard deviation
Muceli et al.,(2012)	6 able-bodied, 64 electrodes	Flexion, extension, radial, ulnar of the wrist, pronation and supination of the forearm, flexor and extensor muscles	Linear envelope	ANN for wrist kinematics estimation	Mean relative error

Ngeo et al. (2014) presented a simultaneous and multi finger kinematics estimation method based on surface EMG. The forearm EMG signals together with the finger kinematics of 10 able-bodied subjects were used to model the EMG-to-muscle activation features that also parameterize the electromechanical delay. A model free approach for each joint was used to estimate the complex finger kinematics. Machine learning regression techniques, the ANN and GP regressor employed have shown viable estimation results with ANN outperforming the GP. The authors claimed that the proposed muscle activation has successfully improved the estimation accuracies. However, the results are based on data that is analysed separately between subjects. Similarly, Shirao et al. (2009) investigated a technique to predict the finger joint angle from the surface EMG measurements of the extensor muscle using neural network models. The sEMG and joint angle measurement for flexion and extension of an index finger were recorded simultaneously at three different speeds; fast, mid and low. The results yielded smaller RMS error for fast speed as compared to the low speed finger extension.

Hahne et al. (2014) presented an independent, simultaneous and proportional myoelectric control for 2 DOF wrist prosthesis by using linear and nonlinear regression methods; linear regression (LR), mixture of linear experts (ME), multilayer perceptron (MLP) and kernel-ridge regression (KRR). Similarly, Muceli et al. (2012) used artificial neural network to estimate wrist and hand kinematics. The result yielded a viable solution that provides practical control for multiple DOFs.

2.5 Issues of Control Design for Exoskeleton Hand

In general, employing EMG signals as part of control strategies will improve control performance as the signals contain important information related to user motion prediction. However, most common controller uses binary methods which open or close, to actuate the gripping motion of the hand. Similar research has been done using the same control methods by Cesqui et al. (2013), Peerdeman et al. (2010), et al., Iqbal et al. (2010) and Hasegawa et al. (2014). Working with surface EMG signals as control input, the control method adopted should be able to cope with the time varying properties of muscle-joint dynamics, subject and day variations, muscle fatigue etc. It is difficult to obtain similar surface EMG signals on same subject at the same muscle

movement as the signals are affected by the physical and physiological condition of muscle contractions. Therefore, adaptation to this condition is crucial. Adaptation can be introduced either in classifying the control input (users' intended motion) in pattern recognition process or in designing the control scheme for the exoskeleton hand.

Meng et al. (2014) proposed an active interaction control method for 6 DOF parallel robot-assisted lower-limb rehabilitation. The interaction control integrates two components: EMG-triggered assistance and the adaptive impedance control scheme. The movement intention and the robot assistance are predicted and triggered through this integration. The robot velocity during the exercise is influenced by the adaptation of impedance controller, the user's muscle activity level is evaluated online and the recovery condition is adapted to the robot impedance. The robot can be driven by the proposed method with a distinct increased in the muscle activity levels between active mode and EMG-triggered mode.

Chen et al. (2011) presented a hybrid control strategy for a five-finger 14 DOF robotic hand. The authors explored several controllers using adaptive neuro-fuzzy interference system (ANFIS) and fuzzy logic (soft control techniques) and proportional-derivative (PD) controller (hard control techniques). The inverse kinematics of the three-link fingers is computed using ANFIS while fuzzy logic is used to tune the PD parameters with 2 input layers using 7 triangular membership function and 49 fuzzy rules. The FL-tuned PD controller exhibit superior performance in comparison to the PD, PID and FL controllers alone.

2.6 Issues of Performance Analysis for Exoskeleton Hand

The performance of the control design should be evaluated to analyse the effectiveness of proposed control techniques. There are many ways to analyse the performance of each proposed methods/techniques regardless of the area of study; features extraction, joint angle estimation, and control methods. Nonetheless, only several researchers have discussed methods adopted for the performance analysis. Meng et al. (2014) analysed the performance of the proposed control method (active interaction controller) by comparing the differences in muscle activity levels between the proposed and traditional methods. The RMS values were compared and the results showed that the proposed method yields higher values compared to the traditional control method. Similarly,

Ngeo et al. (2014) used Normalised Root-Mean-Square Error (NRMSE) and Pearson Correlation Coefficient or known as R-value index to measure the performance of methods employed in extracting the useful information from the EMG as well as the methods used to estimate the complex finger kinematics. They used 3-way ANOVA test with Tukey-Kramers post-hoc comparison test to decide the best methods used in joint estimation between subjects, DOF and the features used. On the other hand, Kang et al. (2014) analysed the stability of their proposed controller (adaptive PID neural network) using Lyapunov method. According to the Lyapunov method, when $\Delta V(k) \leq 0$, in any sampling period, where $V(k)$ is Lyapunov function, the closed loop system is stable.

2.7 Summary

This chapter has presented the research background, a detailed review of the design and development of the orthotic exoskeleton hand for assistive and rehabilitation purposes, the electromyogram control techniques, and the dynamic modelling of the exoskeleton hand. The methodology used to develop the exoskeleton hand alongside its main challenges were studied and discussed.

Despite the fact that there is extensive research focusing on the design and development of exoskeleton hand, more dexterous and combined fingers and wrist control especially for seamless human-machine interaction has not received the same amount of attention. Previously published studies show that the current control schemes employed in controlling the available multiple DOF exoskeleton hands cannot fully utilise the hand function because there are fewer control inputs than the joints that need to be controlled. The most significant step to facilitate an effective control scheme is to extract the useful information within EMG signals to produce high-quality feature sets with significant separability of classes for each finger and wrist movements.

The pattern recognition based control or known as myoelectric control approach is commonly employed in previous research to process and fully utilised the collected EMG data which includes data acquisition, data segmentation, feature extraction and classification. Such approach, however, has failed to efficiently control the exoskeleton hand as direct control using classification commonly process only a single movement at a time, even with extended classification that is able

to process more than one class, some movement limitation might have applied (i.e. two joint commonly cannot be controlled independently if two functions are activated in parallel). Therefore, independent proportional control using regression method to establish the relationship between EMG signal generated by muscles at different handgrip forces and wrist joint angles is needed. Unlike classifier, regressor estimates continuous joint angle values for each DOF of fingers and wrist, allowing an independent, simultaneous and proportional estimation that can facilitate a fluent and natural control for the exoskeleton hand.

In this research, the pattern-recognition process is modified by replacing the classifier with supervised learning method. A feed-forward artificial neural network (ANN) and adaptive neuro-fuzzy inference system (ANFIS) with subtractive clustering are adopted to establish the relationship between forearm electromyogram signals with various finger pinches, handgrip forces, and wrist positions. The in-grip joint angles and handgrip forces were predicted to provide the spectrum of grips, rather than a discrete set for continuous control of the exoskeleton hand.

This chapter portrayed the upmost important platform for this research since it provides the required steps to develop the exoskeleton hand efficiently. The detailed methodologies together with their findings were discussed in the next following chapters; chapter 3 for the design and modelling of the exoskeleton hand in the virtual environment, chapter 4 for the forearm EMG signal analysis, chapter 5 for the dynamic modelling of the hand and chapter 6 for the design and control framework.

Chapter 3

SYSTEM MODELLING AND DESIGN

'Hand is a miraculous creation that no sleek is the same.'

3.1 Introduction

This chapter presents the modelling and design process for the exoskeleton hand. The key is to understand the human hand anatomy, biomechanics and measurements to ensure safe operation and useful function of the device. The human hand is highly articulated with various range of motion (ROM) and its sizes or dimensions vary among individuals. Deep understanding of the hand structure is crucial in obtaining practical design and model of the exoskeleton so that to resemble the actual human hand and provide proper movements/functions. The model is developed based on a systematic knowledge of the human hand following standard anthropometric hand measurements for women.

Technically, a mathematical model of the hand is complex and difficult to derive, and it often requires assumptions and linearisation to be made especially in modelling the nonlinearities associated with the system, making the modelling process tedious and complicated. Some of the assumptions and linearisation may neglect the essential features of the hand and restrain its full functionality when implemented in the real system. Moreover, simplified mathematical model is not sufficient to investigate the overall system performance, and it leads to the deficiency in validation of the control algorithm. Thus, in this research, physical modelling software; SimMechanics embedded with Solidworks design tool is chosen over the complex and lengthy formulations of mathematical equations to aid the designing and modelling process for the exoskeleton.

Solidworks is used to design and assemble the exoskeleton, and this is then imported to the SimMechanics software that is compatible and allows verification of the model in MATLAB. The SimMechanics program enables mechanical systems modelling, motions simulation, parts and structures editing, parameters optimization and further analysis within the Simulink environment. The physical model of the exoskeleton hand developed is used as a simulation platform (testbed) to facilitate the validation of the joints angle estimations, control algorithm, and overall system performance before real embodiment is done. It will help to reduce the research cost, require less testing and shorten the time to commercialise the exoskeleton.

The chapter is structured as follows; it starts with a description of human hand anatomy and biomechanics, followed by the anthropometric hand measurements for women, the design of exoskeleton hand in Solidworks, modelling of the exoskeleton hand in SimMechanics environments and ended with a summary.

3.2 Hand Anatomy and Biomechanics

In general, human upper extremity consists of four segments; shoulder, arm, forearm, and hand, and is characterised based on its mobility and ability to grasp/manipulate. The hand is composed of five fingers; four medial fingers (index, middle, ring, and pinky fingers) and a thumb, palm, dorsum of hand and wrist. The skeleton of a human hand (Figure 3.1) is consists of 27 bones, which can be divided into three groups: 8 carpal bones that make up the wrist, 5 metacarpal bones as the root of the hand, and 14 phalanges for the fingers. The phalanges are divided into three intercalated bony segments: distal, intermediate, and proximal phalanges. The distal phalange is located at the fingertip, connected to the proximal phalange that is located at the base of the finger through an intermediate phalange. The proximal phalange is also connected to the metacarpal bones in the palm.

Anatomically, each of the phalanges is connected through finger joints: metacarpophalangeal (MCP), proximal interphalangeal (PIP), and distal interphalangeal (DIP) joints. The MCP joint of the hand has two degrees of freedom (DOF) (adduction/abduction and flexion/extension) while the PIP and DIP joints both are single DOF (flexion/extension). The PIP and DIP joints are interdependent as the DIP joint is a passive DOF that is driven by the rotation at the PIP. Hence,

each natural finger can be considered as a 4 DOF mechanism with three active and one passive joint (Gilardi et al., 2010; Gopura et al., 2011; Moore et al., 2014)

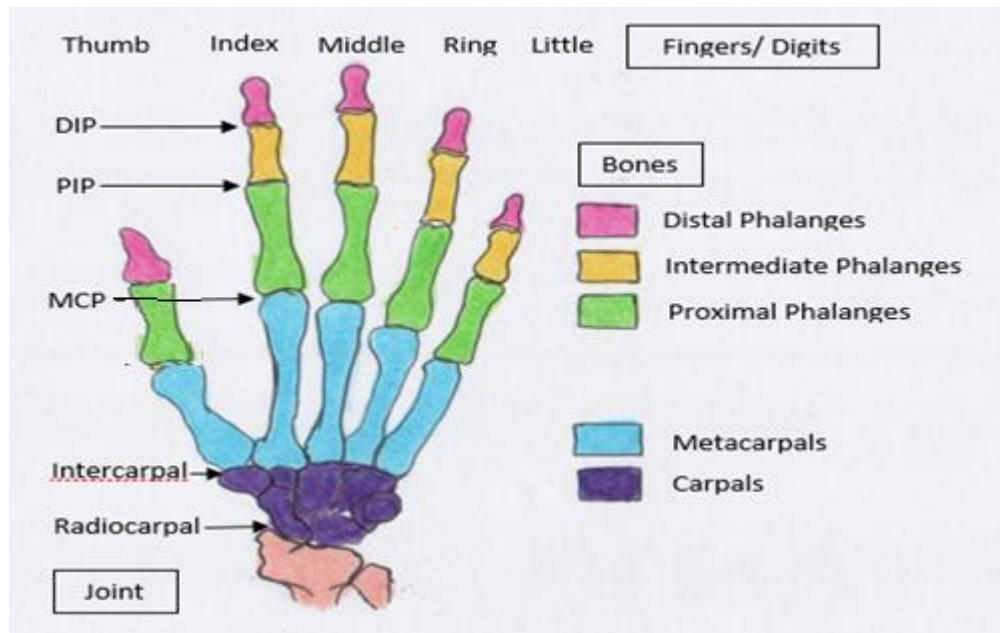


Figure 3.1: Sketch for bones and joints of a human hand

3.3 Anthropometric Hand Measurements for Women

There is a large amount of variation in the dimensional features; size and shape of the human hand between and within individuals and populations. Commonly, the hand length is about one-tenth of the individual's height and one-quarter the length of their upper extremities. The assessment of the physical dimensions of the hand is obtained based on anthropometric measurements. Anthropometry, which refers to the measurement of the human body, where data about the distribution of body dimensions in populations is studied and analysed, can provide crucial information for exoskeletons design. In the context of this research, several anthropometry on women hand measurements, performed by other researchers (Cakit et al., 2014; Esmaili et al., 2011; Jee et al., 2016; Kong and Kim, 2015; McLain, 2010; Nag et al., 2003) were studied and employed to ascertain human-machine compatibility and accurate size of exoskeleton.

During the measurement process, the hand is positioned in a straight and flat position instead of in a relaxed position. The dimensions of the flat side are significantly longer than in the relaxed

hand; there is a possible unconscious tendency to curl the hand. The measurements for finger, hand, palm, wrist breadth and hand depth were recorded using several appropriate measurement tools; electronic digital calliper, finger circumference gauge, and digital measurement tape based on the hand measurement diagram in Figure 3.2. The diagram illustrates three different hand positions; straight and flat, maximum reach and finger grip, for the right hand of a woman. The definitions for hand dimensions and biomechanics measurements of the diagram are as listed in Table 3.1:

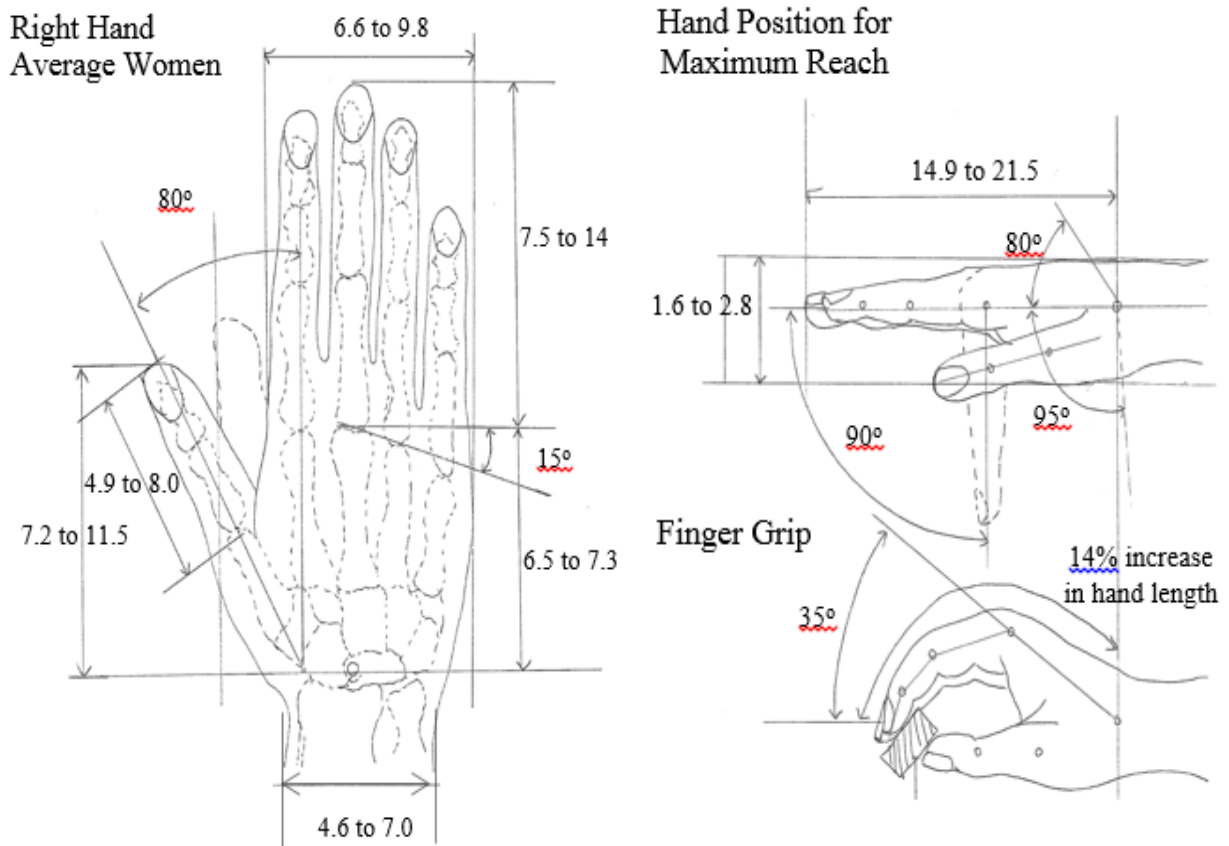


Figure 3.2: Hand measurement diagram (unit is in cm unless otherwise specified)

Table 3.1: Hand dimension and biomechanics measurement definition

Hand Dimension	Definition
Hand length	The distance from distal wrist crease baseline to the top of the middle finger measured alongside the axis of the hand.
Hand width	The breadth of hand measured across the palm; from one side to the other side of the hand with all fingers closed together.
Hand depth	The diameter between anterior to posterior of the hand held in a position with palm facing down; fingers are closed together with the thumb held against the side of the hand.
Wrist breadth	The breadth of the wrist measured alongside the distal wrist crease baseline of the hand from the ulnar to the radius side.
Biomechanics Measurement	Definition
Flexion/extension for each digit	The angle between two phalanges when the respective joint of the finger are moved through the entire range of motion (flexion/extension).
Wrist angle	The angle between metacarpal bones to the neutral line (hand is in a straight and flat position) when the radiocarpal joint is moved from full flexion to full extension.

Based on the selected literature (McLain, 2010; Nag et al., 2003), there are thirty-seven essential hand dimensions for women from different ethnicity considered in this research, as listed in Table 3.2. All these dimensions were selected as most of the measurements are relevant to the design of the hand exoskeleton and cover a wide range of hand parts (the bony segment of fingers and wrist), functionality and range of motion which are essentials and important to produce an exoskeleton that emulates the real human hand. Moreover, the dimensions have been measured and studied in

different women population. The dimensions are in terms of range (minimum and maximum measurements, except for British women data) within sufficient sample size.

Table 3.2: Comparison of selected hand dimensions

Population	Asian	American	British
Sample Size	95	300	5.1
Hand length	13.5-19.0	14.9-21.5	17.43
Hand width	4.7-8.0	6.6-9.8	7.72
Hand depth	1.6-2.8	-	2.57
Wrist breadth	3.6-6.2	4.6-7	5.16
Digit 1 distal phalanx link length	-	2.2-4.1	-
Digit 1 proximal phalanx link length	-	1-2.9	-
Digit 1 tip to finger crotch length	4.4-7.4	4.9-8	-
Digit 1 tip to wrist crease length	-	10.3-15.4	-
Digit 1 interphalangeal breadth	1.0-2.4	1.7-2.5	-
Digit 2 distal phalanx link length	-	1.9-3.2	-
Digit 2 intermediate phalanx link length	-	1.4-2.8	-
Digit 2 proximal phalanx link length	-	4.1-8	-
Digit 2 tip to finger crotch length	5.0-7.9	5.6-8.4	7.83
Digit 2 tip to wrist crease length	-	14.0-20.3	-
Digit 2 distal interphalangeal breadth	0.6-1.4	1.4-2.3	-
Digit 2 proximal interphalangeal breadth	0.8-1.7	1.6-2.4	-
Digit 3 distal phalanx link length	-	2.1-3.4	-
Digit 3 intermediate phalanx link length	-	1.7-3.6	-
Digit 3 proximal phalanx link length	-	3.7-7	-
Digit 3 tip to finger crotch length	5.7-8.8	6.2-9.6	7.7
Digit 3 tip to wrist crease length	-	14-21.3	-
Digit 3 distal interphalangeal breadth	0.6-1.5	1.4-2.1	1.49
Digit 3 proximal interphalangeal breadth	0.75-1.7	1.6-2.4	1.75
Digit 4 distal phalanx link length	-	1.9-3.3	-
Digit 4 intermediate phalanx link length	-	1.6-3.5	-

Digit 4 proximal phalanx link length	-	3.7-6	-
Digit 4 tip to finger crotch length	5.2-8.0	5.5-9	8.62
Digit 4 tip to wrist crease length	-	13.8-20.3	-
Digit 4 distal interphalangeal breadth	-	1.5-2.3	-
Digit 4 proximal interphalangeal breadth	-	1.3-2.1	-
Digit 5 distal phalanx link length	-	1.6-3.0	-
Digit 5 intermediate phalanx link length	-	1.0-2.4	-
Digit 5 proximal phalanx link length	-	2.8-4.9	-
Digit 5 tip to finger crotch length	3.9-6.6	4.1-7.3	5.67
Digit 5 tip to wrist crease length	-	11.4-18	-
Digit 5 distal interphalangeal breadth	-	1.2-1.9	-
Digit 5 proximal interphalangeal breadth	-	1.3-2.0	-

Legend:

- The units for all measurements are in centimetre (cm).
- The (-) indicates that data is not available in the literature selected.
- The numbering of the digit is 1 to 5 representing the thumb, index, middle, ring, and pinky fingers respectively.

3.4 Design of the Exoskeleton Hand using Solidwork

The conceptual design of the exoskeleton hand is completed using SolidWorks tools. SolidWorks is a solid modelling software that facilitates products design in 3D; the sketch is done in 2D profiles, featured into 3D to produce the solid shape. Technically, a broad range of computer-aided design (CAD) software with specialised programs is available for practical design purposes such as SolidWorks, AutoCAD, CATIA etc. SolidWorks is chosen over others for its functionality to employ a parametric feature-based approach in modelling the part that allows editing of the design to be done at any stage in the design process and its compatibility to be embedded with SimMechanics in Matlab.

In designing the prototype hand, few essential design criteria were considered to achieve the most effective hand design that emulates the actual human hand. First, the hand anatomical and

biomechanical abilities were established. The designed hand as illustrated in Figure 3.3, consists of five fingers attached to a palm that is connected to a wrist with a proper choice of DOF; total 15 DOF with 14 DOF at the fingers and 1 DOF at the wrist joint.

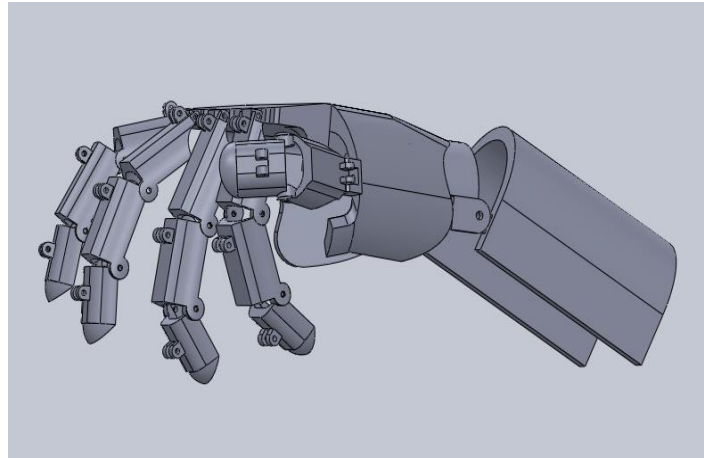


Figure 3.3: The exoskeleton hand in SolidWorks

The bony segments of the human hand are closely followed in designing the exoskeleton, with exceptions in the palm and the wrist. The design of index, middle, ring and pinky fingers contain three intercalated body segments: proximal, middle and distal phalanges (Figure 3.4a), while the thumb contains only two intercalated body segments: proximal and distal phalanges (Figure 3.4b). The palm is designed without metacarpal shaft which makes it fixed, while the wrist is designed without carpal bone which allows only flexion and extension movements.

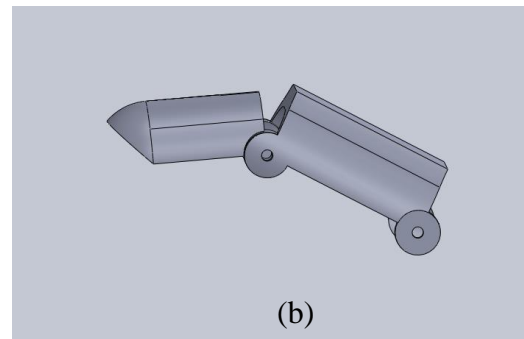
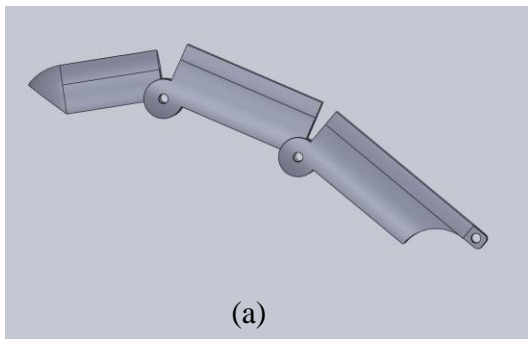


Figure 3.4: The exoskeleton fingers: (a) Design for the index, middle, ring and little fingers, (b) Design for the thumb

The dimensions and specifications of the exoskeleton hand are shown in Table 3.3. Due to the limitation in the literature, the dimensions were chosen for the range that could cater the Asian and American women hand measurements. Small tolerances were considered in each link to allow room for the frame in case additional comfort material should be added to make it more comfortable to be worn in future.

Table 3.3: Dimensions and specifications of the hand exoskeleton

Hand measurements					
Hand length	19				
Hand width	7.5 / 9.5 (with the thumb)				
Hand depth	3.5				
Wrist breadth	6				
	Digit 1	Digit 2	Digit 3	Digit 4	Digit 5
Distal phalanx link length	2.5	2.5	2.5	2.5	2.0
Intermediate phalanx link length	-	2.5	2.8	2.5	2.0
Proximal phalanx link length	3.0	4.0	4.0	4	3.0
Tip to finger crotch length	5.5	9	9.3	9	7.0
Tip to wrist crease length	11.5	16.5	19	19	17
Distal interphalangeal breadth	-	1.7	1.7	1.7	1.7
Proximal interphalangeal breadth	-	2.0	2.0	2.0	2.0
Interphalangeal breadth	2.0	-	-	-	-

Legend:

- The unit for all measurements are in centimetre (cm).
- The (-) is indicating that data is not relevant to the digit.
- The numbering of the digit is 1 to 5 representing the thumb, index, middle, ring, and pinky fingers respectively.

The hand compatibility was targeted to ensure that the designed hand is capable of exerting and assisting daily hand motions. The fingers were designed to trace out a path in space that closely resembles the path of natural fingers during a normal grasp. The natural range of motion and ratio of tip force exerted upon an object are also considered in the design. Additionally, the hand was designed to be directly driven at each joint to achieve the actual performance of the human hand

and to avoid the underactuation problems especially difficulties in path tracking of each fingers during hand grasping.

In order to develop better representation of the system, a few assumptions were made to further define the exoskeleton hand model. These are as follows:

1. All the joints (DIP, PIP, and MCP joints) are assumed to have 1 DOF, allowing only flexion/extension.
2. All the joint angles (DIP, PIP and MCP joints) for each finger are based on Lee et al. (2014), for rectangular object power grip with a grip diameter of 25 cm (the diameter of hand dynamometer).
3. During the finger pinch, the force is exerted at the middle pulp of distal phalanx and all external forces are assumed as single unit.
4. All the joint actuators receive forces as input and render angles as the output (adopting admittance control theory).

Even though careful measurement has been considered in designing the exoskeleton hand, there are several issues associated with the kinematic compatibility of the exoskeleton with human hand making human-exoskeleton attachment difficult. The designed exoskeleton has rigid structure that hinders a full kinematic compatibility when attached to the human joints. It is very challenging to model and replicate the biological joints of human hand using only a single DOF. In order to cope with this issue, a passive joint should be introduced for joint supporting more than one dominant joint and suitable linkages should be designed to avoid possible collision between the device and the anatomical hand.

3.5 Modelling of the Exoskeleton Hand using SimMechanics

Physical modelling is frequently preferred over traditional method in product development due to the nonlinear factors and complex restrictions associated with the intricate system like the exoskeleton hand. It involves the employment of simulation-driven product development software such as Simscape Multibody, Visual Nastran, SimWise, etc, to validate the mechanical design before committing to make a real/physical prototype. Designers are allowed to model, simulate

and visualise the system behaviour under real-application operating conditions and rapidly refine the design without needing to produce multiple physical prototypes for testing purposes.

In this research, the first generation of Simscape Multibody (or previously known as SimMechanics) was chosen for the system modelling as it can be interfaced seamlessly with Simulink block diagram; an existing toolbox in Matlab which is used as a plug-in for GUI-based simulation environment. The combination of SimMechanics and Simulink form an efficient tool for simulating rigid-body mechanical systems especially for control design and performance validation.

The geometric Solidworks assembly of the hand is transformed into a physical model in SimMechanics, where the standard Newtonian dynamics of forces and torques is employed to model and simulate the design of the exoskeleton hand and its motions. It enables interconnection between physical components with geometric and kinematic relationships of the hand in the form of interconnected blocks. This integration allows verification of the model, whether it corresponds to the actual human hand and whether it behaves according to the presumptions and set requirements (Fedák et al., 2014). Two major steps are involved in the transformation process; exporting the Solidworks assembly into ‘.xml’ file and importing the file to create a SimMechanics model (Figure 3.5).

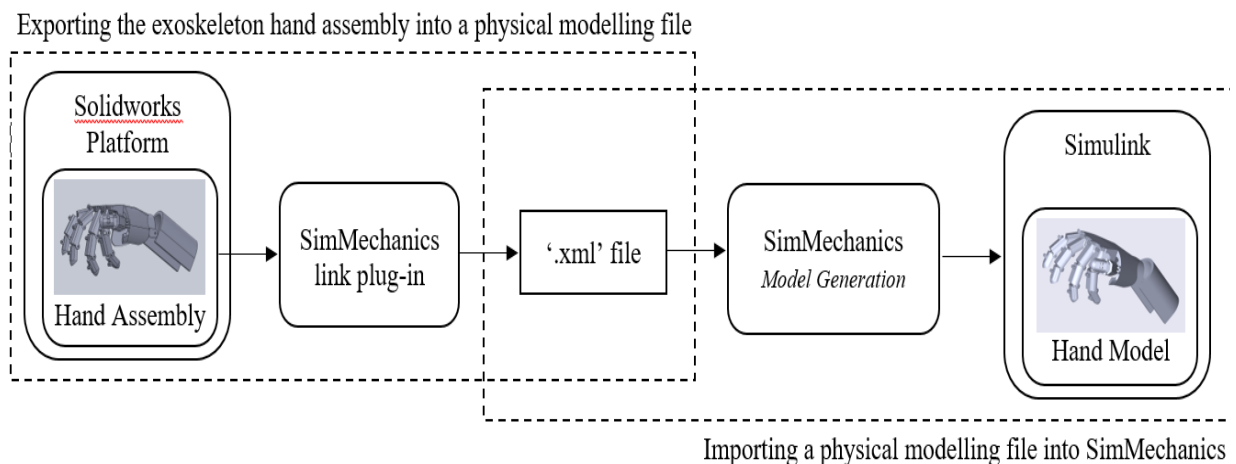


Figure 3.5: Transformation process; from conceptual design in Solidworks into the exoskeleton hand model computed in the Simulink environment

Technically, the SimMechanics link plug-in creates the physical modelling file by converting the assembly's parts into bodies and maps the constraints between parts into joints. The procedure used for the integration is as follows:

- 1) First, the SimMechanics link plug-in is downloaded and installed. The plug-in provides the primary interface for exporting the Solidworks assemblies into SimMechanics software.
- 2) To install the plug-in, MATLAB need to run as administrator and use the 'install_addon' command prompt.
- 3) Command prompt 'smlink_linksw' is entered in MATLAB to add SimMechanics as a Solidworks plugin to the windows registry.
- 4) Then, the plug-in is enabled in the Solidwork application; the SimMechanics checkbox is selected in the add-ins command window and will appear in the menu bar when the assembly is started.
- 5) The assembly design of the exoskeleton hand is loaded and exported to the SimMechanics link first generation. The file is saved and the '.xml' file is generated.
- 6) Finally, the Solidworks 3D design is automatically converted into a SimMechanics model and imported to MATLAB using the 'smimport' command prompt.

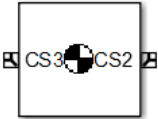
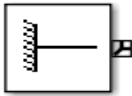
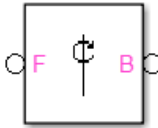
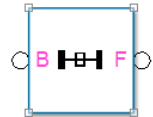
The computed exoskeleton hand model is made up of bodies with geometric and mass information composed of a palm, connected to five fingers and a wrist. It is populated by body parts that are connected to joints corresponding to the assembly parts and constraints saved in the physical modelling file. More intuitive and precise specifications for the body parts and joints of the hand model are discussed in the next sub-section.

3.5.1 Body and Joint Specifications

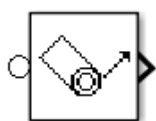
In general, most of the Solidworks-based models have the same properties and standard features; exactly one ground block that is connected to machine environment block, fundamental root that is represented as ground connected to root weld and root body, joints with degree of freedom containing the right joint primitives between two bodies, and weld parts to represent fixed joints. The imported model also contains the system parameters such as masses of the bodies, the tensor of inertia, and graphics.

Similarly, the exoskeleton hand model comprises several parts denoted by the body and joint blocks; the body blocks depict the respective body segments (the phalanxes of the fingers, the palm and the forearm), while the revolute joints represent the constraints used to assemble two parts with a single DoF. For motion analysis, each joint is actuated and the motion is sensed using the interfaces that transform the signal between SimMechanics and Simulink environments and vice versa. The joint actuator block applies the desired torque to the link/body through the revolute joint block, and the joint sensor block detected the position of the link/body. The joint actuator takes either force or motion as the input and outputs a similar parameter through sensing process carried out by the joint sensor. The block types and their functions are listed as in Table 3.4.

Table 3.4: Description of the block parameters and their functions employed in the exoskeleton hand model

Group	Block Type	Block Name	Functions
Bodies		Body block	Represents the user-defined rigid body with mass, frames, coordinate origin, inertia and geometry.
		Machine environment	Categories the mechanical simulation environment for the machine to which the block is connected; gravity, constraint, tolerances, etc.
		Ground	Fixes one side of a joint to a location in the World coordinate system.
Joints		Revolute joint	Allows one rotational degree of freedom; the follower body rotates about a single rotational axis relative to the base through collocated coordinate system origins.
		Weld joint	Represents zero DoF and cannot be actuated but sensor ports can be added to it.

Sensor and Actuator



Joint sensor

Measures the motion (position, velocity and acceleration) as well as computed and reaction force/torque of a primitive joint. It needs to be connected to a joint block (output).



Joint actuator

Actuates a primitive joint using generalised force/torque desired motion signals (position, velocity and acceleration). It needs to be connected to a joint block (input).

For a better relation of the mapping process, the program scheme for four medial fingers after importing together with the corresponding Solidworks parts is illustrated in Figure 3.7. The finger consists of three phalanxes connected by constraints, which are converted into three body parts by revolute joints.

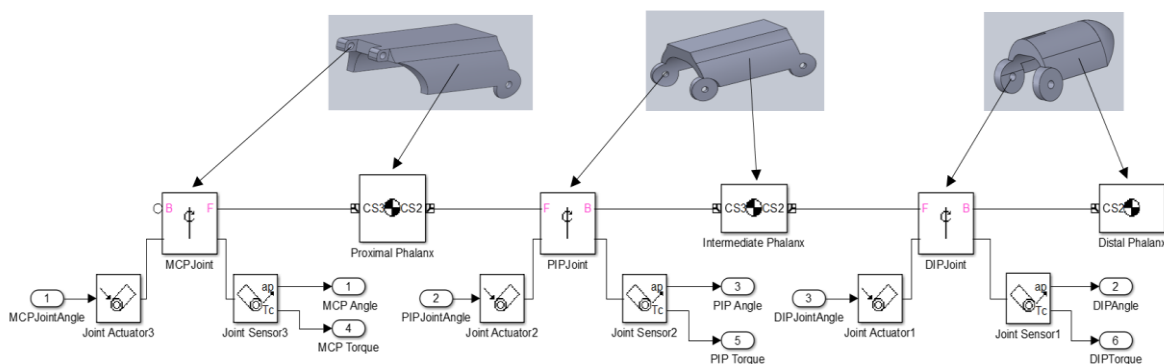


Figure 3.6: The SimMechanics block diagram for four medial fingers (index, middle, ring, and pinky fingers) that are mapped to the respective Solidworks-based assembly parts and constraints

The SimMechanics scheme in Figure 3.7 shows the basic configuration of the exoskeleton hand after importing the physical modelling file to Simulink; the palm body block is firmly connected to ground and machine environment block at one side and connected to the five fingers and a wrist at the other side.

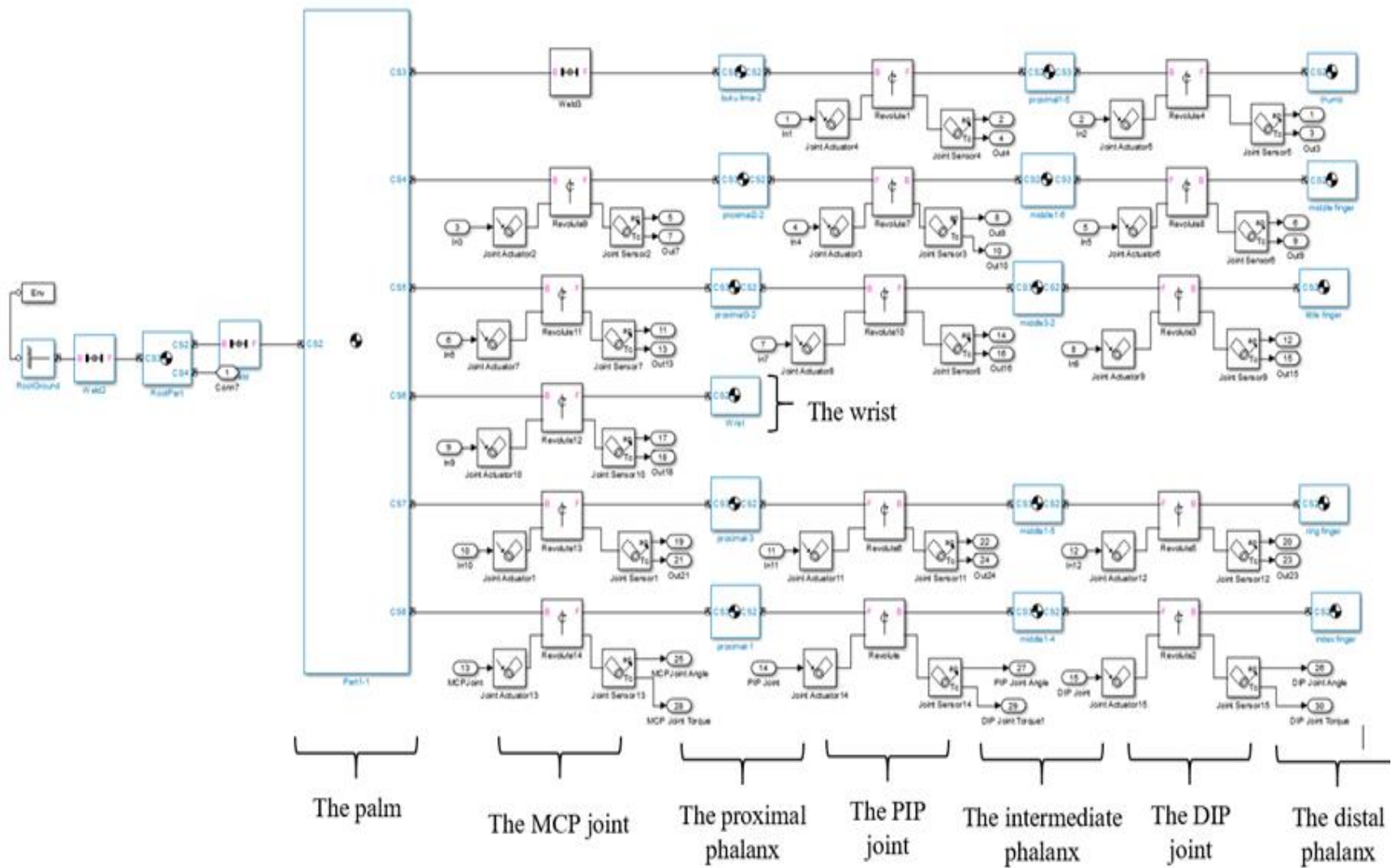


Figure 3.7: The SimMechanics scheme for the exoskeleton hand

3.5.2 Physical Model Visualization and Motion Analysis

The physical model contains a visualization mode; a customized graphics figure window, that is enabled when the simulation is started. It includes the graphical appearance of the exoskeleton hand that resembles the Solidworks assembly with negligible differences, like the colors and graphics quality (Figure 3.8). The visualization contains graphic toolbar features that cater for various display and animation functions such as various viewpoint (isometric, top, etc.), zoom-in and zoom-out, record simulation animation etc. One of the useful features is the simulation time feature that can be slowed down or accelerated, and useful for accurate rapid dynamics system observation and motion analysis.

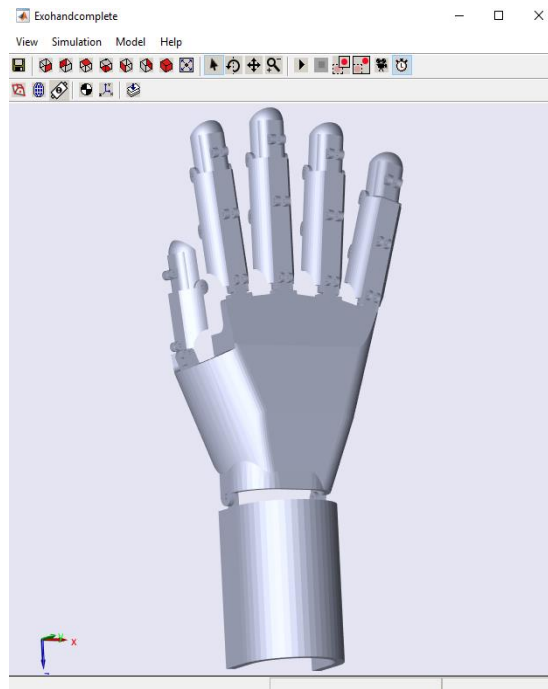


Figure 3.8: The SimMechanics visualization window displaying the exoskeleton hand model

In SimMechanics, Newtons Law is employed to analyse the motion for either forward or inverse dynamics. In forward dynamics, a set of forces or torques are applied to accelerate the bodies of a mechanical system which will be integrated twice by SimMechanics to yield the motion parameters; velocities and positions as functions of time. In contrast, the inverse dynamics analyses the given motions and differentiates them twice to calculate the forces and torques needed to accelerate the system. Depending on the topology of the system used, both cases can be analysed

in SimMechanics by selecting the appropriate analysis mode; forward dynamics, trimming, inverse dynamics and kinematics.

The motion of the exoskeleton hand model is analyzed using forward dynamics, which takes joint angles as the control parameters and senses the orientation of the hand end effectors and the torque computed. The joint actuator block operates in the generalized forces mode for actuation and the mode of calculation in the machine environment block is set to the forward dynamics mode. The sensors are connected to the respective joints to determine the torques computed that are necessary to perform the defined angular orientation of the hand end effectors. This setting is vital to help verify and validate the EMG based controller designed for the exoskeleton hand.

3.6 Summary

This chapter has described the exoskeleton hand developed in the SimMechanics software as the system model to provide testing platform for the EMG based controller developed in this research. The human anatomy and its biomechanics have been studied and referred in designing the exoskeleton hand in Solidworks following the anthropometric data of women hands. The design has been imported to SimMechanics for modelling process. All necessary descriptions regarding the measurements, body and joint specification including the limitation when attaching the hand to anatomical human hand are discussed. The testbed of this research is complete, the simulation diagram of the designed exoskeleton hand shows a satisfactory result and ready to be used for testing and validating the EMG based controller developed in the next chapters.

FOREARM ELECTROMYOGRAPHY SIGNALS ANALYSIS

4.1 Introduction

In defining the user motion intention, the forearm EMG signals need to be properly analysed to extract useful information and for use as control input for the overall system control. This chapter explains the signal analysis that includes detection and processing techniques for the forearm EMG signals collected from seven muscles contributed to finger pinches and hand grasping at various wrist positions. The EMG datasets utilised in this research are collected after obtaining research ethical approval from the Ethical Committee of University of Sheffield, United Kingdom. The purpose of collecting the forearm EMG signals is to investigate the inter-relation between EMG signals with various finger pinches and handgrip forces at different wrist angles. A series of experiments were designed to collect the data. The collected data were processed in four steps; (1) normalisation step using maximum activation levels (peak amplitude) during maximum voluntary contractions, (2) filtering step using band-pass filter, (3) data segmentation step where the data is segmented using overlapping segmentation, and (4) feature extraction step using four time-domain features analysis. In investigating the inter-relation between EMG signals, handgrip force and wrist angles, the muscle excitation and finger pinching/hand grasping forces at different finger/wrist angles are simultaneously measured. Figure 4.1 illustrates the block diagram for the experimental set-up for EMG signals detection process before the data is sent for signal processing.

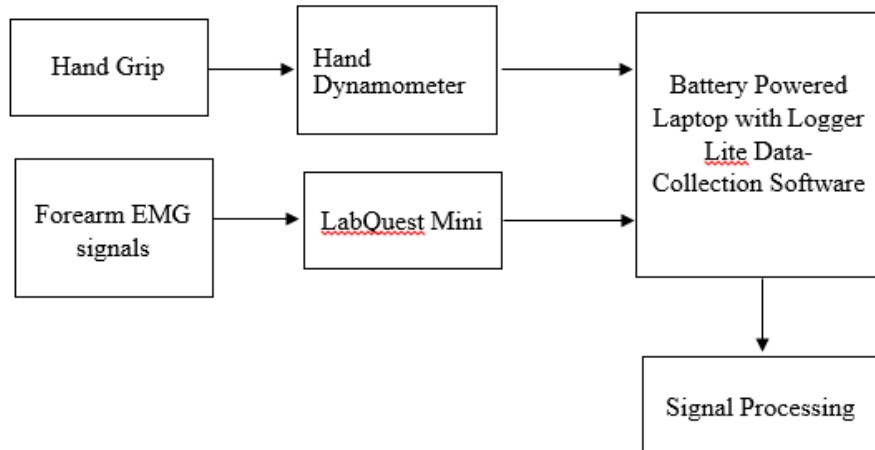


Figure 4.1: Block diagram for the experimental set-up

4.2 EMG Data Collection

The data collection procedure starts with the identification of relevant forearm muscles that are responsible for various hand movements. Here, the anatomy of human hand is extensively studied to select the prominent muscles where the muscles are identified and the procedure to locate the exact position of the muscles are recorded for inclusion in the experimental procedure documentations. After completing the muscle selections, the experimental set-up is done before the experimental procedure for data collection is carried out.

In collecting the data, eight subjects were randomly selected; male and female aged between 30 – 40 years old. The subjects chosen were normally limbed without any neuro-muscular problems. They were briefed (orally or using a visual aid, ie recorded video) and provided with informed consent prior to the study (please refer to Appendix B for the documentation used in the data collection).

The data is collected from healthy subjects to generalise the inter-individual differences to assist the design, testing and validation of the proposed control framework. Commonly, the muscle weaknesses of stroke survivors are contributed from the interruption of the corticospinal tract and muscle atrophy. The EMG features collected from the stroke survivals contains inter-individual differences contributed from the disturbed motor control and needs to be examined and analysed

individually based on subjects. It makes the analysis to be tedious and complicates the research. Besides, limited access to stroke survivors will slow down the research progress.

4.2.1 Muscle Selection Procedures

According to Heo et al. (2012), combination and coordination action of both extrinsic and intrinsic musculature contribute to dexterous movement of the hand. The extrinsic muscles are originated from the arm and forearm while the intrinsic muscles are located entirely within the hand. In order to establish the relationship between forearm EMG signals, handgrip force/joint and wrist angles, the EMG data are collected from the muscles, which show higher levels of muscular activity only. In collecting the data, muscles, which show higher performance during an isometric contraction, are considered and differentiated from muscles that show lower performance. Along the forearm, the muscles that are coordinated for hand gripping are also involved in the flexion and extension of the fingers and the wrist. Some flexor muscles flex the fingers towards the palm of the hand and/or flex the wrist towards the anterior of the forearm. They are located within forearm posterior and anterior compartments. In the posterior compartment, the muscles are commonly known as extensor muscles while they are known as flexor muscles in the anterior compartment. Based on the actions intended to be tested seven potential muscles (Figure 4.2 and Figure 4.3) were selected for further investigation.

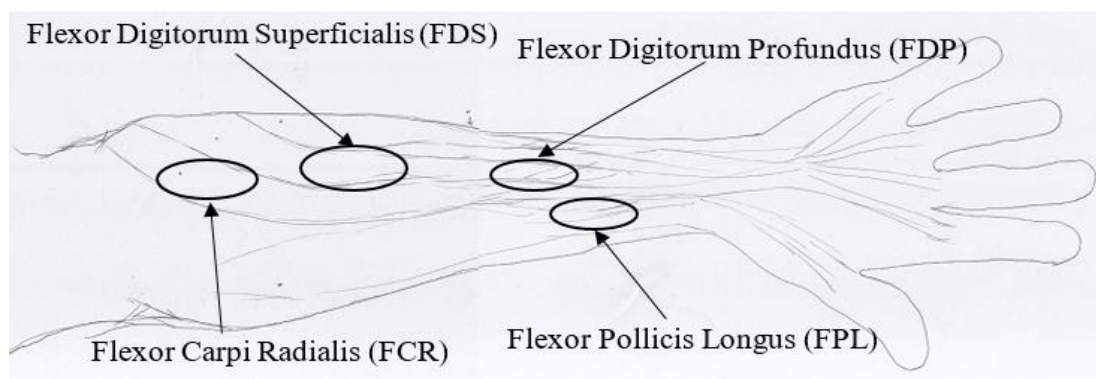


Figure 4.2 Sketch for anterior compartment of a human forearm with location of muscles under consideration: FDS, FDP, FPL and FCR

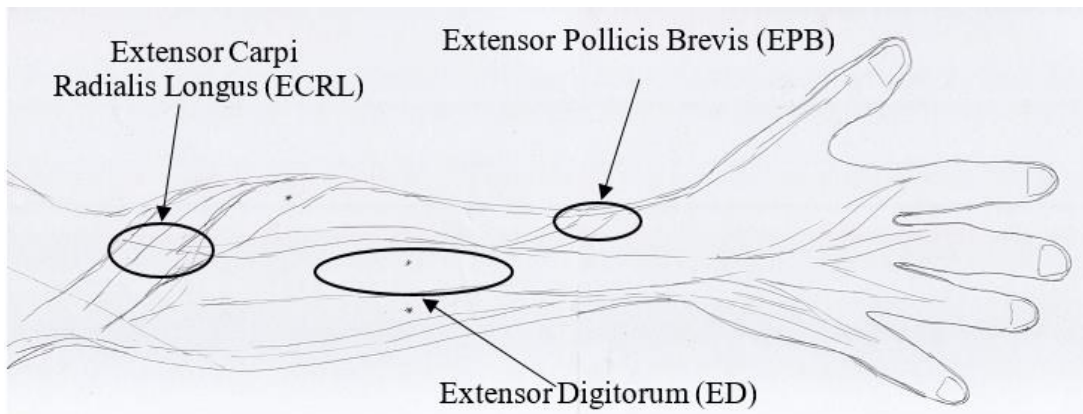


Figure 4.3: Sketch for posterior view of a human forearm with location of muscles under consideration: ED, EPB and ECRL

Among those muscles, five extrinsic muscles contribute to the flexion and extension of the four medial fingers and the thumb while another two muscles are responsible for the wrist movements. The list of muscles and their characteristics are shown in Table 4.1. (Moore et al., 2014)

Table 4.1: Muscles under consideration with their characteristics

No	Muscle	Distal Attachment	Forearm Location	Main Actions
1	Flexor Digitorum Superficialis (FDS)	Middle phalanges of medial four digits	Anterior	Flexes middle and proximal phalanges at PIP and MCP joints of medial 4 digits.
2	Flexor Digitorum Profundus (FDP)	Distal phalanges of medial four digits	Anterior	Flexes distal phalanges at DIP joints of medial four digits; assists the hand flexion.
3	Extensor Digitorum (ED)	Extensor expansion of medial four digits	Posterior	Extends MCP and interphalangeal joints of medial four digits and extends hand at wrist joint

4	Flexor Pollicis Longus (FPL)	Distal phalanx of first digit	Anterior	Flexes phalanx of first digit (thumb).
5	Extensor Pollicis Brevis (EPB)	Proximal phalanx of first digit	Posterior	Extend proximal phalanx of first digit (thumb) at MCP joint.
6	Flexor Carpi Radialis (FCR)	Base of 2 nd metacarpal bone	Anterior	Flexes and abducts hand at wrist.
7	Extensor Carpi Radialis Longus (ECRL)	Base of 2 nd metacarpal bone	Posterior	Extends and abducts hand at wrist.

In general, the estimation of muscle excitation can be done by analysing the amplitude of the EMG signals generated. More motor units and higher firing rates are needed in order to maintain or increase the pinching/gripping forces. The quality and accuracy of the EMG signals collected were improved by ensuring accurate electrodes placement for each muscle under consideration for specific movement. The subjects were instructed to perform several tests to detect the right location of each muscle as described based on Moore et al. (2014) and listed as in Table 4.2.

Table 4.2: Muscles identification test and location for electrode placement

No	Muscle	Test	Location
1	Flexor Digitorum Superficialis (FDS)	Forearm in supination, one finger is flexed at the PIP joint, while the DIP are kept extended against resistance and the other three fingers are held extended to inactivate the FDP.	Middle of the forearm, index fingers flexed towards biceps tendon, just medial to the finger.

2	Flexor Digitorum Profundus (FDP)	Forearm in supination, the PIP joint, and middle phalanx are held in the extended position while the person attempts to flex the DIP joint against resistance.	Lower 1/3 of the forearm and two fingerbreadths, volar to the ulna.
3	Extensor Digitorum (ED)	Forearm in pronation, the fingers are extended at MCP joints while pressure is exerted at the PIP joints by attempting to flex them.	Upper 1/3 of the forearm between radius and ulna.
4	Flexor Pollicis Longus (FPL)	Forearm in supination, the proximal phalanx of the thumb is held, and distal phalanx is flexed against resistance.	Middle of the forearm, volar to the radius.
5	Extensor Pollicis Brevis (EPB)	Forearm in pronation, the thumb is extended at the MCP joint against resistance.	Lower 1/3 of the forearm between radius and ulna.
6	Flexor Carpi Radialis (FCR)	The wrist is flexed against resistance.	Three or four fingerbreadths away from the midpoint of a line connecting the medial epicondyle and biceps tendon.
7	Extensor Carpi Radialis Longus (ECRL)	The wrist is extended and abducted with the forearm pronated	Two fingerbreadths away from lateral epicondyle.

4.2.2 Experiment Set-up

Following completion of muscle selection procedure, pre-task procedure is carried out where the general information about each subject is recorded; weight, height, age and hand length. Then, the subjects are seated on an armchair, with their forearm supported and fixed at one position to avoid the effect of different limb movements on the generated EMG signals. The muscle excitation and finger pinch force are simultaneously measured using multi-channel EMG sensors and a hand dynamometer by Vernier (HD-BTA). The hand dynamometer is a strain gauge based isometric force sensor that amplifies handgrip force applied to its pressure pads and converts the force value into a corresponding voltage value.

The experiment set-up is based on surface EMG technique that measures the muscle activity noninvasively and does not involve any extensive medical procedure. The electrodes are placed on the skin and do not penetrate the skin surface. Unlike needle electromyography, the protocol can be easily carried out, especially for home based assistive and rehabilitative devices.

Before placing the electrodes, the areas of the skin are scrubbed with a paper towel to remove skin oil and moisture. (Detailed skin preparation procedure will only be carried out if necessary). The electrode patches (Kendall 5400 Diagnostic Tab Electrodes) will be used for the data collection. These are specifically designed for most diagnostic applications. No extensive skin preparation procedure will be needed since the electrodes include:

- i. Conductive adhesive hydrogel to provide firm adhesion, repositionability and low impedance for clear, reliable tracing as well as minimizing adhesive residue to facilitate subject clean up.
- ii. Different adhesive levels to accommodate different skin types, applications and monitoring situations
- iii. Laminated Carbon Vinyl to provide conformability to the skin, torsion relief and radiolucency
- iv. Silver/Silver Chloride (Ag/AgCl) sensing element to assist in making the electrode defibrillation recoverable.

Electrode patches are then placed on the selected forearm muscle on subject's dominant hand and connected to the LabQuest mini data acquisition through the interfacing wire (3channels; red, green and black wire with alligator clip). The red (or positive) alligator clip is connected to the electrode patch that measures the muscle activation while the green (or negative) alligator clip is connected to the other electrode patch on the same muscle with 24mm spacing between the electrodes. The black (or reference) alligator clip is connected to electrode patch that is placed at the reference point (near to bone). Next, the hand dynamometer is connected to the LabQuest mini data acquisition and it is connected to a laptop (battery powered). Finally, Logger Lite software is launched, the hand dynamometer is calibrated and data is recorded. The sampling rate is 2 kHz (2000 data values collected in 10 sec). The experimental set-up in Figure 4.4 illustrated the experimental set-up for the data collection. The equipment and material used in the experimental set-up are listed in Table 4.3.

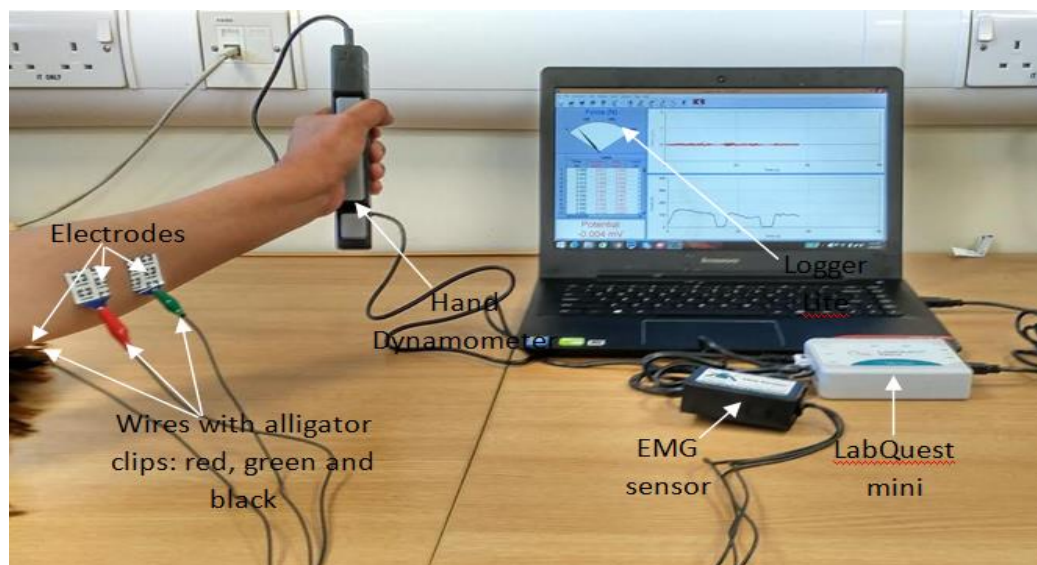


Figure 4.4: Experimental set-up for EMG and hand grip force measurement

Table 4.3: List of research equipment and material

No.	Equipment/Material	Unit	Function
1.	LabQuest Mini data acquisitions with a computer (battery powered)	1 unit	Acquiring EMG signals
2.	Logger Lite data-collection software	1 unit	Recording EMG signals
3.	EMG sensor	2 unit	Measuring the EMG signals
4.	Interfacing wires	2 unit	Measuring the EMG signals
5.	hand dynamometer	1 unit	Measuring hand grip force
6.	Angular scale	1 unit	Measuring wrist angle
7.	Kendall 5400 diagnostic tab electrodes	100 unit	Detecting the EMG signals
8.	Alcohol prep pad	100 unit	Skin preparation
9.	Wet tissues	3 packs	Skin preparation
10.	Paper towel	1 roll	Skin preparation

4.2.3 Experimental Procedures for Data Collection

The purpose of the data collection is to investigate the inter-relation between EMG signals with various finger pinches and hand grip forces at different wrist angles. This will be used for signal processing and joint angle estimations for use as control input for controlling the exoskeleton hand. The EMG signals are extracted from forearm and upper arm muscles using surface electrodes, thus non-invasive. The EMG data collection is carried-out with two experimental procedures; extraction of EMG signals contributing to the finger(s) pinching and extraction of EMG signals contributing to the hand grasping at various wrist movements. The first part of the experiment involves five classes of finger pinches; finger at rest (FR), index to thumb finger pinch (FP1),

middle to thumb finger pinch (FP2), ring to thumb finger pinch (FP3), and pinky to thumb finger pinch (FP4) as illustrated in Figure 4.5. 25 classes of datasets will be collected at different finger pinch strengths (20, 40, 60, 80, and 100% of MVC). The data will be collected for 5 datasets at each session.

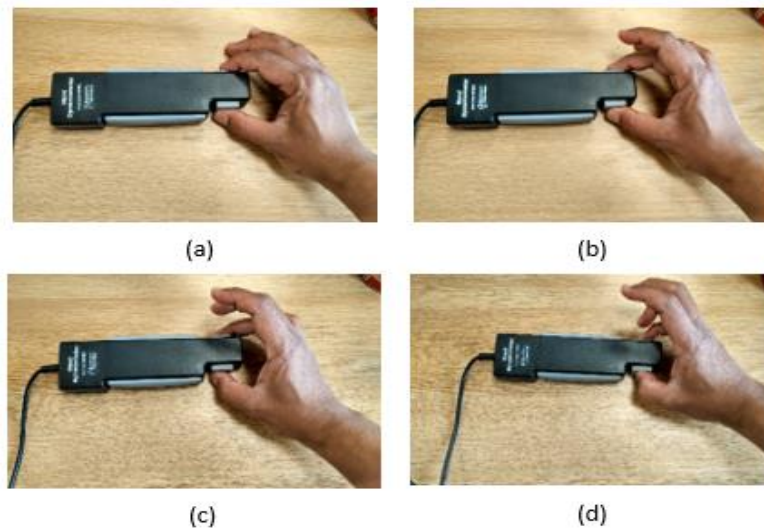


Figure 4.5: Fingers pinch muscle contractions of forearm with 4 groups of movement and angles: (a) index to thumb finger pinch, (b) middle to thumb finger pinch, (c) ring to thumb finger pinch and (d) pinky to thumb finger pinch

The experimental procedure is as follows:

1. Subjects are instructed to pinch the hand dynamometer for 5 seconds using different finger groups (index finger pinch, middle finger pinch, ring finger pinch and little finger pinch) with maximum pinch strength. 2 seconds rest sessions are incorporated within each pinch to prevent muscle fatigue. The maximum finger pinch strengths for each finger group are recorded and considered as subject's maximum activation level (peak-amplitude) during maximum voluntary contraction (MVC).
2. Electrode patches are placed on the selected forearm muscles. Then, the subjects are instructed to pinch the hand dynamometer for 10 seconds using index to thumb finger pinch with various pinching strengths (20, 40, 60, 80, and 100% of MVC). 5 seconds rest sessions are incorporated within each pinching to prevent muscle fatigue. The raw EMG signals extracted are recorded in Logger Lite software.

3. Next, step 2 is repeated for different finger pinches.
4. Finally, steps 1 to 3 are repeated four times with different pinching time (for approximately 10-15 second or until fatigue) with rest intervals (5 seconds).

The second part of the experiment involves six classes of movements; hand rest and hand grasping at three different wrist positions which are 45-degree flexion, at neutral and at 45-degree extension, as illustrated in Figure 4.6. Prismatic power grip (adducted thumb) is used as the grasping pattern. 30 classes of datasets will be collected at different hand grip strengths (20, 40, 60, 80, and 100% of MVC) at various wrist positions. Details of the experimental procedure are as follows:

1. Subjects are instructed to grasp the hand dynamometer for 5 seconds with maximum hand grip strength. 2 seconds rest sessions are incorporated after each grasp. The maximum hand grip strengths are recorded and considered as subject's maximum activation level (peak-amplitude) during maximum voluntary contraction (MVC).
2. Electrode patches are placed on the selected forearm muscles. Then, the subjects are instructed to grasp the hand dynamometer for 10 seconds using different hand grip strengths (20, 40, 60, 80, and 100% of MVC) at neutral (90° of wrist angle). 5 seconds rest sessions are incorporated after each grasping. The raw EMG signals extracted are recorded in Logger Lite software.
3. Next, step 2 is repeated for different wrist positions (at 45-degree flexion and at 45-degree extension).
4. Finally, steps 1 to 3 are repeated four times with different grasping time (for approximately 10-15 second or until fatigue) with rest intervals (for 5 seconds).

4.3 Processing Techniques for the Forearm Electromyogram Signals

The structure of the EMG based control method can be categorized as pattern-recognition or non-pattern recognition based. Non-pattern recognition normally consists of a simple structure with only few processing techniques. The data acquisition of the forearm EMG signals is carried out with a sampling frequency of 2 kHz obeying the Nyquist sampling theorem, which suggests that the sampling frequency should be at least twice the highest frequency contained in the signal. The usable energy of the surface EMG signal is limited to 0 to 500 Hz frequency range, with the dominant energy being in the 50-150 Hz range. In this research, the collected data is processed in

four steps; normalisation step using maximum activation levels (peak amplitude) during maximum voluntary contractions, filtering step using band-pass filter, data segmentation step where the data is segmented using overlapping segmentation, and feature extraction step using four time-domain features analysis.

Technically, the amplitude and frequency characteristics of the raw EMG signals are highly variable and sensitive. Luca (1979) and Konrad (2006) have provided a detailed discussion on how the raw EMG signals can vary when recorded between same and/or different subjects at same and/or different times. It includes and is not limited to extrinsic factors like electrode configuration and placement, muscle selections, skin preparation, temperature, etc., and intrinsic factors like physiological and anatomical factors of the muscles, fiber type compositions, etc. These factors affect the raw EMG signals collected causing difficulties to describe its level of amplitude without any reference value.

The normalisation procedure was first introduced by Eberhart, Inman and Breslar in 1954, and refers to the conversion of the signal to a standard scale. It provides a relative measure of muscle activation and compares it to the reference value. It is usually performed by dividing the EMG signals during a task with a reference amplitude value (the maximum peak value) obtained from the same muscle. The reference value should be chosen in the sense that it allows comparisons between individuals and/or between muscles. In general, the accepted methods to obtain the normalisation reference value include; maximum activation levels (peak amplitude) during maximum voluntary contractions (MVC), peak or mean activation level during specific tasks, activation level during submaximal isometric contractions and peak-to-peak amplitude of the maximum M-wave. However, no method has been declared as the best method for the normalisation of the EMG raw data (Halaki and Gi, 2012).

In this research, maximum activation level (peak amplitude) during MVC is employed to normalise the EMG signals recorded from seven forearm muscles during manual muscle test. (Please refer to section 4.2.1 for detailed information about the selected muscles and their functions). The test involved isometric finger pinches and handgrip forces at different wrist position and grip strength (20 to 100% grip strength). Each subject was asked to pinch and grasp the hand dynamometer for 10 seconds producing maximum forces with 5 seconds rest in between

for three trials. The maximum forces were recorded and used in the experimental procedure for the data collection. (Please refer to the experimental procedure explained in section 4.2.3 for detailed information about how the MVC forces are utilized). The MVC tests were performed for each investigated muscle separately using multi-channel EMG devices.

The EMG signals collected are rectified and filtered before defining the maximum amplitude indicating the maximum voluntary contraction of the specific muscles. The maximum value obtained during the test is used as the reference value for normalising the EMG signals from the muscles of interest. The EMG signal during a task is then divided with the reference value obtained from the same muscle of interest using

$$\text{normalisation} = \frac{\text{amplitude value}}{\text{reference value}} \times 100\% \quad (4.1)$$

Normalisation is important to accurately interpret the muscle excitation and is very useful to highlight the statistical significant differences between the classes of the data collected especially when used with standard hypothesis testing like t-test, Anova test, etc.

After normalisation is done, the data is filtered using second-order bandpass filter (20 Hz – 450 Hz) before segmentation using overlapping segmentation technique with 256 ms window size and 128 ms window increment in MATLAB environment. The overlapping method has advantages over disjoint segmentation as it increases the processing time and provides better classification performance. The number of training samples is estimated as

$$\text{No of training sample} = \frac{\text{Data length} - \text{window size}}{\text{window increment}} + 1 \quad (4.2)$$

Next, feature extraction method is carried out. It plays a critical role in extracting useful information hidden in the forearm EMG signals by transforming the raw data into a reduced representation of features vector. It is also essential in removing the unwanted signal part and interferences. Based on studies conducted by Phinyomark et al. (2012), time domain features; mean absolute value (MAV), integrated EMG (IEMG) and waveform length (WL), that belong to energy and complexity information together with frequency information method groups are

selected for used in this research to avoid redundancy and because it yields better performance when compared to others. Moreover, due to normality, root mean square (RMS) feature is considered to be part of the analysis. All of these features were also chosen due to their computational simplicity.

The Root Mean Square (RMS) is widely adopted for feature extraction. It is modelled as amplitude modulated Gaussian random process. It is related to the constant force and non-fatiguing contraction of the EMG signal (Phinyomark et al., 2013) and can be defined as

$$RMS = \sqrt{\frac{1}{N} \sum_{i=1}^N x_i^2} \quad (4.3)$$

where, N represents the total number of samples considered, and x the signal sample amplitude.

Mean Absolute Value (MAV) is the average of the absolute value of EMG signal measured for certain duration of time. It is an easy way for detection of muscle contraction levels and is one of the most popular used in EMG signal analysis. MAV feature can be defined as

$$MAV = \left(\frac{1}{N}\right) \sum_{i=1}^N |x_i| \quad (4.4)$$

Integrated EMG (IEMG) refers to the absolute summation of the EMG signal amplitude that represent the EMG signal sequence firing point. The absolute summation is normally analysed over a window length of EMG samples. The IEMG can be define as

$$IEMG = \sum_{i=1}^N |x_i| \quad (4.5)$$

Wave length (WL) is the accumulative length of the EMG waveform over the time segment and can be considered as extended version of the integrated EMG. It is defined as

$$WL = \sum_{i=1}^{N-1} |x_{i+1} - x_i| \quad (4.6)$$

4.4 Results and Analysis

Results obtained at each analysis stage are presented in this section. An example of raw EMG data collected based on different handgrip strength showing the muscle excitation is presented. This is followed by normalisation results, features extracted for finger movements with its analysis and finally the features extracted for wrist movements with its analysis.

4.4.1 Samples for Raw and Normalised EMG Signals

The effectiveness of muscle selected and accuracy of raw EMG signal collected are evaluated by analysing the change in signal amplitude towards different finger pinch and handgrip strength. Figure 4.6 illustrates the raw EMG signal collected at different handgrip strengths (20, 40, 60, 80 and 100% of MVC) for FDS muscle at neutral wrist position. It reveals that the amplitude increases proportionally with increase in the handgrip strength. Based on the EMG trace, the signal envelope of EMG activities show many spikes indicating the brain activity to electrically activate or excite the muscle to produce the desired handgrip strength. In the case of fatigue, the envelope of the muscle will increase even though the force actually decreases indicating that the brain is driving the muscle harder and harder but the muscle fatigue makes it weaker. Also noted in the trace is the AC line interference, which contains noises that need to be pre-processed, and can be avoided by conducting the data collection in a room that is away from large electrical devices and power cords.

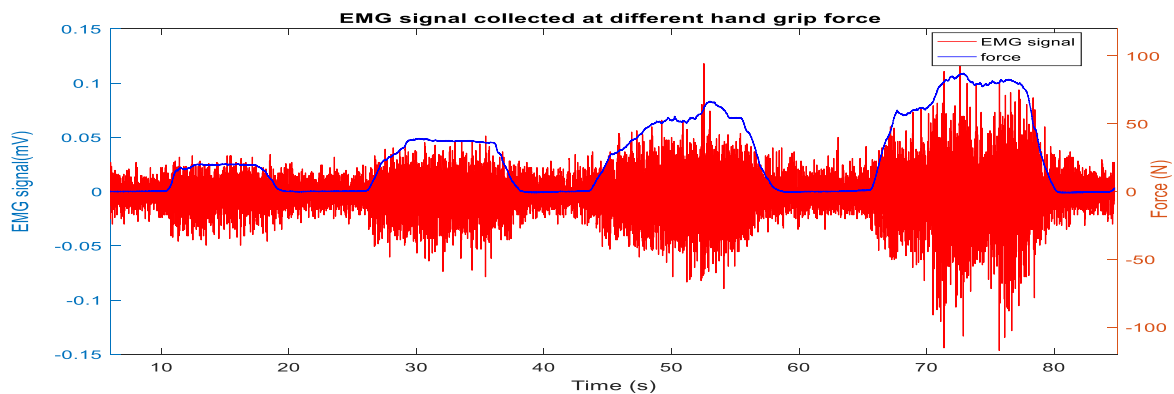


Figure 4.6: The raw EMG collected at different handgrip strength (20, 40, 60, and 80% of MVC) for FDS muscle at neutral wrist position

The scatter plots of the raw EMG data with and without normalisation are illustrated in Figure 4.7 and Figure 4.8. The raw EMG data is collected at 20% of MVC of pinching strength that is contributed from three muscles responsible for the flexion and extension of four medial fingers; FDS, FDP and EDC muscles. The Figure 4.7 shows that without normalisation, the data between classes of movement indicated as index to thumb finger pinch (FP1), middle to thumb finger pinch (FP2), ring to thumb finger pinch (FP3), and pinky to thumb finger pinch (FP4) were overlapping except for finger at rest (FR).

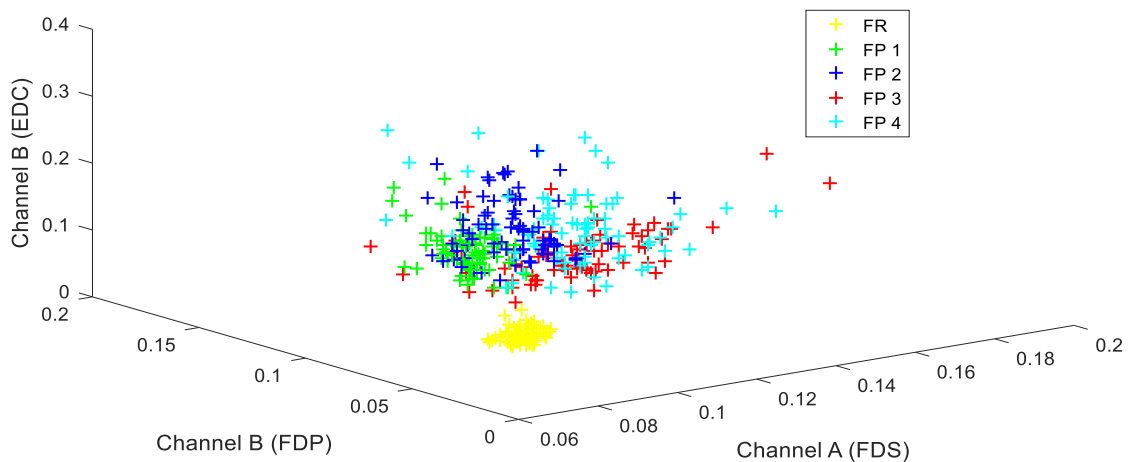


Figure 4.7: The raw EMG signals contributed to the movement of four medial finger without normalisation

Meanwhile, the distribution of the data in the projected space with normalisation shows a significant separability between classes. Minimum overlapping between classes is observed with a higher value range for features at finger rest, as illustrated in Figure 4.8. The FR class gets higher value range due to normalisation that divides the amplitude of the EMG signal during a task (finger at rest), with reference value represented by the maximum amplitude during the maximum voluntary contraction of the same task. At rest, the finger is static, causing the muscle contraction to be negligible regardless of the percentage of MVC. Therefore, the amplitude is expected to be small throughout the task causing the normalisation to yield bigger feature value as compared to other classes.

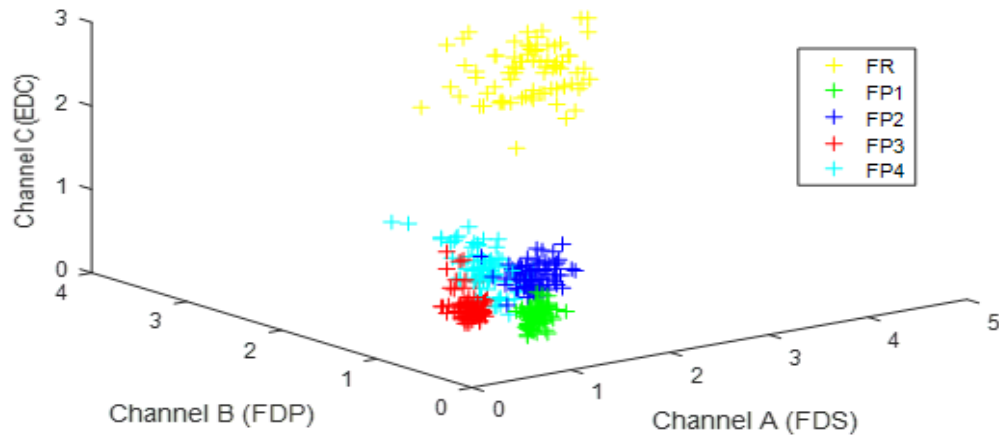


Figure 4.8: The raw EMG signals contributed to the movement of four medial finger with normalisation

4.4.2 Features for Finger Movement

The scatter plots of the four time-domain features (RMS, MAV, IEMG and WL features) extracted at 20% of MVC pinching strength for four medial fingers and a thumb are shown in Figure 4.9 and Figure 4.10. (Please refer to Appendix C and Appendix D for more samples of results). Five classes of movement were studied and analysed; finger rest (FR), index to thumb finger pinch (FP1), middle to thumb finger pinch (FP2), ring to thumb finger pinch (FP3), and pinky to thumb finger pinch (FP4). Based on the obtained results, all features were examined to find the optimal feature that will be used in joint angle estimations. Similar discriminative patterns were obtained by RMS, MAV and IEMG feature values extracted for four medial fingers with poor class separability as shown in Figure 4.9 (a), (b) and (c). The scatter of feature values obtained by WL showed good class separability with minimum overlapping between classes.

Patterns orders observed for all four features were similar with arrangement of feature values (from smallest to the largest value) as FP3, FP1, FP2, FP4 and FR as shown in Figures 4.10(a) to 4.10(d). However, the scatter plot for WL showed better class separability when compared to the other three classes. Similar patterns were also observed for features extracted at 40% of MVC pinching strength for four medial fingers and a thumb as shown in Figure 4.11 and Figure 4.12.

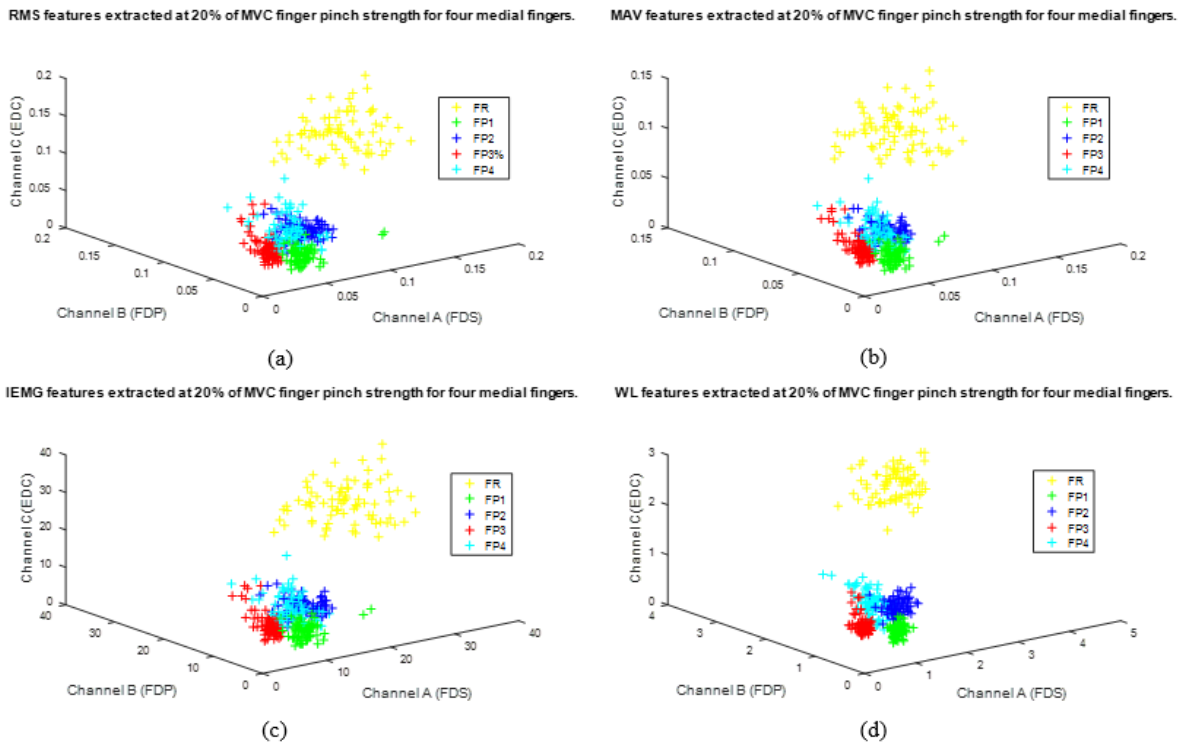


Figure 4.9: Features extracted (from FDS, FDP and EDC muscles) at 20% of MVC finger pinch strength for four medial fingers (a) RMS (b) MAV (c) IEMG (d) WL

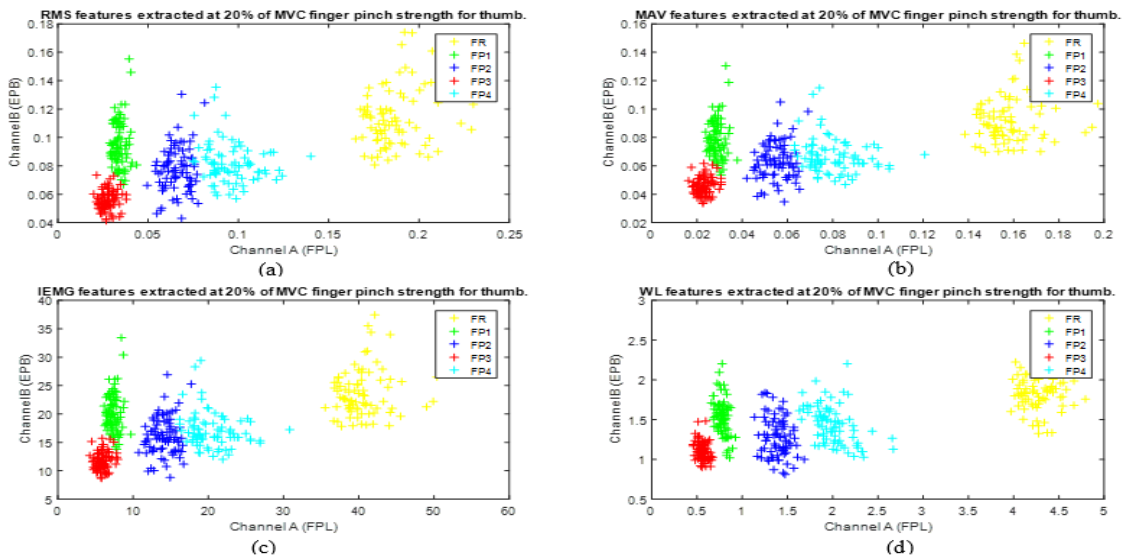


Figure 4.10: Features extracted (from FPL and EPB muscles) at 20% of MVC finger pinch strength for a thumb (a) RMS (b) MAV (c) IEMG (d) WL

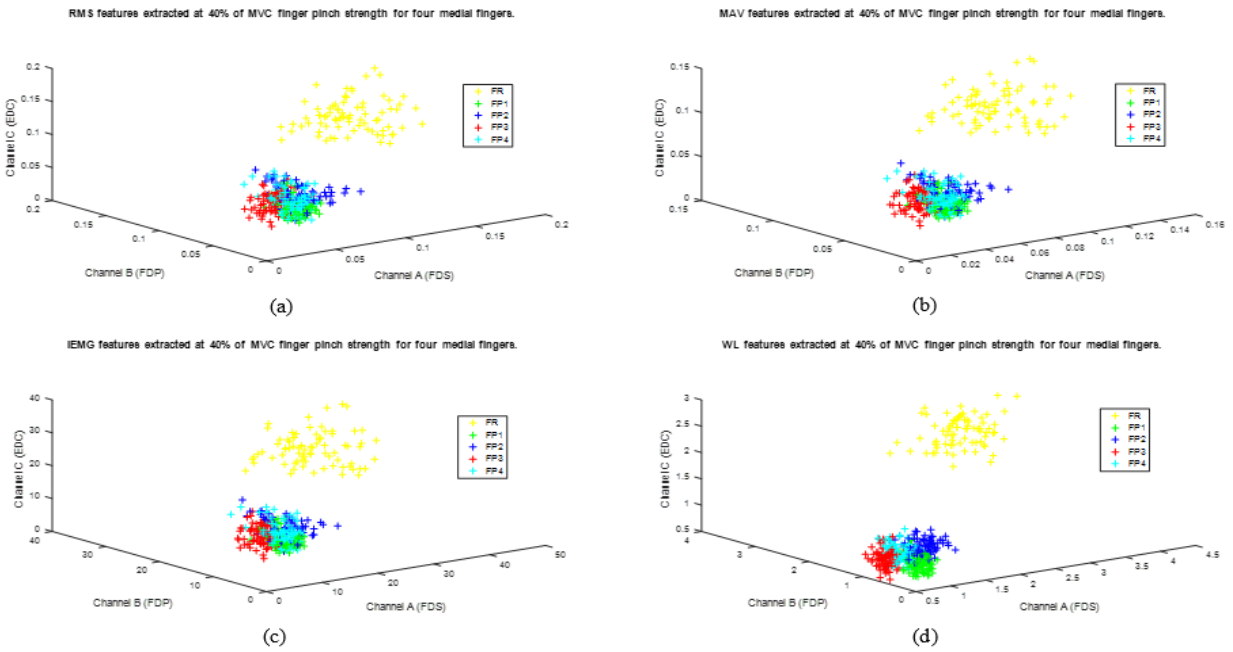


Figure 4.11: Features extracted (from FDS, FDP and EDC muscles) at 40% of MVC finger pinch strength for four medial fingers (a) RMS (b) MAV (c) IEMG (d) WL

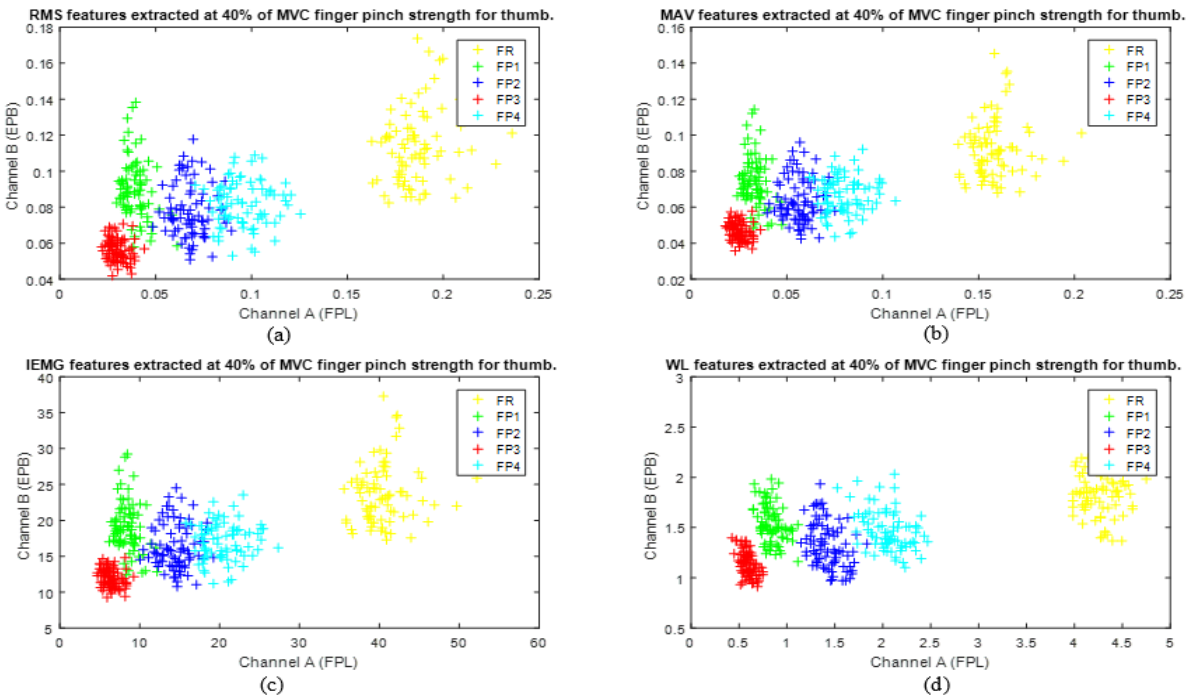


Figure 4.12: Features extracted (from FPL and EPB muscles) at 40% of MVC finger pinch strength for a thumb (a) RMS (b) MAV (c) IEMG (d) WL

4.4.3 Features for Wrist Movement

Six classes of hand movement at various wrist positions were studied and analysed; hand open at neutral (HON), hand grasping at neutral (HGN), hand open at 45-degree wrist flexion (HOF), hand grasping at 45-degree wrist flexion (HGF), hand open at 45-degree wrist extension (HOE), and hand grasping at 45-degree wrist extension (HGE). The scatter plots of the four time-domain features (RMS, MAV, IEMG and WL features) extracted at 20% of MVC grasping strength (prismatic power grips) at different wrist positions are shown in Figures 4.13, 4.14 and 4.15. (Please refer to Appendix F and Appendix G for more samples of results). Likewise, all features were examined to find the optimal feature that will be used in joint angle estimations.

In all scatter plots, the features at hand open (slight differences were noted between classes for hand open at neutral, flexion and extension wrist positions) yielded higher value features as compared to hand close. Similar to the finger movement analysis, the distribution of data in the projected space shows higher value range due to normalisation that divides the amplitude of the EMG signal during a task (hand open), with reference value represented by the maximum amplitude during the maximum voluntary contraction of the same task. When the hand is open, the muscle contraction is negligible regardless of the percentage of MVC as there are no muscle activities involved (no hand movement). Therefore, the amplitude is expected to be small throughout the task causing the normalisation to yield bigger feature value as compared to other classes.

Figure 4.13 shows the discriminative patterns for time domain features extracted from the flexion-extension muscles; FCR and ECRL muscles that are responsible for the flexion and extension of the wrist. Based on the obtained results, the scatter plot for WL feature showed good performance with small variation between features within the same class of movements whereas the RMS, MAV and IEMG features presented similar pattern with poor class separability.

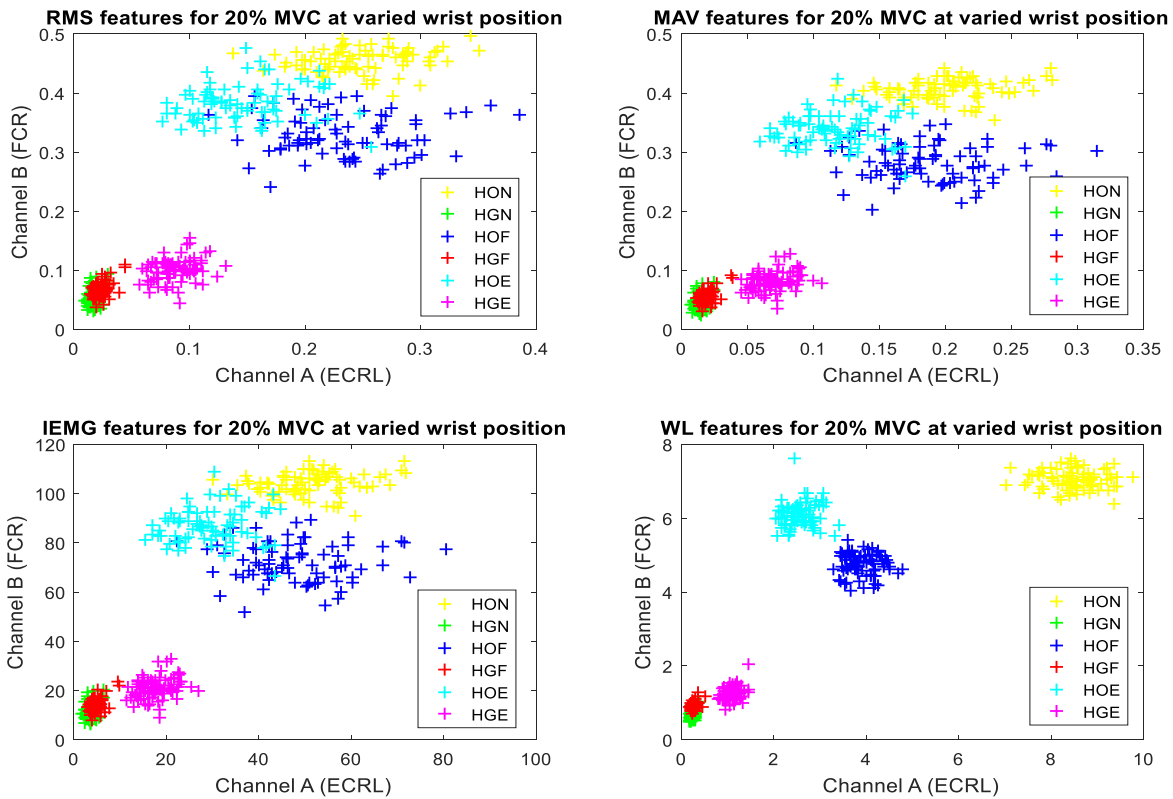


Figure 4.13: Features extracted from flexion-extension muscles (ECRL and FCR muscles) at 20% of MVC for handgrip strength at wrist positions with prismatic power grip (adducted thumb)

The same observation was obtained for flexion muscles (the FDS and FCR muscles) plot and extension muscles (the EDC and ECRL muscles) plot as illustrated in Figures 4.14 and 4.15 respectively. The same findings were obtained by Phinyomark et. al (2012) in their research that studied thirty-seven time-domain and frequency-domain features for six classes of movement, namely hand open, hand close, wrist extension, wrist flexion, forearm pronation and forearm supination. The WL feature was recommended for use as the optimal feature representing the time-domain feature group employing MAV, RMS IEMG and several more features.

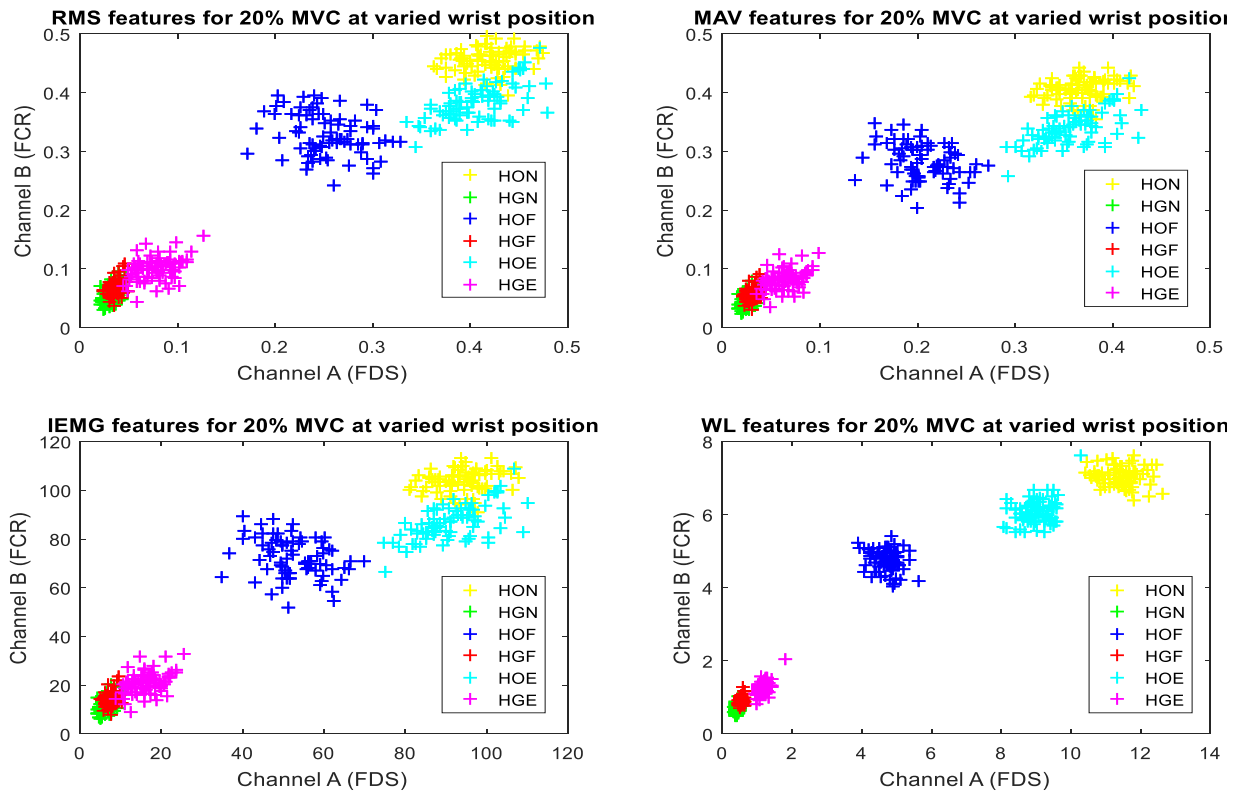


Figure 4.14: Features extracted from flexion muscles (FDS and FCR muscles) at 20% of MVC for handgrip strength at wrist positions with prismatic power grip (adducted thumb)

In terms of pattern orders, different results are expected to have slight change in the pattern orders between the flexion-extension movements depending on the prominent muscles used. Based in the obtained results, the pattern orders observed in flexion muscles plots for all four features were similar with arrangement of feature values (from smallest to the largest value) as HGN, HGF, HGE, HOF, HOE, and HON. However, the scatter plot for WL showed better class separability when compared with the other three classes. Slight change was observed in the pattern orders for extension muscles plot with arrangement of feature values (from smallest to the largest value) as HGF, HGN, HGE, HOE, HOF, and HON as shown in Figure 4.15.

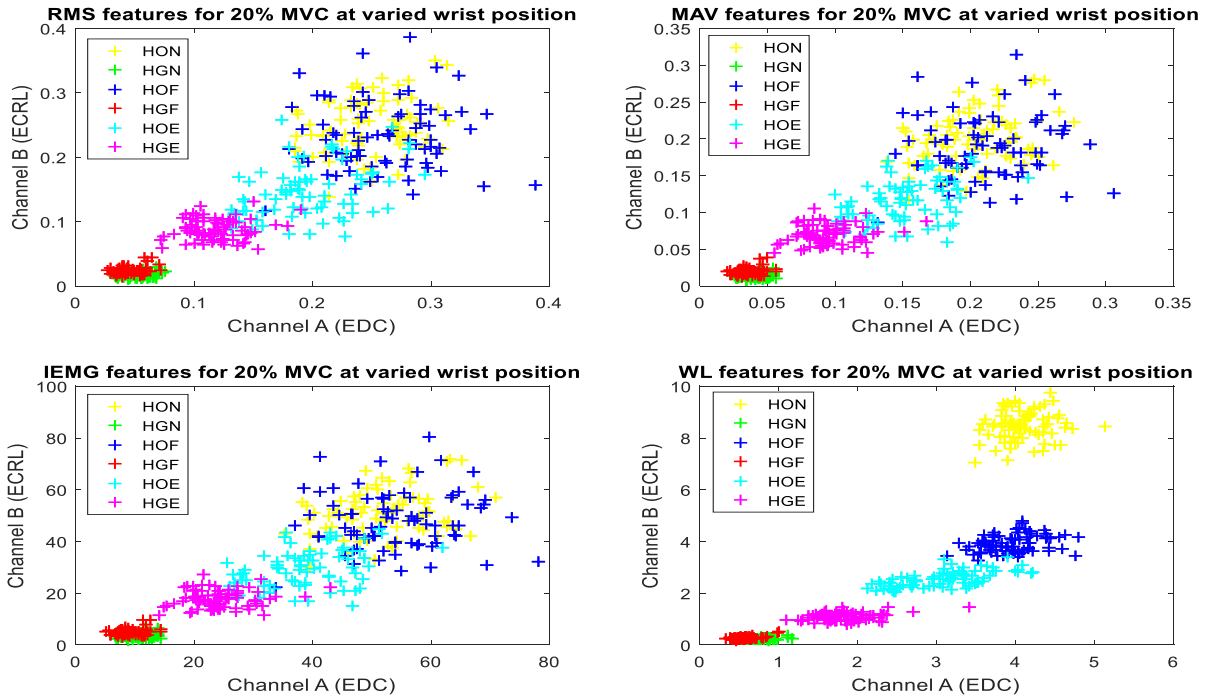


Figure 4.15: Features extracted from extension muscles (EDC and ECRL muscles) at 20% of MVC for handgrip strength at wrist positions with prismatic power grip (adducted thumb)

4.4.4 Performance Analysis for Feature Selections

The performance of the RMS, MAV, IEMG and WL features are analysed and the best features at different percentage of MVC with significant class separability is selected for joint angles estimation. Visual observation together with two statistical approaches were employed in the analysis; the standard deviation is used to select the data with appropriate finger pinches and handgrip strength, while the ANOVA test is used to select the best features with significant class separability. The standard deviation is computed to measure the variation of the feature values between different finger pinches and handgrip strength (at 20%, 40%, 60%, 80% and 100% of MVC). Features with lower standard deviation value show that most of the feature values are very close to the average in a specific feature vector. Predicting the handgrip force would require all of the data to be analysed, but not for joint angle estimations where specific percentage of MVC should be sufficient as the same method can be easily replicate to analyse different dataset in future.

Table 4.4 shows the standard deviation computed for the index to thumb finger pinches at different percentage of MVC for 5 different muscles. Smaller deviation is observed for the features that belong to the 20% of MVC classes as highlighted in bold. This suggests that the features in this class are recommended to be further analysed to choose the optimal feature for use in finger/wrist joint angle estimation. Please refer to Appendix E for more sample data (different finger pinches).

Table 4.4: The standard deviation computed for the index to thumb pinch (FP1)

Feature	Muscles	Standard deviation values				
		20% of MVC	40% of MVC	60% of MVC	80% of MVC	100% of MVC
RMS	FDS	0.0115	0.0062	0.0139	0.0197	0.0187
	FDP	0.0047	0.0092	0.0213	0.0204	0.0229
	EDC	0.0076	0.0107	0.0139	0.0156	0.0207
	FPL	0.0032	0.0060	0.0066	0.0207	0.0368
	EPB	0.0165	0.0165	0.0181	0.0194	0.0182
MAV	FDS	0.0074	0.0052	0.0095	0.0144	0.0126
	FDP	0.0039	0.0072	0.0171	0.0170	0.0184
	EDC	0.0063	0.0078	0.0104	0.0123	0.0132
	FPL	0.0027	0.0050	0.0058	0.0153	0.0302
	EPB	0.0137	0.0135	0.0143	0.0151	0.0145
IEMG	FDS	1.9009	1.3236	2.4298	3.6853	3.2184
	FDP	0.9890	1.8378	4.3677	4.3563	4.7075
	EDC	1.6203	2.0040	2.6676	3.1512	3.3872
	FPL	0.6793	1.2706	1.4800	3.9162	7.7377
	EPB	3.5056	3.4676	3.6596	3.8666	3.7036
WL	FDS	0.0841	0.1002	0.1818	0.2846	0.2821
	FDP	0.0412	0.1333	0.3260	0.3779	0.4293
	EDC	0.1080	0.1227	0.1959	0.2718	0.3126
	FPL	0.0542	0.1047	0.1292	0.2369	0.5166
	EPB	0.2269	0.1888	0.2234	0.3330	0.3068

ANOVA is utilized to demonstrate the statistical significance of the features with the most separable classes. It is a hypothesis test to compare the means of more than two populations. One-way ANOVA with a single factor is designed completely randomized by setting the null (H_0) and the alternative (H_a) hypothesis as

$$H_0 : \mu_1 = \mu_2 = \mu_3 = \mu_4 \quad (4.7)$$

$$H_a : \text{At least two treatment means differ} \quad (4.8)$$

The test statistic (F) was then calculated using

$$F = \frac{\text{variance between the treatments}}{\text{variance within the samples}} \quad (4.9)$$

In designing the ANOVA, the dependent variable is set to be the EMG features generated, in this case the four treatments are RMS, MAV, IEMG and WL methods, while the finger pinch is set as the independent variable with ‘FR’, ‘FP1’, ‘FP2’, ‘FP3’, and ‘FP4’ as the level of independence variables. Table 4.5 shows the summary for ANOVA test between the four treatments; the time domain EMG features with $\alpha=0.05$ for each finger pattern. The summary includes the number of data, sum, average and variance for each data groups that are used in the analysis.

Table 4.5: The summary of data used in the ANOVA test

<i>Finger Pinch Pattern</i>	<i>Groups</i>	<i>Count</i>	<i>Sum</i>	<i>Average</i>	<i>Variance</i>
Finger at rest (FR)	RMS features	390	108.58	0.28	0.01
	MAV features	390	92.76	0.24	0.01
	IEMG features	390	23746.91	60.89	741.44
	WL features	390	1454.87	3.73	2.64
Index to thumb finger pinch (FP1)	RMS features	390	27.60	0.07	0.00
	MAV features	390	23.09	0.06	0.00
	IEMG features	390	5910.96	15.16	75.16
	WL features	390	325.83	0.84	0.18
Middle to thumb finger pinch (FP2)	RMS features	390	31.79	0.08	0.00
	MAV features	390	26.13	0.07	0.00
	IEMG features	390	6689.71	17.15	19.14
	WL features	390	377.19	0.97	0.04

Ring to thumb finger pinch (FP3)	RMS features	390	24.16	0.06	0.00
	MAV features	390	20.11	0.05	0.00
	IEMG features	390	5147.07	13.20	40.94
	WL features	390	287.86	0.74	0.12
Pinky to thumb finger pinch (FP4)	RMS features	390	25.93	0.07	0.00
	MAV features	390	21.43	0.05	0.00
	IEMG features	390	5487.30	14.07	49.39
	WL features	390	320.78	0.82	0.11

Table 4.6 show the results for the ANOVA test. Based on the table, the generated F value for each finger pattern are higher than F critical and considering the $\alpha=0.05$ that were set for each finger pattern, it can be concluded that the p-value generated are lower than the set p-value ($p < 0.05$). Therefore, it can be concluded that the null hypothesis (no difference) for the assumption of homogeneity of variance can be rejected and that there is a significant difference between the two treatment groups.

Table 4.6: The results for ANOVA test

<i>Finger Pinch Pattern</i>	<i>Source of Variation</i>	<i>SS</i>	<i>df</i>	<i>MS</i>	<i>F</i>	<i>P-value</i>	<i>F crit</i>
Finger at rest (FR)	Between Groups	1037751	3	345917.1	1859.5	1E-262	2.61
	Within Groups	289456.2	1556	186.0			
	Total	1327207	1559				
Index to thumb finger pinch (FP1)	Between Groups	64522.72	3	21507.6	1141.8	8.15E-239	2.61
	Within Groups	29309.28	1556	18.8			
	Total	93832	1559				
Middle to thumb finger pinch (FP2)	Between Groups	82577.98	3	27526.0	5739.9	6.3E-233	2.61
	Within Groups	7461.856	1556	4.8			
	Total	90039.84	1559				
Ring to thumb finger pinch (FP3)	Between Groups	48899.45	3	16299.8	1588.1	1.1E-205	2.61
	Within Groups	15970.59	1556	10.3			
	Total	64870.04	1559				
Pinky to thumb finger pinch (FP4)	Between Groups	55494.61	3	18498.2	1494.7	1.7E-237	2.61
	Within Groups	19256.42	1556	12.4			
	Total	74751.03	1559				

Even though the null hypothesis is rejected, it is difficult to determine which group of treatments that have means that are significantly different from each other. If based on ANOVA test alone, the results computed a general statement without clearly highlighting the significant features that can be used for further analysis. Therefore, a statistical test is computed to determine which pairwise group of features are significant. Tukey-Kramer test compares the means of each treatment and identifies any significant differences between the group of treatments. The Tukey-Kramer procedure was performed for six-factor levels to select the best features amongst four features and the result is shown in Table 4.7. The wavelength feature pair shows significantly different means (when WL feature paired with any features, the means are significantly different), which suggest to be the dominant or the best feature.

Table 4.7: Tukey-Kramer significance test

<i>Finger Pinch Pattern</i>	<i>Comparison</i>	<i>Absolute Difference</i>	<i>Critical range</i>	<i>Results</i>
Finger at rest (FR)	WL to RMS	3.450	2.510	Means significantly different
	WL to MAV	3.490	2.510	Means significantly different
	WL to IEMG	57.16	2.510	Means significantly different
	RMS to MAV	0.040	2.510	Not significantly different
	RMS to IEMG	60.61	2.510	Means significantly different
	MAV to IEMG	60.65	2.510	Means significantly different
Index to thumb finger pinch (FP1)	WL to RMS	0.765	0.798	Not significantly different
	WL to MAV	0.776	0.798	Not significantly different
	WL to IEMG	14.321	0.798	Means significantly different
	RMS to MAV	0.079	0.798	Not significantly different
	RMS to IEMG	0.035	0.798	Not significantly different
	MAV to IEMG	0.044	0.798	Not significantly different
Middle to thumb finger pinch (FP2)	WL to RMS	0.8856	0.403	Means significantly different
	WL to MAV	0.9001	0.403	Means significantly different
	WL to IEMG	16.1860	0.403	Means significantly different
	RMS to MAV	0.0145	0.403	Not significantly different
	RMS to IEMG	17.0716	0.403	Means significantly different
	MAV to IEMG	17.0861	0.403	Means significantly different

The multi-comparison test was conducted on all grip pattern, but only three finger pinches were included in the table as the results were repeated (similar for the other grip pattern). Overall, based on the visual observation and the significance test results, separable classes of features were noticed with WL as the method produced more significant features when compared to RMS, MAV

and IEMG methods. In particular, it shows that WL features appear to be the best sensing technique to represent the intention of the user. Thus, the WL features were chosen in classifying the control input.

4.5 Summary

This chapter has described the methods used in analysing the forearm EMG signals. The procedures for EMG data collection, data processing and analysis using appropriate techniques have been described for producing reliable feature datasets that can be used as the input for joint angle estimations. The features extracted have significantly presented separable classes and range that can be used as user defined input signals. Based on the visual observation, the standard deviation value, and the ANOVA test conducted, wavelength feature for 20% of MVC is recommended to be used as the representative feature and is expected to provide better estimation. It has significant class separation with small standard deviation that offer reliable and continuous input for the supervised learning methods employed in the next chapter. As previously stated, predicting the handgrip forces would require all of the data (every % of MVC) to be analysed but since this work only focussed on predicting the grip pattern, specific range of datasets are sufficient.

Chapter 5

MODELLING FRAMEWORK FOR JOINT ANGLE ESTIMATION

5.1 Introduction

Over the years, pattern recognition schemes have been extensively studied and applied to classification of hand gestures with decoding accuracies of above 90% (refer to section 2.3 for details). However, the applicability of this scheme is limited and can be used in controlled laboratory condition only. This control strategy normally uses a sequential process that activates only a single class of movement at a time, which is inadequate to actuate and control the exoskeleton hand to resemble the actual human hand. Besides, the human hand is highly articulated with a wide range of degrees of freedom. Therefore, its movements are not limited only to discrete gestures but more to continuous and coordinated gestures allowing various and complex movements. The issues pertaining to the pattern classification control approach has led to the development of proportional myoelectric control strategy with growing attention to the joint angles estimation for exoskeleton hand. The major differences between classification and regression method is that the regressor provides continuous estimated joint angle values for each DOF, allowing an independent, simultaneous and proportional estimation to be computed which facilitate a fluent and natural control (provided that good regression performance is viable).

The regression model has been used and proven useful in modelling and providing valuable predictions for decades. It can model the relationship between one or more independent variables (the input of the model) and a dependent variable (the predicted variables). However, in predicting the joint angles estimation based on EMG signals, supervised learning method is preferred over the traditional regression due to the EMG signal characteristics that is highly nonlinear and

nonparametric causing fitting the data to the regression equation difficult and weighty. The supervised learning method is adopted for its flexibility to adapt itself to the shape of the EMG data and model the complex relationship between the forearm EMG signals, various finger pinches/hand grasping and various finger/wrist joint angles.

The modelling framework for the joint angle estimation for the exoskeleton hand is discussed in this chapter. The proportional joint angles estimation based on forearm EMG signals recorded during various finger and wrist movements is explored utilizing two supervised learning approaches, namely an artificial neural network (ANN), and an adaptive neuro-fuzzy inference system (ANFIS) with subtractive clustering. All methods are trained and tested using the features selected as discussed in Chapter 4. The models developed for each finger/wrist are validated using the validation data set collected from normally limbed subjects.

5.2 Artificial Neural Network Model

Artificial Neural Networks (ANN) are renowned for function fit problems and have been extensively used for classification and regression of surface EMG signals. ANN is a computational model developed for information processing inspired by biological neural systems. Human brain comprises of biological neurons that are interconnected to one another, enabling signals transmission and acting as a tool that will process information of biological senses. The similar concept is adopted in the ANN model that consists of layers of nodes known as artificial neurons that have the characteristics of transmission and reception of information. The artificial neuron will receive a signal and process it before signals an additional artificial neuron connected to it. It plays an essential role in defining the function and operation of the network.

The connections of neurons in the network will form a layer patter and determine the type of the ANN architecture; either feed-forward or feedback neural network. The example of a feed-forward neural network model as illustrated in Figure 5.1 comprises an input layer that is connected to a hidden layer and an output layer by a set of connection weights. It does not have a feedback link and allows the signals to move in one direction only. Hence, the output of each layer will not affect the previous layer.

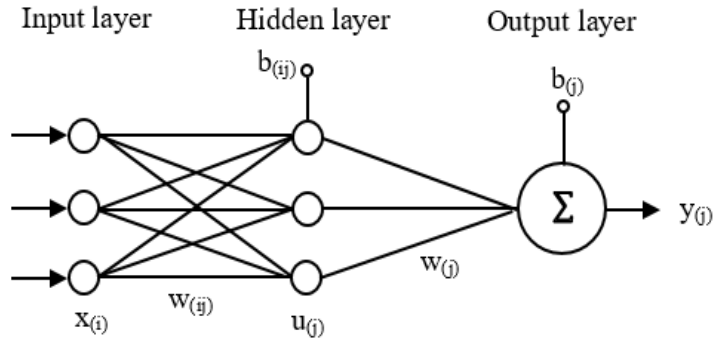


Figure 5.1: The example of a feed-forward neural network with 3 input neurons, 3 hidden neurons and one output neuron

In general, the feed-forward network often has one or more hidden layers (sigmoid neurons) followed by an output layer (linear neuron). The multiple layers of tangent-sigmoid neurons allow the network to learn nonlinear relationships between the input and output vectors while the linear output layer is used to approximate the function in solving the nonlinear regression problems.

The mathematical model of the network can be represented as follows:

$$u_j = \sum_{i=1}^R w_{ij}x_i + b_{ij} \quad (5.1)$$

$$y_j = \sum_{j=1}^S w_j u_j + b_j \quad (5.2)$$

where R is the number of inputs, S is the number of the hidden neurons, $u_{(j)}$ is the output value of the hidden neurons and $y_{(j)}$ is the output of the adder function neuron model with $x_{(i)}$ as the i th input, $w_{(ij)}$ and $w_{(j)}$ as the weight variables, and $b_{(ij)}$ and $b_{(j)}$ as the bias variables.

5.2.1 Feed-forward Neural Network with Backpropagation Algorithm

In this research, a multilayer feed-forward neural network is employed to deal with the complicated relationship between surface EMG and finger/wrist joint angles. In designing the network, the first step is to choose an appropriate learning process. There are two types of learning process that are commonly used; supervised and unsupervised learning. It depends on the information provided by the network. The supervised learning requires sample patterns that are labelled while the unsupervised learning works oppositely.

In this work, supervised learning is used by providing the network with sample of pattern of the selected time-domain features that has been categorised and labelled. Each pattern is fed to the network with a known output; the respective finger/wrist joint angles. The signal will be passed to the neurons and will continue to spread out along the network until it reaches the end layer of the neurons in the output layer before generating the output pattern and compared it with the desired output. In case of any error signals generated during the process, the network weights will be modified to correct the learning so that the actual output will be in accordance as the desired output.

Next, the learning algorithm or learning rule that is used to train the network is selected. A Levenberg-Marquardt backpropagation algorithm is used to train the neural network until it can approximate a function by associating the elements in the input matrices (time-domain features) with elements in the target matrices (finger/wrist joint angles). The Levenberg-Marquardt algorithm will adjust the weight and bias variables while the backpropagation algorithm will compute the Jacobian matrix of the performance function that will update the weights and biases, which are used by the network to further estimate the respective finger/wrist joint angles. Finally, the network is assessed to check the learning capacity, the required training sample and the learning time required to complete the estimations. The architecture of the proposed feed-forward neuron network training is illustrated in Figure 5.2.

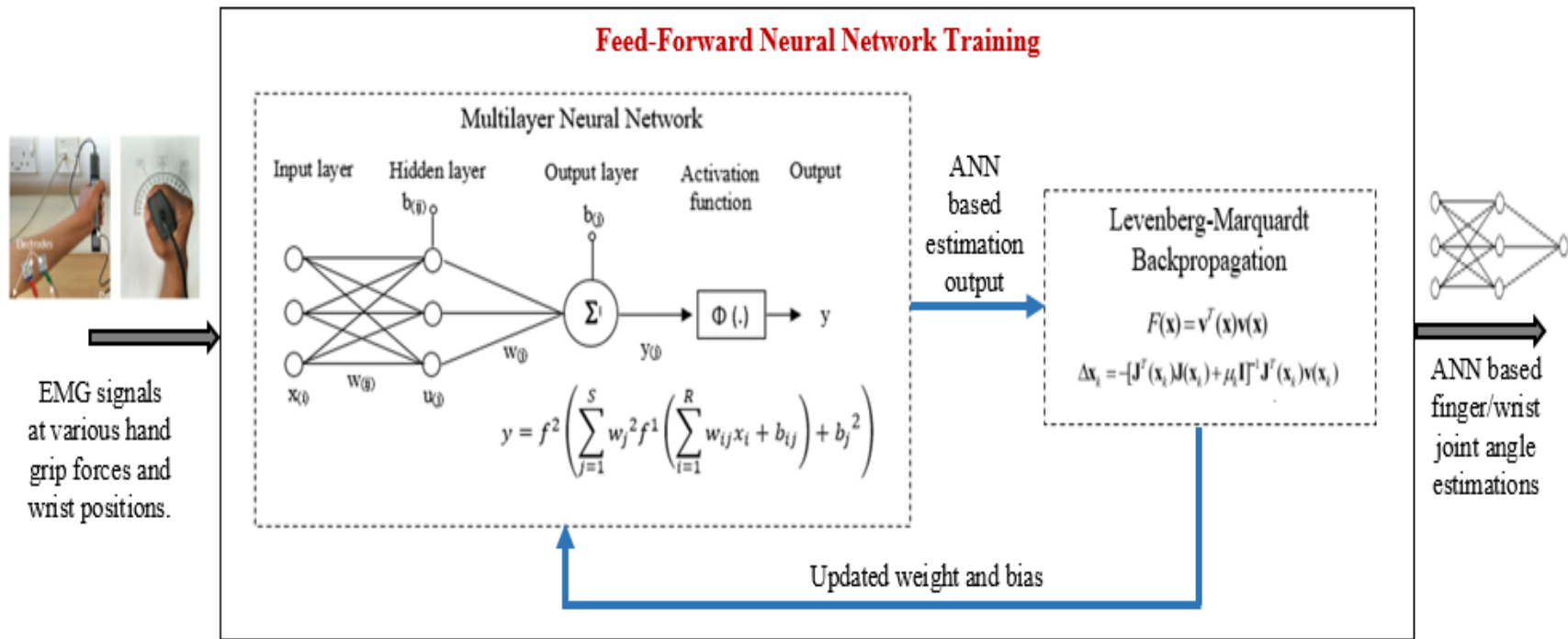


Figure 5.2: The proposed feed-forward neural network with Levenberg-Marquardt backpropagation algorithm for finger/wrist joint angle estimations. The number of input changes depend on the respective output estimation (either finger or wrist joint angles)

5.2.2 Modelling of the Finger Joint Angle

In modelling the four medial fingers and the thumb, two separate ANN models are used where each model is studied, trained and tested with different input data sets that are mapped to specific joint angle as the output. The joint angles measurement used are based on the flexion and extension of resting fingers presented by Lee et al. (2014), as mentioned in section 3.3.

The four medial fingers are modelled based on the WL features for five classes of finger movements (extracted from FDS, FDP, and EDC muscles at 20% of MVC pinching strength) that are mapped with the joint angles (DIP, PIP and MCP joints) for specific finger (index, middle, ring and pinky fingers). Whereas, the thumb is modelled based on the WL features extracted from FPL and EPB muscles for similar classes of movement that is mapped to the joint angles (DIP and MCP joints) of the thumb. Each network is modelled based on the EMG data collected from a single and multi-subjects and is trained with different number of hidden neurons depending on the complexity of the input.

Each input samples (the WL features for four medial finger and the thumb for either single or multi-subjects) were randomly divided between three sample groups; training dataset, validation dataset, and testing dataset. 70% of the input samples are used as training dataset to fit the parameters of the model where the model is trained using the chosen learning method. While, 30% of the input samples are equally divided and are used as validation and testing datasets. The validation dataset is used by the fitted model to predict the desired output and to measure the network generalization so that the training can be stopped if the generalization stops improving. The testing dataset is used to evaluate the network performance.

At first, WL features extracted from individual subject are presented to the network as the input dataset with desired target data. The network architecture for individual joint angle model consists of three-layer network; an input layer with three neurons, a tangent-sigmoid hidden layer with ten neurons and a pure linear output layer with one neuron. Figure 5.3 to Figure 5.5 show the prediction results for the mapping between WL features for five classes of movement with the DIP, PIP, and MCP joint angles.

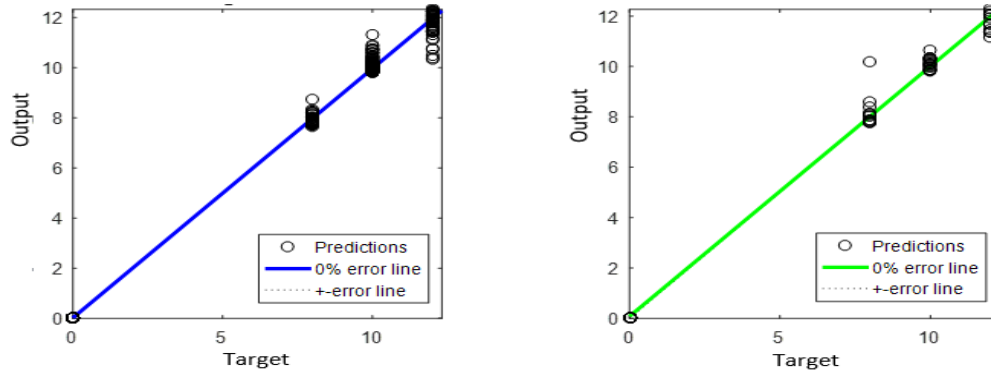


Figure 5.3: Prediction results for the DIP joint angle model (a) modelling dataset (b) validation datasets

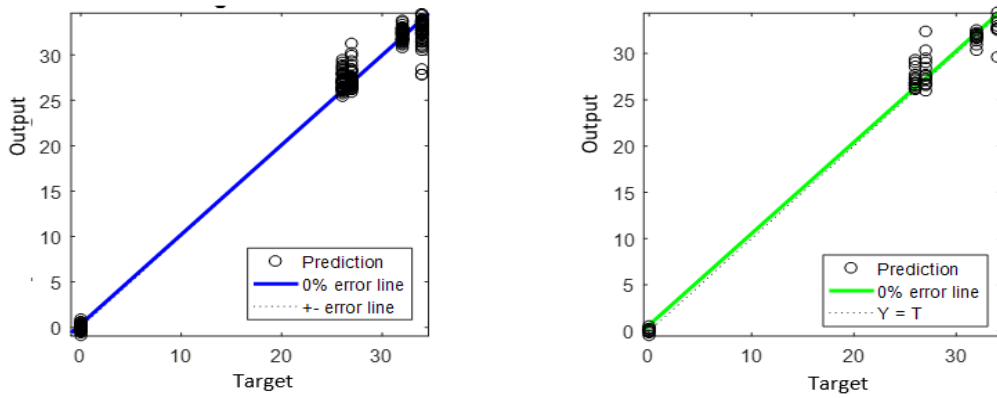


Figure 5.4: Prediction results for the PIP joint angle model (a) modelling dataset (b) validation datasets

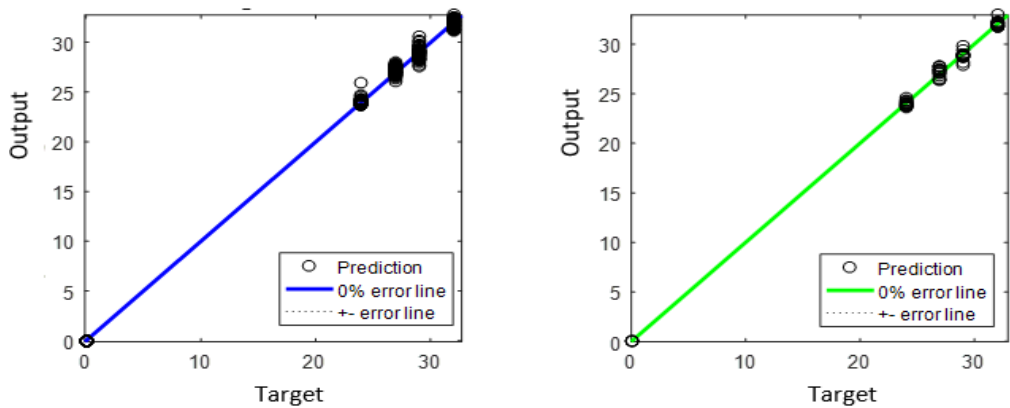


Figure 5.5: Prediction results for the MCP joint angle model (a) modelling dataset (b) validation datasets

Figure 5.3 shows four prediction groups for both modelling and validations dataset indicating that there is overlapping in predicting the DIP joint angle for two finger movements whereas Figure 5.4 and Figure 5.5 show five prediction groups that represents PIP and MCP joint estimations for five finger movements. Based on the obtained results, the DIP, PIP and MCP joint models produced acceptable mean square error (MSE) and correlation coefficient values (R) indicating small variation between the actual and estimated samples.

The DIP joint model produced MSE of 1.038 and correlation coefficient of 0.997 for training datasets and MSE of 1.552 and correlation coefficient of 0.995 for validation datasets. Meanwhile the PIP joint and MCP joint produced MSE of 1.517 and 1.554, and correlation coefficient of 0.995 and 0.994 for training datasets and MSE of 2.160 and 1.513, and correlation coefficient of 0.991 and 0.998 for validation datasets respectively. The performance index of each model is presented in Table 5.1.

Table 5.1: Performance index for the four medial finger joint models of a single subject

Test subjects	Joint angle	Datasets		No of hidden layer	Mean Square Error (MSE)	Correlation Coefficient Value
		Type	No. of sample			
Single subject	DIP joint	Training	272	10	1.038	0.997
		Validation	59		1.552	0.995
		Testing	59		6.671	0.998
	PIP joint	Training	272	10	1.517	0.995
		Validation	59		2.160	0.991
		Testing	59		1.255	0.998
	MCP joint	Training	272	10	1.554	0.994
		Validation	59		1.513	0.998
		Testing	59		5.890	0.997

Similar method was repeated using input dataset for multi-subjects to model the four medial fingers. The larger input samples are used to produce adaptation on the overall joint angle estimation network. The architecture of the neural network consists of three-layer network; an input layer with three neurons, a tangent-sigmoid hidden layer with ten neurons and a pure linear output layer with one neuron. The network for PIP joint angle was adjusted by adding more hidden layers to yield smaller MSE. The example of prediction results for training and validation datasets are shown in Figure 5.6. The joint angle estimations for the DIP, PIP, and MCP joints are

combined using a single ANN network. Overall, the DIP model yielded smaller MSE for training and validation datasets, while PIP and MCP models produced acceptable MSE values. The performance index of the model is presented in Table 5.2.

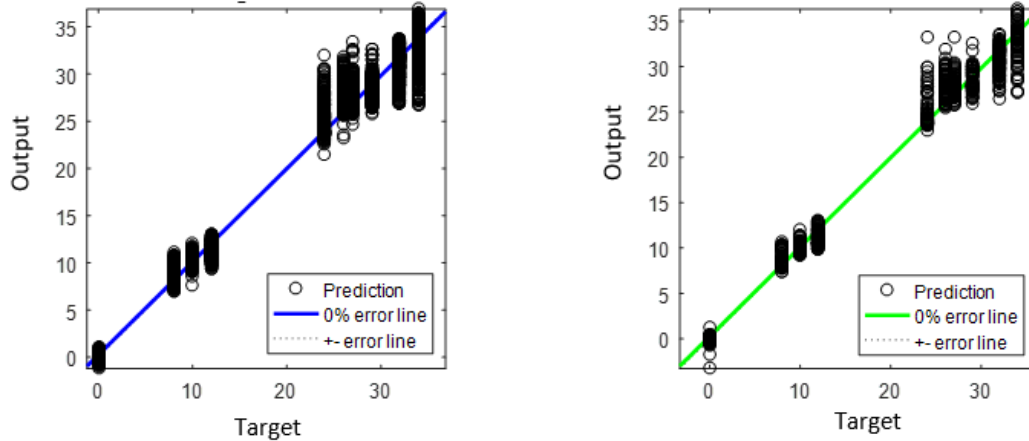


Figure 5.6: Prediction results for the DIP, PIP and MCP joint angle model for multi-subjects
(a) modelling dataset (b) validation datasets

Table 5.2: Performance index for the four medial finger joint models of multi-subjects

Test subjects	Joint angle	Datasets		No of hidden layer	Mean Square Error (MSE)	Correlation Coefficient Value
		Type	No. of sample			
Multi subjects	DIP joint	Training	1638	10	0.322	0.990
		Validation	351		0.335	0.998
		Testing	351		0.561	0.994
	PIP joint	Training	1638	10	2.884	0.903
		Validation	351		3.498	0.988
		Testing	351		2.384	0.923
	PIP joint	Training	1638	15	2.615	0.914
		Validation	351		2.345	0.909
		Testing	351		2.982	0.903
	MCP joint	Training	1638	10	1.673	0.935
		Validation	351		1.712	0.940
		Testing	351		3.005	0.988
DIP, PIP & MCP joint	Training	1638	10	1.997	0.993	
	Validation	351		2.196	0.992	
	Testing	351		1.740	0.994	

5.2.3 Modelling of the Wrist Joint Angle

Modelling the wrist joint angle requires only a single ANN model that takes four inputs and two outputs. The input samples are the WL features extracted from FCR, FDS, ECRL and EDC muscles at 20% of MVC grasping strength at different wrist positions; neutral, flexion and extension. It is mapped to the grasping and wrist joint angles based on the flexion and extension of resting wrist presented by Lee et al. (2014). The network architecture for the wrist joint angle model consists of three-layer network; an input layer with four neurons, a tangent-sigmoid hidden layer with ten neurons and a pure linear output layer with two neuron.

Figure 5.7 and Figure 5.8 presented the prediction results for the wrist joint angles for six class of movements; hand open at wrist neutral, wrist flexion and wrist extension, and hand grasping at wrist neutral, wrist flexion and wrist extension. The obtained results shows similar pattern for both modelling and validation datasets with six prediction groups.

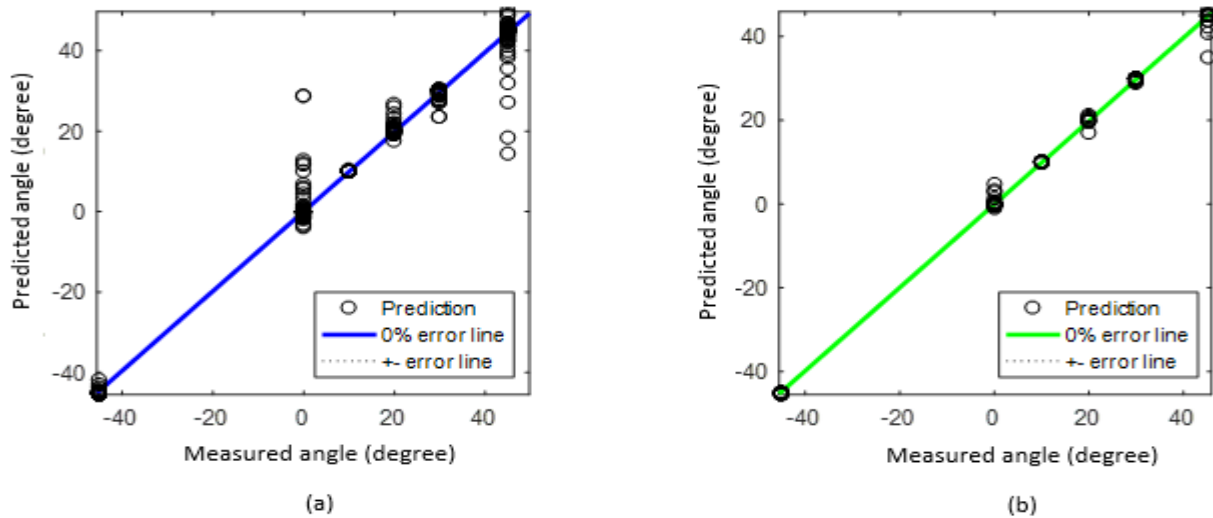


Figure 5.7: Prediction results for the wrist joint angle model for single subject (a) modelling dataset (b) validation datasets

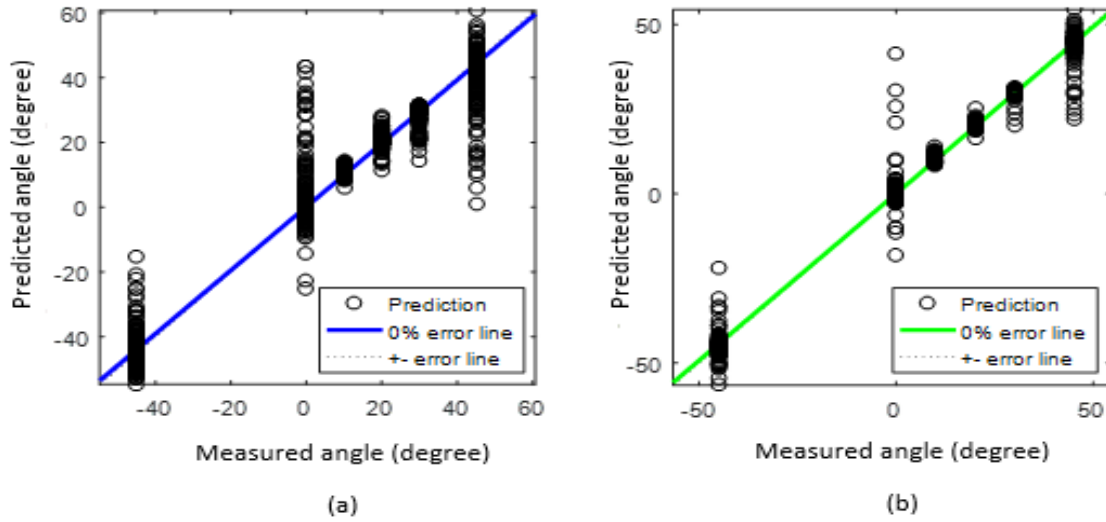


Figure 5.8: Prediction results for the wrist joint angle model for multi-subject (a) modelling dataset (b) validation datasets

The performance index of each model is presented in Table 5.3. The joint model for single subject produced MSE of 7.82 and correlation coefficient of 0.94 for training datasets and MSE of 1.552 and correlation coefficient of 0.995 for validation datasets. Meanwhile, for multi-subjects, the MSE are 15.11 and 13.12, with correlation coefficient of 9.90 and 9.91 for training and validation datasets respectively. The MSE value for modelling and validation datasets of multi-subjects was higher compared to single subject. It seems possible that these results are due to the pattern of the input dataset that resulted from the overlapping and poor class separability within the WL features.

Table 5.3: Performance index for the wrist angle model of single and multi-subjects

Test subjects	Datasets		No of hidden layer	Mean Square Error (MSE)	Correlation Coefficient Value
	Type	No. of sample			
Single subject	Training	328	15	7.82	9.94
	Validation	70		1.39	9.99
	Testing	70		1.67	9.98
Multi subjects	Training	1966	20	15.11	9.90
	Validation	421		13.12	9.91
	Testing	421		19.26	9.98

5.3 Artificial Neural Fuzzy Inference System Models

Fuzzy inference systems are known for their ability to deal with ill-defined and nonlinear system that is difficult to model and solve analytically using conventional mathematical tools. A fuzzy inference system (FIS) consists of interpretable linguistic rule base (fuzzy if-then rule), fuzzy set membership functions, and fuzzy logic operators that can qualitatively model human knowledge and reasoning processes into decision-making. The fuzzy inference process involves three basic steps; fuzzification that translates crisp inputs into a truth table, rule evaluation that computes output truth-value and defuzzification that transfers the truth values into crisp output.

The functional block of FIS is illustrated in Figure 5.9. It comprises of five functional blocks, namely rule base, database, decision-making unit, fuzzification and defuzzification interface units. The rule base contains fuzzy if-then rules, and is often associated with the database, which defines the membership functions of fuzzy sets used in the fuzzy rules. Both are referred to as knowledge base and are very important for the decision-making.

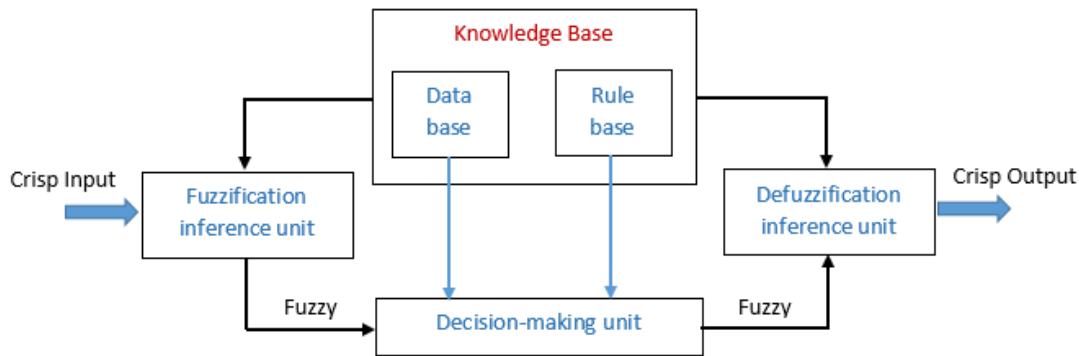


Figure 5.9: The fuzzy inference system

In this work, the fuzzy rule is extracted based on sugeno-type fuzzy model that determines the output as a constant or linear term (normally the output is determines as a fuzzy set). First, the decision points are found based on the WL features selected from the respective muscles. Then, the ranges used to distinguish every level of the input data are defined. Finally, the fuzzy rule extracted by sorting the data points based on their importance is done. The number of rules set for each model is depends on the number of inputs and the number of linguistic variables assigned to each input. The standard fuzzy-if-then rules are applied (for example, the two fuzzy rules):

If x is A_1 and y is B_1 , then $f_1 = a_1x + b_1y + c_1$.

If x is A_2 and y is B_2 , then $f_2 = a_2x + b_2y + c_2$.

where x and y are the inputs with membership functions defined as A_1, A_2, B_1, B_2 , while $a_1, a_2, b_1, b_2, c_1, c_2$, are the output parameters.

In the FIS model, there is no defined method to acquire the knowledge to build the fuzzy rule, and tuning the parameters in the membership functions is often challenging and requires a lot of effort. To address this limitation, ANN that has a higher learning capability is combined with the FIS to automatically adjust the membership functions and reduce the error in formulating the fuzzy rules so that the readability and learning ability can be effectively achieved in parallel. The combination of the ANN and fuzzy logic forms neuro-fuzzy system or simply called as ANFIS and it was first introduced by Jang (1993).

The basic architecture of ANFIS consists of 5 layers with specific node types; a square (adaptive) node has parameter while circle (fixed node) has none, as illustrated in Figure 5.10.

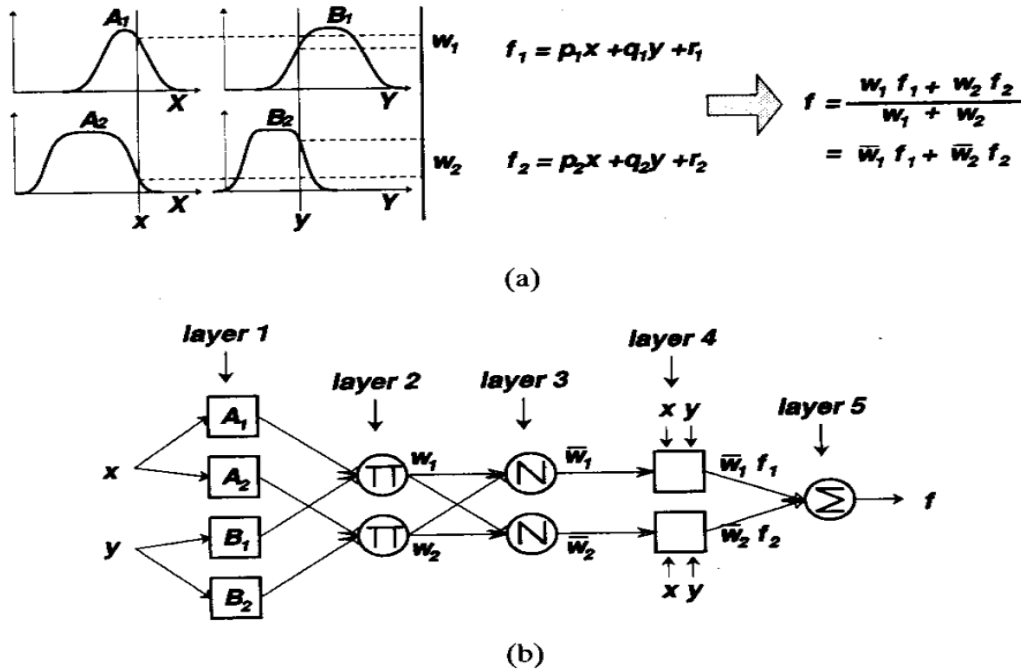


Figure 5.10: (a) Type-3 fuzzy reasoning and (b) Equivalent ANFIS (Jang, 1993)

Details of the layers are as follows:

- Layer 1 - The fuzzification layer. Each node in this layer is an adaptive node, and adapts to a function parameter (premise parameters). Its output is in terms of membership value that is given by the input of the membership functions.
- Layer 2 - The rule layer. Each node in this layer is a fixed node, and provides firing strength of the rule. Each node multiplies the incoming signal in producing the output.
- Layer 3 - The normalisation layer. Each node in this layer is a fixed node, and works as normalised firing strength node that calculates the ratio of the rule's firing strength to the sum of all rule's firing strengths.
- Layer 4 - The defuzzification layer. Each node in this layer is an adaptive node, and adapts to a function parameter (consequent parameters). It provides a product operation between the normalised firing strength and the corresponding rule.
- Layer 5 - The output layer. Each node in this layer is fixed node, and sums up all the incoming inputs.

5.3.1 ANFIS with Hybrid Learning and Subtractive Clustering

In this work, the ANFIS architecture employed for finger/wrist joint angle estimation is based on an adaptive network that uses supervised learning that adopts Takagi-Sugeno fuzzy model. The output of each rule is a linear combination of the inputs and a constant term that is weighted average to produce the final output. The adaptive learning is based on a hybrid back propagation and least-mean-square algorithm. Through the learning process, the parameters in the membership functions are changed and adjusted using a gradient vector that measures how well the FIS is modelling the input/output data based on the given parameters. Here, the hybrid-learning algorithm is applied to optimize and adjust the parameters to reduce the error. The hybrid algorithm is chosen to overcome the drawback of back propagation that has slow convergence with tendency of being stuck in local minima during the training process.

To further improve the ANFIS model, clustering technique is used to optimize the fuzzy data sets. In the fuzzy system, each data point has a certain membership grade associated with specific

patterns that can provide a concise representation of behaviour or characteristics. Partitioning the input datasets into a degree of membership functions usually requires experience and takes a long time. It can be achieved by applying clustering techniques to improve the performance and interpretability of the fuzzy model as well as reduce the development time. Fuzzy clustering will divide the data space into fuzzy clusters that represent a particular system behaviour to determine its membership function.

In this research, a subtractive clustering technique is used to automatically determined and optimise the fuzzy sets. It is an unsupervised clustering technique that requires no pre-defined reference for the vectors. The subtractive clustering is applied to a Takagi-Sugeno FIS model and resolves the growing dimension issues by using a data point (instead of grid point as used in grid partition method) as a potential centre of the cluster. It is able to yield a quick cluster estimation and is more consistent than the fuzzy C-Means clustering method.

The applied subtractive clustering method is based on the method proposed by Chiu (1994). Considering a collection of n wavelength feature points $\{wl_1, wl_2, \dots, wl_n\}$ in an M dimensional space. Each data point is assumed to be normalised in each dimension making the coordinate ranges in each dimension to be equal. Considering each data point as a potential cluster centre, a density measure of data point wl_i is defined as:

$$P_i = \sum_{j=1}^n \exp \left[-\frac{\|wl_i - wl_j\|^2}{\left(\frac{r_a}{2}\right)^2} \right] \quad (5.3)$$

where r_a is a neighborhood radius in which data outside this radius will have little influence on the potential data. The data point with the highest potential is selected as the first potential cluster with wl_{ci} as the location of the first cluster and P_{ci} as the potential value. The potential value is revised and defined as:

$$P_i = P_i - P_{ci}^* \exp \left[-\frac{\|wl_i - wl_j\|^2}{\left(\frac{r_b}{2}\right)^2} \right] \quad (5.4)$$

where r_b is a neighborhood radius that has measureable reduction in density. The process is repeated until $P_{ck} < \epsilon P_{ci}$ with ϵ as a small fraction.

5.3.2 Modelling of the Finger Joint Angle

In modelling the finger joint angle, three ANFIS models were independently trained, validated and tested for each finger joints; the DIP, PIP, and MCP joints. The fuzzy rules employed were based on the input data that were substantively clustered using subtractive clustering technique. Each model consists of five fuzzy rules with three inputs and a single output, which are:

If in1 is in cluster1 and in2 in cluster1 and in3 is in cluster1, then Out1 is outputcluster1.

If in1 is in cluster2 and in2 in cluster2 and in3 is in cluster2, then Out2 is outputcluster2.

If in1 is in cluster3 and in2 in cluster3 and in3 is in cluster3, then Out3 is outputcluster3.

If in1 is in cluster4 and in2 in cluster4 and in3 is in cluster4, then Out4 is outputcluster4.

If in1 is in cluster5 and in2 in cluster5 and in3 is in cluster5, then Out5 is outputcluster5.

where in1, in2 and in3 are the inputs (WL features extracted from FDS, FDP and EDC muscles respectively), while cluster1, cluster2, cluster3, cluster4, cluster5 are the membership functions based on the finger pinches FR, FP1, FP2, FP3, and FP4. The out1, out2, out3, out4, out5 are the output with parameters that were clustered based on the joint angles for respective joint and finger pinches (ie DIP joint for FR1, FP1, FP2, FP3 and FP4).

The prediction results for the DIP, PIP and MCP joints angle using ANFIS subtractive clustering model are shown in Figures 5.11 to Figure 5.13. As noted in the Figure 5.11, the DIP joint estimations produced acceptable prediction errors when tested using different target datasets. The DIP joint angle ranges between 8 to 12 degrees with overlapping joint angle output denoted at 10 degree for FP1 and FP2 (as highlighted in the dotted-line box). Meanwhile, based on Figure 5.12 and Figure 5.13, the PIP and MCP joint estimations produced acceptable prediction errors when tested using different target datasets.

The results confirmed that with proper input datasets, the ANFIS models are capable of predicting the respective joint angles for different finger movements. The overlapping between FP1 and FP2 can be avoided if more distinguished joint angle are used to define the output range

for different finger pinches. Biologically, the DIP, PIP and MCP joint angles between four medial fingers during finger pinching and/or hand grasping are quite similar, therefore, precise measurements are needed.

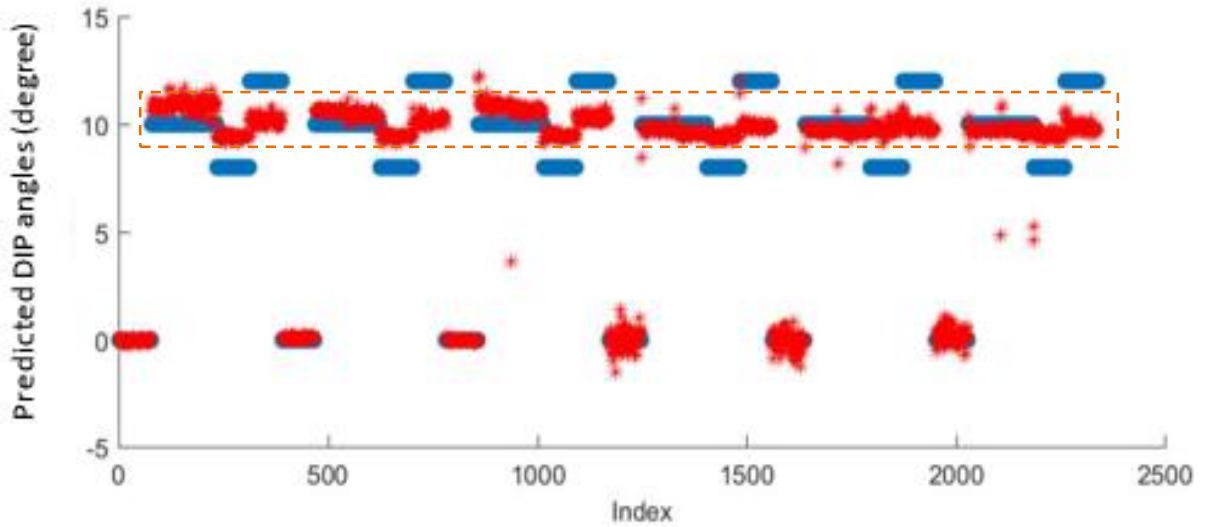


Figure 5.11: The prediction results for DIP joint estimations using ANFIS subtractive clustering model

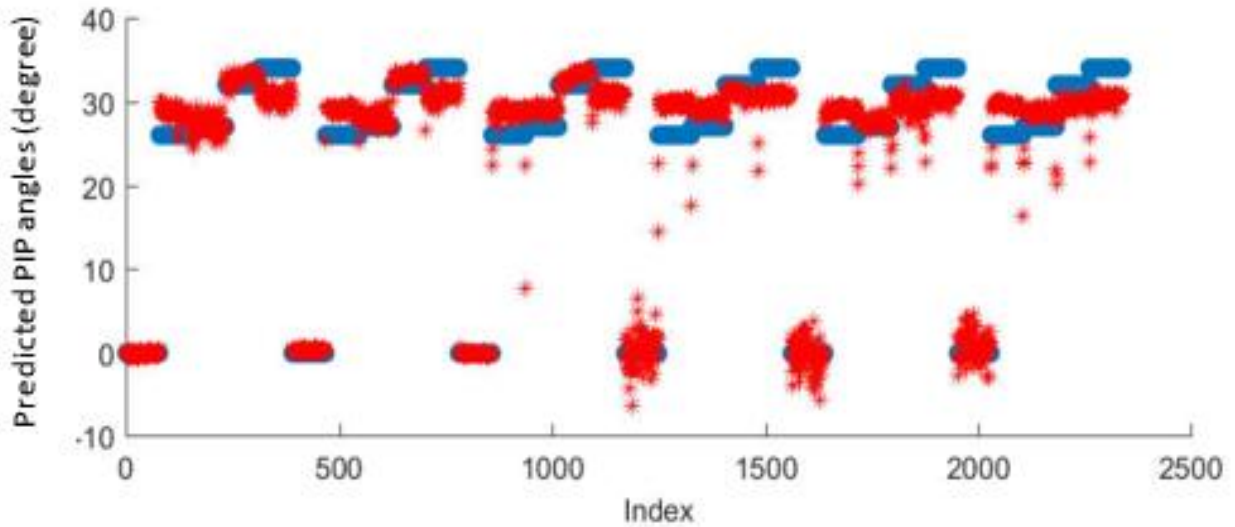


Figure 5.12: The prediction results for PIP joint estimations using ANFIS subtractive clustering model

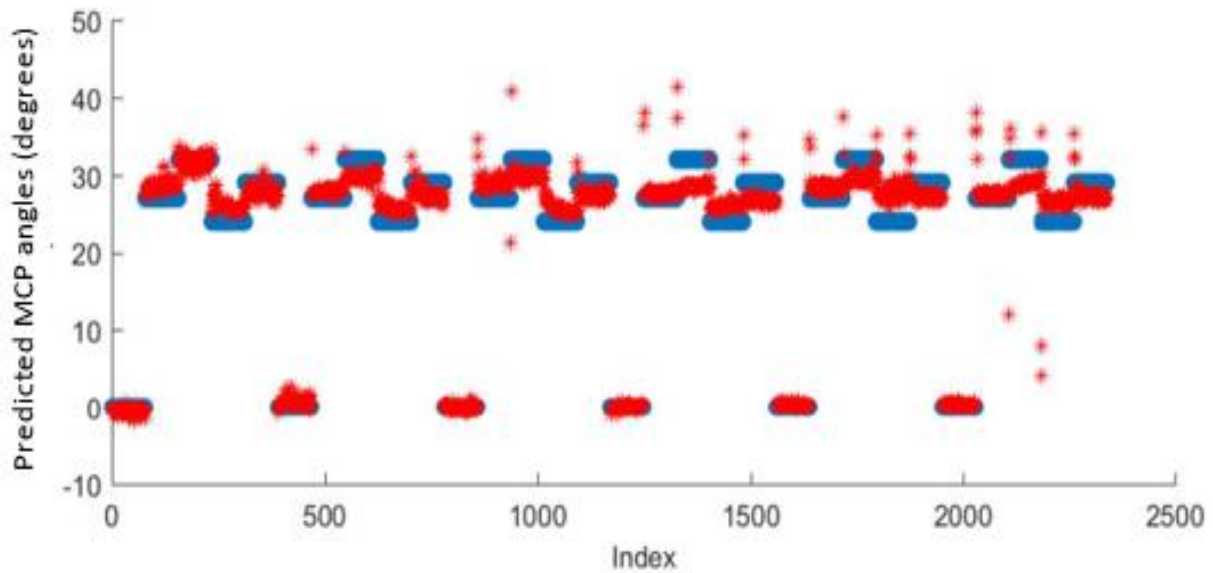


Figure 5.13: The prediction results for MCP joint estimations using ANFIS subtractive clustering model

5.3.3 Modelling of the Wrist Joint Angle

A similar method was employed to model the wrist joint angles. A single ANFIS model was trained, validated, and tested based on the input data that were clustered following to the defined hand grasping movements; hand open and hand grasping at different wrist positions (neutral, flexion and extension). The fuzzy rule used are based on the WL features extracted from four muscles (FDS, FCR, EDC and ECRL muscles) at 20% of MVC of handgrip strength that is mapped to a single output, the wrist joint angles. Each input and output are clustered in six clusters. The fuzzy rule employed are as follows:

If in1 is in cluster1 and in2 in cluster1 and in3 is in cluster1 and in4 is in cluster1,
then Out1 is outputcluster1.

If in1 is in cluster2 and in2 in cluster2 and in3 is in cluster2 and in4 is in cluster2,
then Out2 is outputcluster2.

If in1 is in cluster3 and in2 in cluster3 and in3 is in cluster3 and in4 is in cluster3, then Out3 is outputcluster3.

If in1 is in cluster4 and in2 in cluster4 and in3 is in cluster4 and in4 is in cluster4, then Out4 is outputcluster4.

If in1 is in cluster5 and in2 in cluster5 and in3 is in cluster5 and in4 is in cluster5, then Out5 is outputcluster5.

If in1 is in cluster6 and in2 in cluster6 and in3 is in cluster6 and in4 is in cluster6, then Out6 is outputcluster6.

The prediction results for wrist joint angle using ANFIS subtractive clustering model are shown in Figures 5.14. Overall, prediction results for wrist joint angle model yielded slightly larger error as compared to prediction results for the finger joint angle model. Based on the results, the estimations were overlapping with most of the input data were interpolated to be at neutral wrist position.

Technically, ANFIS is capable in providing precise prediction if proper input data is provided to the model. This suggests that the WL features provided as the input datasets to model the wrist joint angles contained overlapping classes, perhaps due to repetitive muscles that were selected; FDS with FCR and EDC with ECRL. Since both flexor and extensor muscles are responsible for wrist movement, reducing the input data into only WL features extracted from FCR and ECRL muscles will improve the model performance.

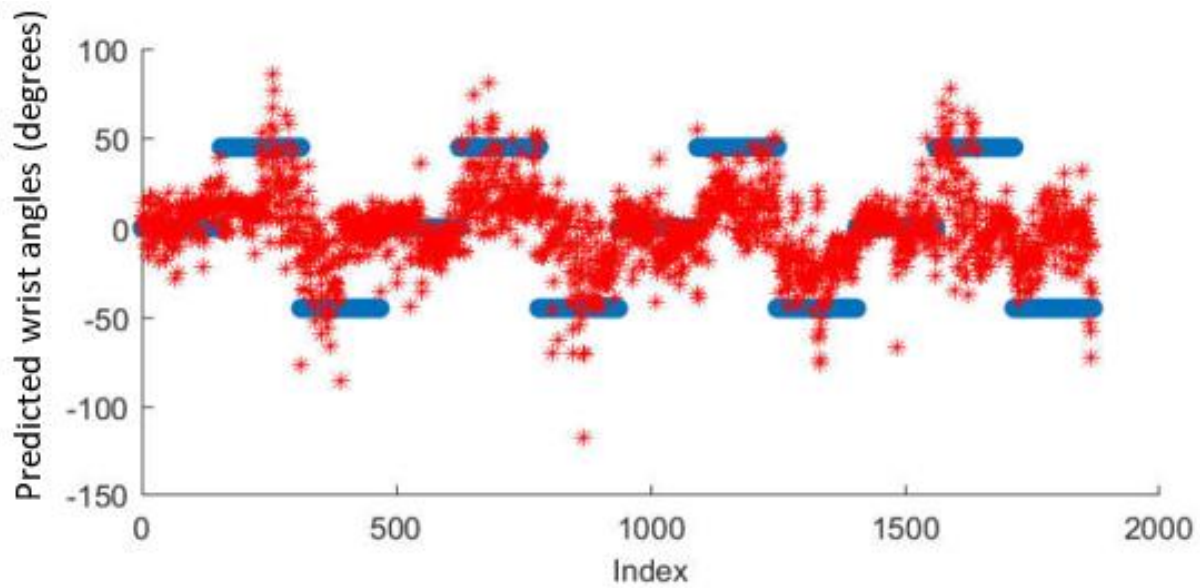


Figure 5.14: The prediction results for wrist joint estimations using ANFIS subtractive clustering model

5.4 Validation of the Joint Angle Estimations

The ANN models developed are used in the validation of the finger and wrist angle estimations. It is selected based on the regression value and the MSE value computed for ANN model that is better when compared to the ANFIS with subtractive clustering model. (Please refer to Appendix H and Appendix I for more samples of results for ANN and ANFIS model validations).

5.4.1 Validation for the Finger Joint Angle

Several datasets comprising of WL features from the single and multi-subjects are used as the input to the ANN model. Figure 5.15 to Figure 5.17 show the corresponding DIP, PIP and MCP joint angle estimated by the neural network for the four medial fingers. The performances of each of the neural networks are evaluated by calculating the Mean Absolute Error (MAE) between the output values estimated by the neural network with the desired values. It can be concluded that the neural networks used estimated the joint angles for the fingers with acceptable MAE values.

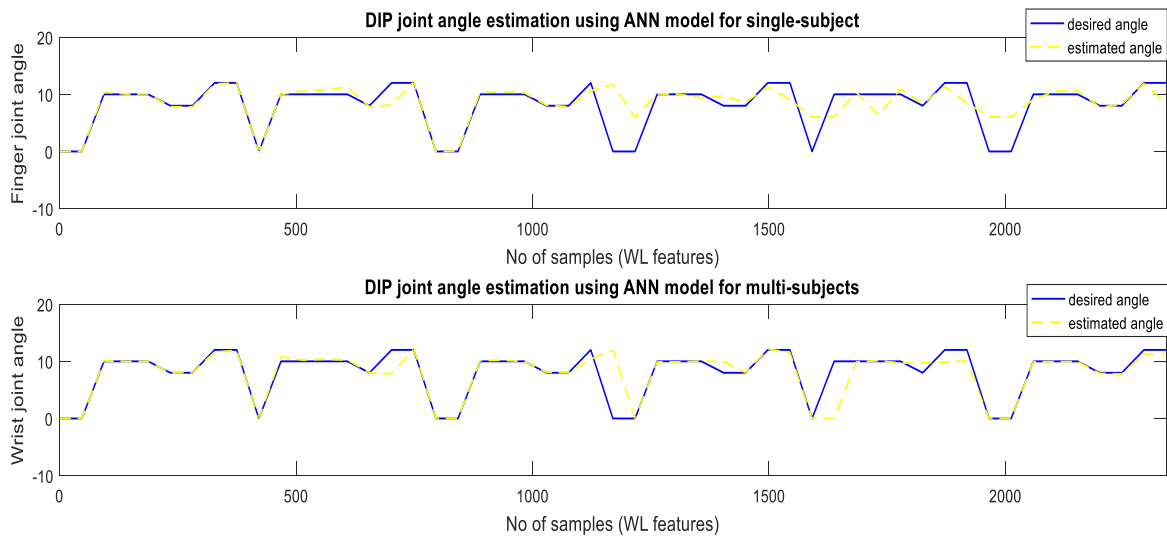


Figure 5.15: The DIP joint angle estimated from the ANN model for four medial fingers based on wavelength features at 20% MVC for different finger pinches (FR, FP1, FP2, FP3, & FP4)

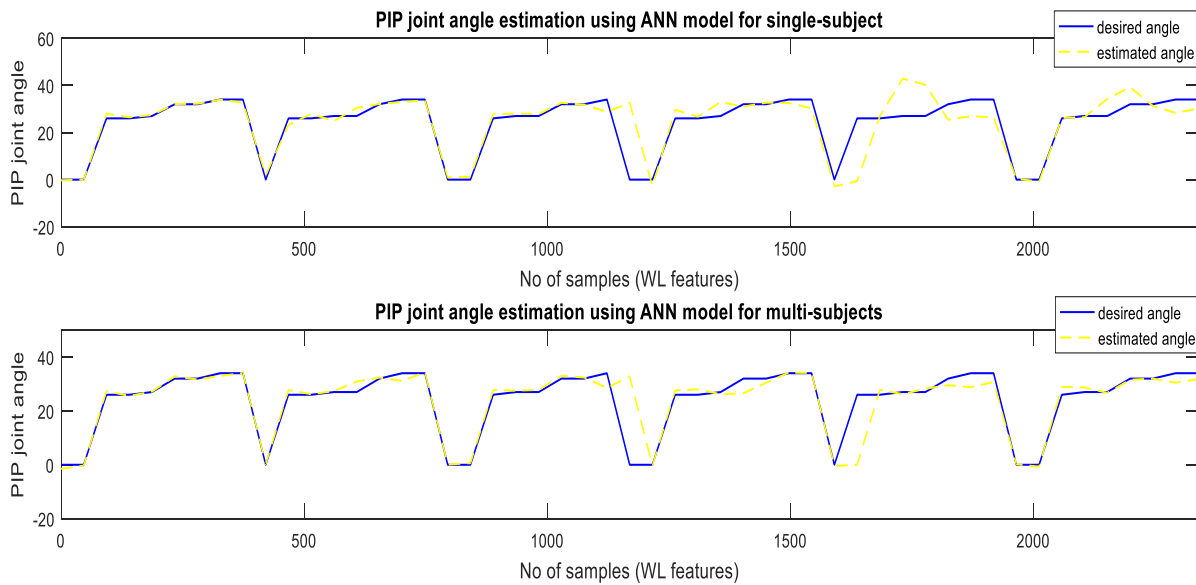


Figure 5.16: The PIP joint angle estimated from the ANN model for four medial fingers based on wavelength features at 20% MVC for different finger pinches (FR, FP1, FP2, FP3, & FP4)

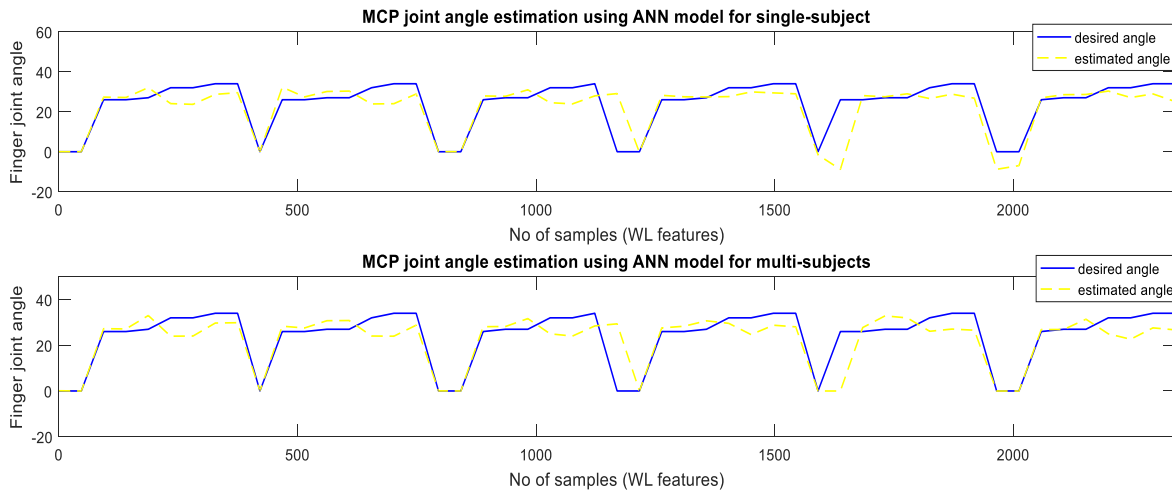


Figure 5.17: The MCP joint angle estimated from the ANN model for four medial fingers based on wavelength features at 20% MVC for different finger pinches (FR, FP1, FP2, FP3, & FP4)

5.4.2 Validation for the Wrist Joint Angle

Figure 5.18 and Figure 5.19 show the validation results for the hand grasping and wrist angle estimations using the ANN model. The obtained results show significant differences between each class of movements especially for wrist flexion and extension with prismatic power grip. The validation was done using input data for single and multi-subjects.

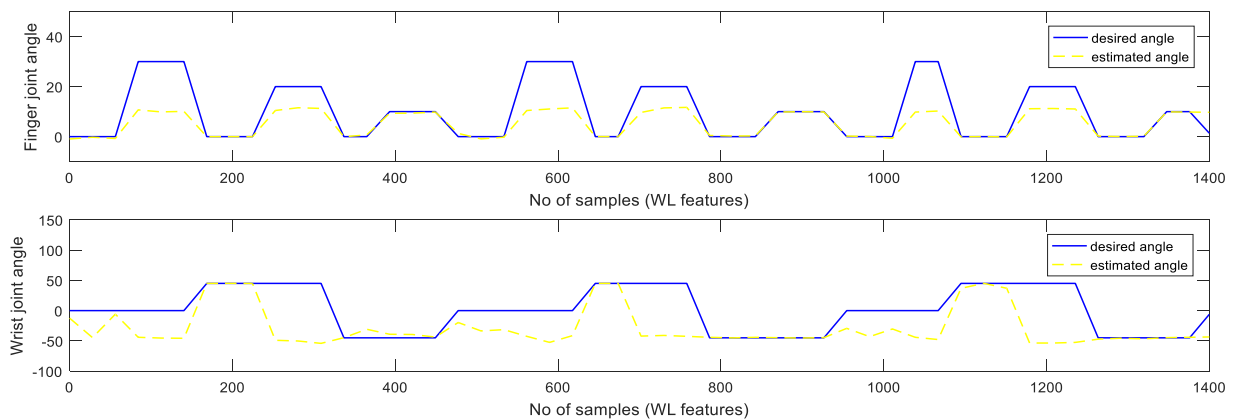


Figure 5.18: The grasping and wrist angles estimated from the ANN model based on wavelength features at 20% MVC using target data for a single subject

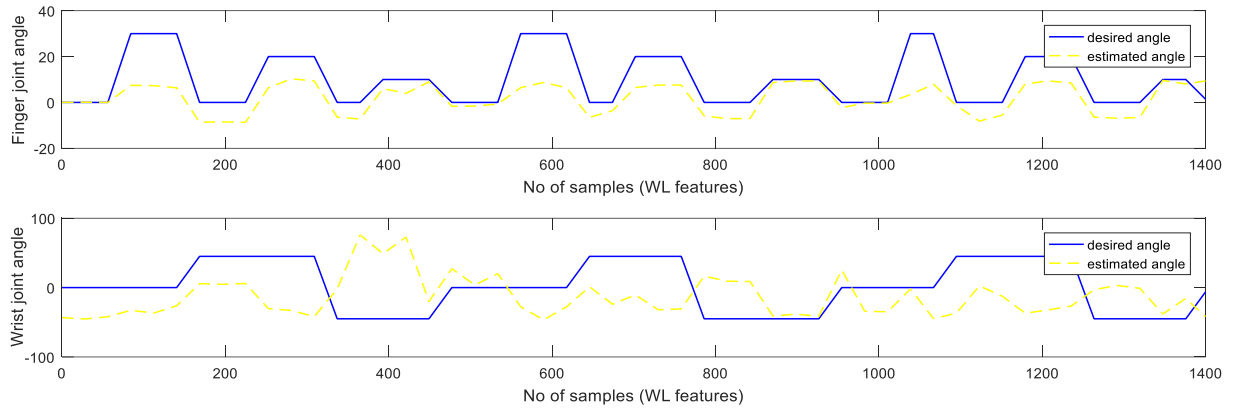


Figure 5.19: The grasping and wrist angles estimated from the ANN model based on wavelength features at 20% MVC using target data for multi-subject

5.5 Summary

The experimental results show that the feed-forward ANN provides better joint angle estimation with a correlation coefficient of 0.98 ± 0.008 and mean square error less than 3%, when compared to the ANFIS model with subtractive clustering. This result suggests that ANN with WL features provides a viable and effective estimation for finger joint kinematics and demonstrates a potential control strategy, which can be applied for continuous control of robotic devices. The estimation results obtained for each joint angle will be used to design a finite state controller for the overall control of exoskeleton hand in chapter 6.

Chapter 6

DESIGN AND CONTROL FRAMEWORK FOR EXOSKELETON HAND

6.1 Introduction

In this chapter, the control framework for the exoskeleton hand is presented by employing the results of the estimations obtained in the previous chapter. The control framework includes an EMG based controller that takes into account the user motion intention as part of the control input in designing the overall control scheme. The earliest myoelectric controller was applied around the 1950s to 1960s using simple algorithms based on the comparison between EMG amplitude to a threshold. The technique is inherently limited. Therefore, in the 1960s, pattern recognition based classification techniques were introduced and attracted the interest of researchers working on controlling artificial limbs with performance accuracies greater than 90%. The approach is based on the assumption that the EMG signal patterns are distinguishable and repeatable among different muscles activation. However, this control approach is not applicable in clinical practice and seems to be only successful in the scientific papers.

The main issues with the myoelectric control based on pattern recognition are due to the discrete approximation making the control scheme sequential without a direct proportional control that substantially differs from the natural control of the human hand. The human hand requires continuous control and coordination of multiple degrees of freedom across several joints. Its movements are generally simultaneous with proportional articulation. However, the proportional control degrades the accuracy of the classification and is usually implemented after classifications are made. Thus, control methods that realise continuous and proportional control of multiple DOF should be implemented and realised to control the exoskeleton hand.

In this research, a hierarchical control based strategy is designed to control the exoskeleton hand. Technically, in developing a complex system, the hierarchical control scheme is often introduced to organise and divide the design task as a hierarchy. The higher level of control requires longer execution time and process while the lower layer computes the direct control command based on decisions made by the higher level. The framework of the proposed control method is discussed in the following section, followed by the results and performance analysis of the controller.

6.2 Exoskeleton Hand Control Framework

A three-level hierarchical control framework is employed to control the exoskeleton hand. The proposed framework was inspired by and extended from the control strategies for lower limb prosthesis introduced by Tucker et al. (2015) and Varol et al. (2010). It comprises high-level control, mid-level control and low-level control, as shown in Figure 6.1.

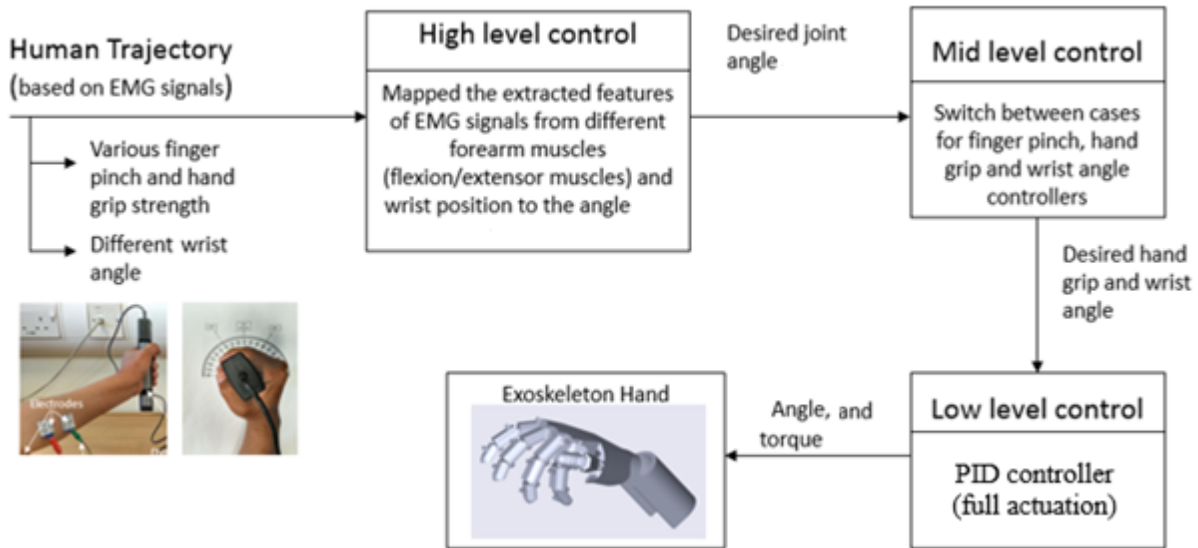


Figure 6.1: Hierarchical control framework for the exoskeleton hand

The hand movement is originated from the user motion intentions whose physiological state and desire can be traced and interpreted. In the high-level control (the perception level), the user motion is perceived and estimated by the activity recognition mode, which comprises the

processing techniques for the EMG signals together with the supervised learning algorithm which translates the muscle excitation into kinematics estimations of the hand, as shown in Figure 6.2. It distinguishes different movements like finger pinches, hand grasping, flexion and extension of the wrist and switches to appropriate mid-level controller.

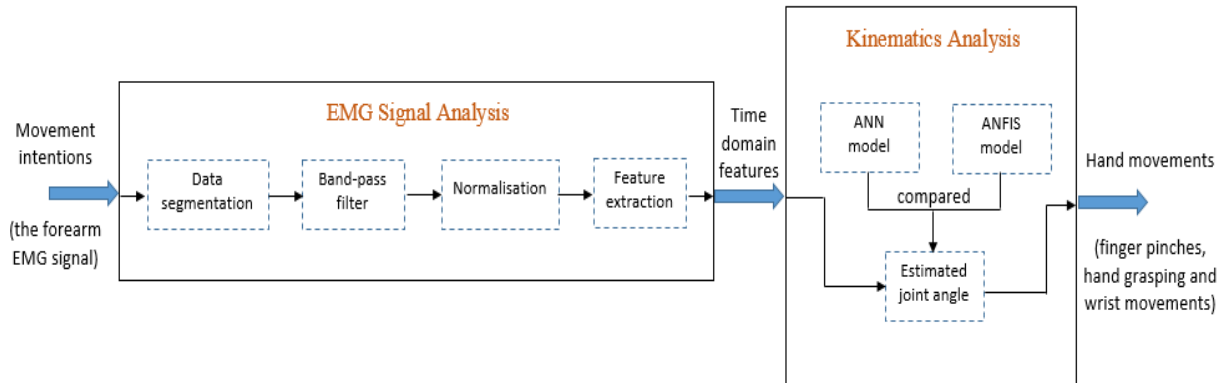


Figure 6.2: The activity mode intent recogniser

The mid-level controller (the transition level) translates the activity mode decisions from the high-level control to the desired device states for the low-level control to track. It generates the angle references for the joint using a finite state machine (FSM) controller that modulates the impedance of the joints depending on the phase of activity. The desired state control action is passed to the low-level controller (the execution level), which executes the control command and signals the actuators to produce the desired hand movement. It computes the error with respect to the current state.

6.3 Hierarchical Control of the Exoskeleton Hand

The control framework proposed in this research is executed and validated using the exoskeleton hand designed in Chapter 3. Figure 6.3 shows a block diagram of the overall control of the exoskeleton hand in Simulink; the graphical programming environment that offers an integration platform with the MATLAB software, developed by MathWorks. The controller integrates the joint angles estimated by the ANN models based on the WL features with the finite state machine that switches among the controller mode and the closed-loop proportional integral derivative (PID)

control position controllers that compensate for the error computed by the actuators of the exoskeleton hand developed in SimMechanics.

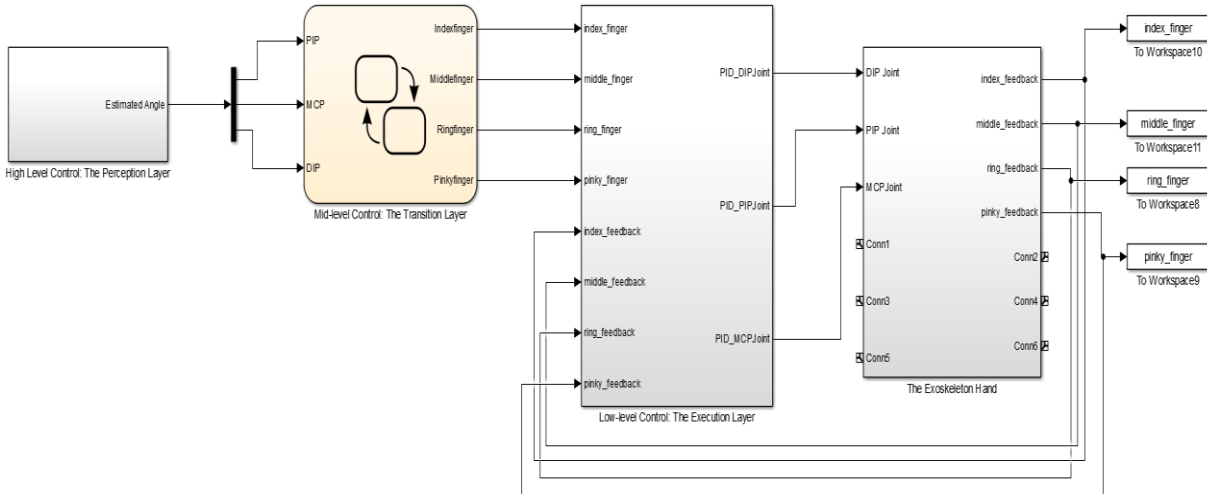


Figure 6.3: Block diagram of overall system controller showing the integration of the proposed hierarchical control framework for the exoskeleton hand; the perception level, the transition level and the execution level.

6.3.1 Finite State Machine Controller

The finite state machine (FSM) is the most popular mid-level controller used in lower limb exoskeletons (Miranda-Linares et al., 2015), upper limb exoskeleton and many others (Tucker et al., 2015), preferably due to its sequential operation. FSM is a computational model of sequential behaviour of a system and is commonly used to represent an execution flow for the system. It is defined by its states, its initial condition and the conditions of each state transition. The FSM comprises a set of pre-defined states with transition states in between; the state is a status of the system waiting to execute the transition that contains the corresponding outputs/actions when a condition is fulfilled.

In this research, the mid-level control is designed using two FSM models that are used to control the finger pinching and hand grasping at different wrist positions. States were defined based on the classification of the movements similar to the classification made during the features extraction

process. Figure 6.4 shows the FSM diagram developed to control the finger pinches for the exoskeleton hand.

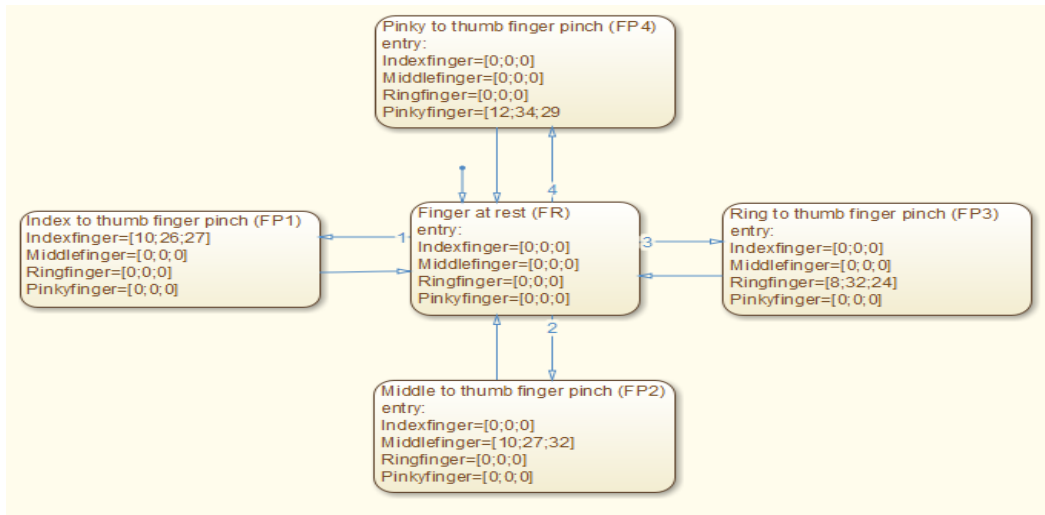


Figure 6.4: Finite state controller for finger pinches

For finger pinches, the FSM was built using five states with ten transitions, which include finger at rest, index to thumb finger pinch, middle to thumb finger pinch, ring to thumb finger pinch and pinky to thumb finger pinch. The five states are represented by the set, $S=\{0,1,2,3,4\}$. The transitions between each states are triggered by three input functions generated continuously by high-level controller. The input set are: $I=\{DIP_{angle}, PIP_{angle}, MCP_{angle}\}$. Meanwhile, three outputs are generated for each finger pinches making the output set to be: $O=\{DIP_{index}, PIP_{index}, MCP_{index}, DIP_{middle}, PIP_{middle}, MCP_{middle}, DIP_{ring}, PIP_{ring}, MCP_{ring}, DIP_{pinky}, PIP_{pinky}, MCP_{pinky}\}$. Each state with its input sets and output functions are as follows:

State 0: Finger at rest. This is the initial state in which all fingers are at resting positions (0 degree for all joints). The next state is activated when the DIP, PIP and MCP joint angles change to the value set for FP1.

State 1: Index to thumb finger pinch. In this state, the DIP, PIP and MCP joint angles are estimated to be the angles for index finger (FP1). Other fingers are not activated. The next state is activated when the DIP, PIP and MCP joint angles change to the value set for FP2.

State 2: Middle to thumb finger pinch. Similar to the previous state, the DIP, PIP and MCP joint angles are estimated to be the angles for middle finger (FP2). Other fingers are not activated. The next state is activated when the DIP, PIP and MCP joint angles change to the value set for FP3.

State 3: Ring to thumb finger pinch. This state triggered when the DIP, PIP and MCP joint angles are estimated to be the angles for ring finger (FP3). Other fingers are not activated. The next state is activated when the DIP, PIP and MCP joint angles change to the value set for FP4.

State 4: Pinky to thumb finger pinch. In this state, the DIP, PIP and MCP joint angles are estimated to be the angles for pinky finger (FP4). Other fingers are not activated.

The corresponding input set and output functions for each states are described in Table 6.1.

Table 6.1: The state with input set and output function for finger pinches

States/phases	State transitions	Output/Actions
Finger at rest (FR)	Finger pinch is off; DIP = 0; PIP=0; MCP=0;	All finger pinches is 0
Index to thumb finger pinch (FP1)	Finger pinch is on; 8.5 < DIP > 10.5; 20.5 < PIP > 26.5; 24.5 < MCP > 28;	Index finger = [10;26;27]; Others is 0
Middle to thumb finger pinch (FP1)	Finger pinch is on; 8.5 < DIP > 10.5; 26.5 < PIP > 32; 24 < MCP > 30.5;	Middle finger = [10;27;32]; Others is 0
Ring to thumb finger pinch (FP1)	Finger pinch is on; 8.5 < DIP > 11.5; 30 < PIP > 32.5; 24 < MCP > 29;	Ring finger = [8;24;32]; Others is 0
Pinky to thumb finger pinch (FP1)	Finger pinch is on; 11 < DIP > 12.5; 29 < PIP > 35; 29 < MCP > 30.5;	Pinky finger = [12;34;29]; Others is 0

The finite state machine controller for wrist movements is based on the hand grasping at different wrist positions (neutral, flexion and extension) as illustrated in Figure 6.5. It was built with six states and 12 states transitions, represented by the set, $S=\{0,1,2,3,4,5\}$. The transitions between each states are triggered by five input functions generated continuously by high-level controller. The input set are: $I=\{Wrist_{angle}, Handgrip_{strength}\}$. Meanwhile, two outputs are generated are set to be: $O=\{Wrist, Handgrasp\}$.

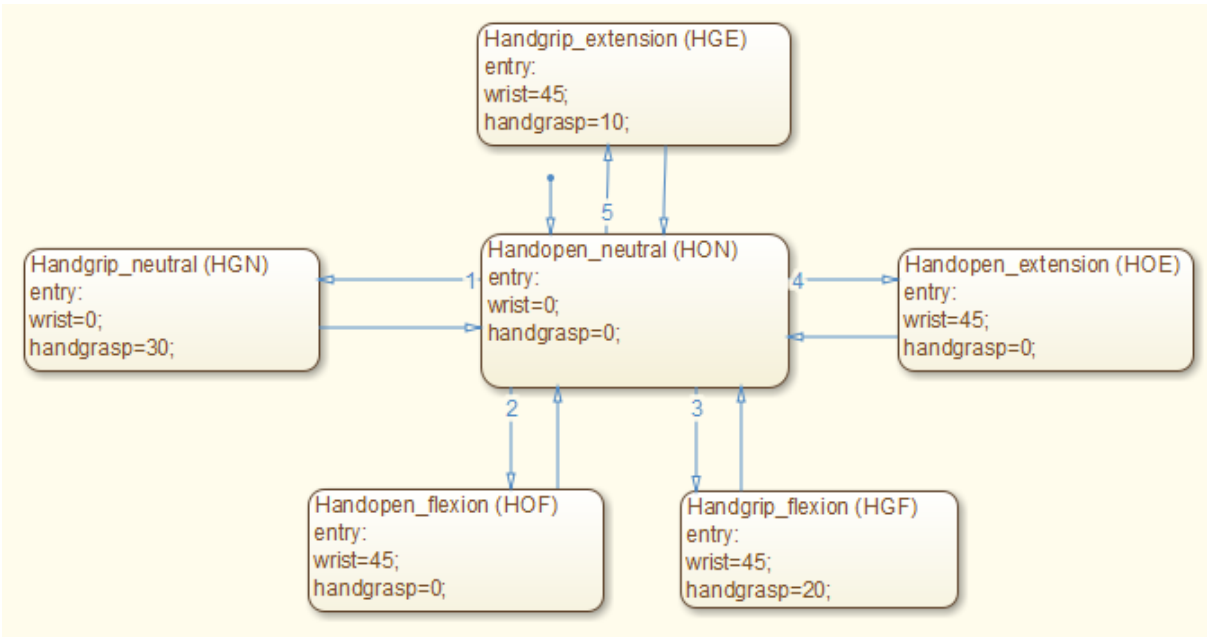


Figure 6.5: Finite state controller for wrist movements

Based on Figure 6.5, each state with its input sets and output functions are as follows:

State 0: Hand open at neutral. This is the initial state in which all fingers and wrist are at resting positions (0 degree for all joint angles). The next state is activated when the handgrip is triggered while the wrist angle is set to be 0 degree. This is based on the predicted angles measured in high-level controller.

State 1: Hand grip at neutral. In this state, the handgrip is triggered at neutral wrist positions. Other states are not activated. The hand will be closed at 0-degree wrist position. The next state is activated when hand open at wrist flexion is triggered.

State 2: Hand open at flexion. This state is triggered when the wrist angle is estimated to be at 45-degree wrist flexion for hand open. The next state is activated when the handgrip is activated at similar wrist angle.

State 3: Hand grip at flexion. In this state, the handgrip is triggered at flexion wrist position. Other states are not activated. The hand will be closed and flexed to 45-degree. The next state is activated when hand open at wrist extension is triggered.

State 4: Hand open at extension. This is the state is in which the hand is open at 45-degree extension. The next state is activated when the handgrip is activated at similar wrist angle.

State 5: Hand open at flexion. In this state, the handgrip is triggered at extension wrist position. Other states are not activated. The hand will be closed and extended to 45-degree.

The corresponding input set and output functions for each states are described in Table 6.2.

Table 6.2: The state with input set and output function for wrist movements

States/phases	State transitions	Output/Actions
Hand open at neutral	Hand grasping is off; $-2 < \text{wrist} < 2$;	Handgrasp = 0; Wrist = 0
Hand grip at neutral	Hand grasping is on; $-2 < \text{wrist} < 2$;	Handgrasp = 20; Wrist = 0
Hand open at flexion	Hand grasping is off; $\text{wrist} > 40$;	Handgrasp = 0; Wrist = +45
Hand grip at flexion	Hand grasping is on; $\text{wrist} > 40$;	Handgrasp = 20; Wrist = +45
Hand open at extension	Hand grasping is off; $\text{wrist} < -40$	Handgrasp = 0; Wrist = -45
Hand grip at extension	Hand grasping is on; $\text{wrist} < -40$;	Handgrasp = 20; Wrist = -45

Based on the data in Table 6.1, the state transition is defined based on the ANN model as shown in Figure 6.6. The estimated angle for DIP, PIP, and MCP joints for each respective finger joint is used as the condition that is needed to be fulfilled before executing the output or action.

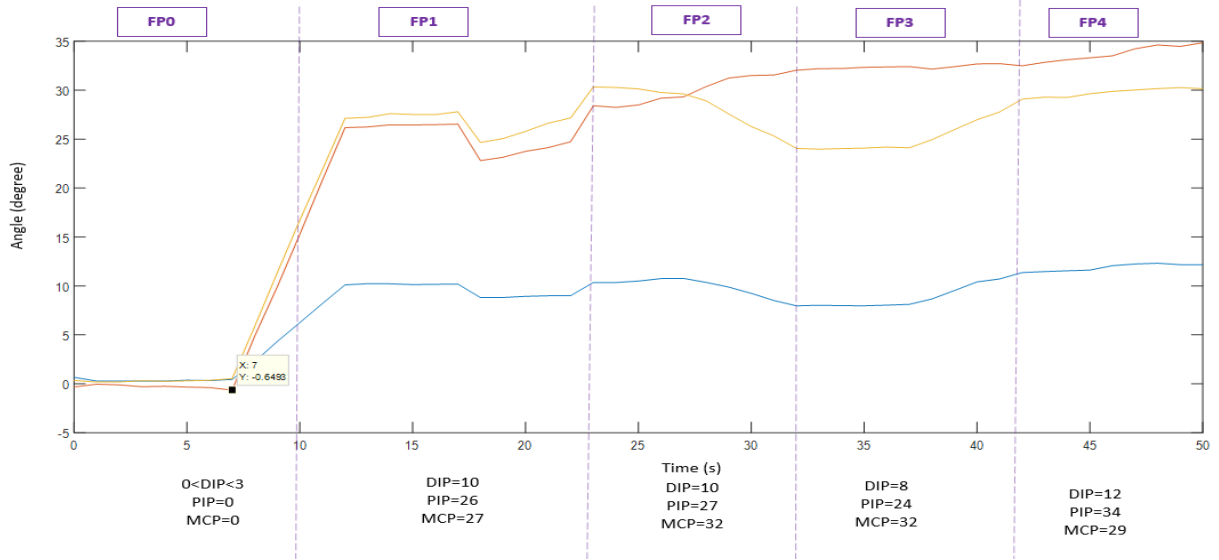


Figure 6.6: The reference trajectories divided by states based on the estimated DIP, PIP and MCP joint angles. (As for the legend; blue line is the DIP joint angle, yellow line is the PIP joint angle, while red line is the MCP joint angle)

The obtained results produced joint angle references for each respective finger joints with acceptable activation periods. A trapezoidal type of signal was observed for each finger pinches with different activation periods for each movement due to the variations in the input data set as shown in Figure 6.7.

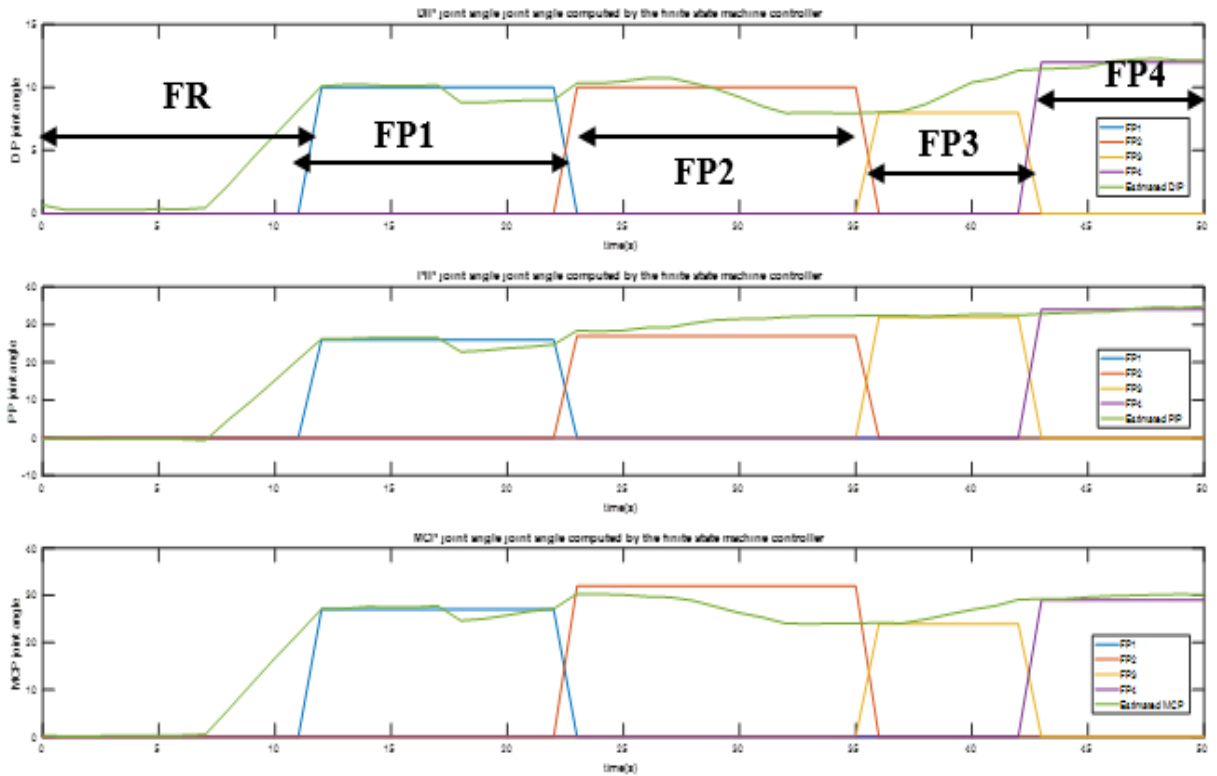


Figure 6.7: The angle references computed by the FSM controller.

6.3.2 PID controller

The computed reference angles are fed to the closed-loop PID controller to compute the desired finger pinches. The exoskeleton hand is assumed to operate with 100% control command with no control input from the human user. The composition of the human hand mass is approximated and incorporated in the exoskeleton model. The exoskeleton hand is designed with full actuation with the intension to produce hand functionality that can emulate the actual human hand. Each of the joints is controlled by separate actuators requiring independent PID controller for each joint. This however has caused the system to be complex, and increase the computational load and time.

Figure 6.8 and Figure 6.9 show the computed joint angles and torque for index to thumb finger pinch (FP1). The control parameters for the PID were manually tuned to produce the desired control response. Initially, all control parameters were set to zero. Then, the proportional (P) gain

was increased followed by the derivative (D) gain and integral (I) gain. The I gain was adjusted to obtain $e_{ss}=0$. It is noted in Figure 6.7, there were small overshoot and undershoot in the control response computed for each joint angle. Therefore, the integral gain was reduced while the derivative gain was adjusted.

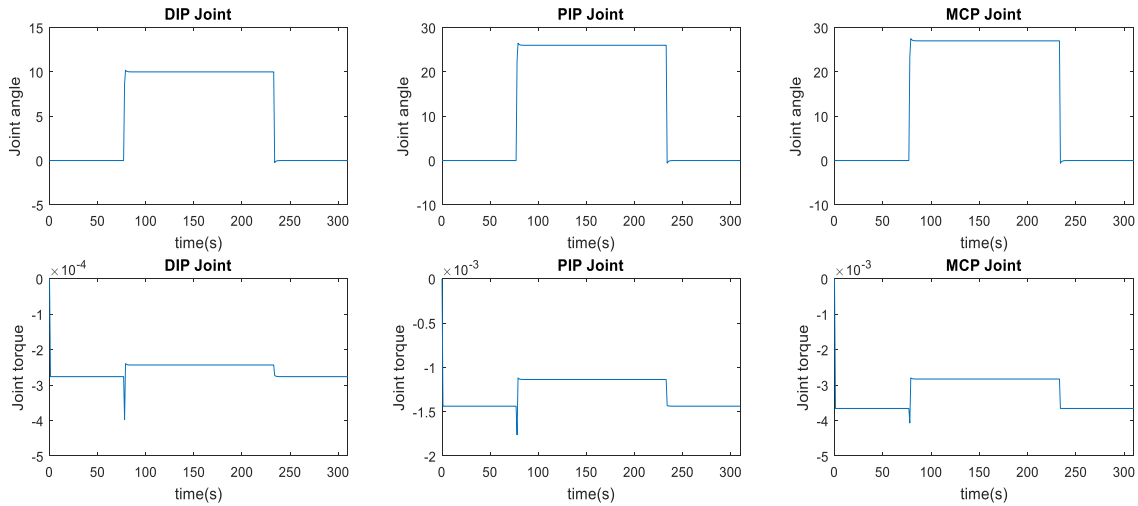


Figure 6.8: The joint angle and torque computed for index finger with the control parameters $K_p=0.5$, $K_d=0.02$, $K_i=1.5$.

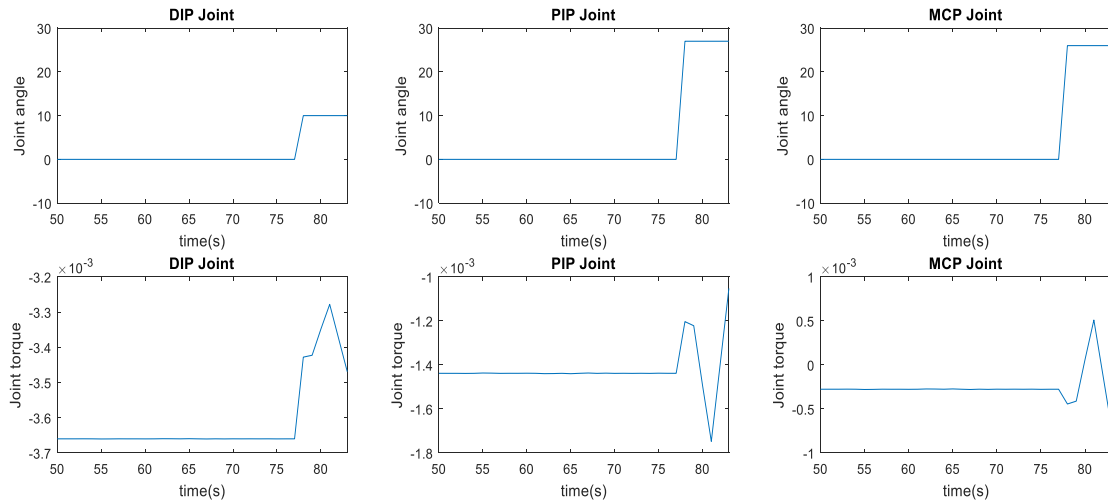


Figure 6.9: The joint angle and torque computed for index finger with adjusted control parameters $K_p=0.5$, $K_d=0.01$, $K_i=1$.

6.5 Summary

This chapter has presented the control framework that integrates all methods described in this research. The proposed framework comprises a 3-level control hierarchy that computes different outputs or control actions. The results have been validated and good results have been achieved. The results produced by the mid-level and low-level control are analysed in terms of variations between the input and the output trajectories. Root mean square error (RMSE) is computed for both mid-level and low-level control while the control response in terms of steady state error and percentage of overshoot is evaluated for the low-level control. It can be concluded that the proposed control design is viable and sufficient to be used in controlling the exoskeleton hand.

Chapter 7

CONCLUSION AND RECOMMENDATION FOR FUTURE WORK

7.1 Discussion

A literature review has been carried out to study the development of exoskeleton hand and its' challenges. Gaps have been identified regarding the development of exoskeleton hand in virtual environments for early design assessments. It was found that most of the publications on the development of the exoskeleton hand described the construction of the mechanical prototype with only a few described the use of virtual environments. The recent advancement in computational tools allow the integration of complex physical and mathematical systems to be carried out in simulations. The geometric Solidworks assembly of the exoskeleton hand is transformed into a physical model in SimMechanics.

The exoskeleton model scheme presented acceptable prototype animation with several limitations. The design structure is designed with the palm that is tied to the ground and attached to a forearm that was freely moved. Technically, this design structure is not following the biological hand movements as supposedly, the forearm is designed as the distal body to the wrist joint and tied to the ground. Even though the simulation model of the exoskeleton hand is not quite right, it still able to produce acceptable results for early control design assessments. Additionally, the designed exoskeleton has a rigid structure (with parallel joints) that hinders a full kinematic compatibility when attached to the human joints. It is difficult to model the biological joints of the hand making human-exoskeleton attachment difficult. This can be improved by introducing 'circuitous joint' that coincides the joint axes between the human and the exoskeleton by extending the link length of the finger in proportion to the joint angular displacement.

It was also found that the most significant step in developing the exoskeleton hand is to design an effective control scheme that includes the user motion intention as part of the control input. It can be done by extracting the useful information within EMG signals to produce high-quality feature sets with significant separability of classes for each finger and wrist movements. Previously published studies show that the current EMG based control schemes employed in controlling the available multiple DOF exoskeleton hands cannot fully utilise the hand function because there are fewer control inputs than the joints that need to be controlled. It is based on pattern recognition that is sequential with limited robustness as it can process only a single movement at a time. The proportional controller is normally applied after classification is done to avoid degradation in the classification performances. Therefore, in this research, the relationship between the forearm EMG signals with various finger pinches and handgrip strength at different wrist positions were established by using nonlinear regression methods.

The EMG data collected were pre-processed and the features were extracted. These steps are crucial and not only significant in extracting useful information, but also essential to be used in removing the unwanted signal part and interferences. The time domain features extracted produced significant class separability when normalised as presented in Chapter 4. Since the EMG data collected were extensively analysed, the remaining normalised and non-normalised features extraction results for different percentage of maximum voluntary contraction were included in the Appendixes.

The EMG pattern-recognition process is modified by replacing the classifier with supervised learning method; a feed-forward artificial neural network (ANN) and adaptive neuro-fuzzy inference system (ANFIS) with subtractive clustering. The learning method are used to predict the finger and wrist joint angles based on the extracted EMG features. The results show that the ANN model provides superior joint angle estimations when compared to the ANFIS model. Even though the EMG signals are proportional to the handgrip force, the estimations for the force is not included in this research work. Instead, the handgrip force was recorded and used only to analyse the maximum voluntary contraction of the finger pinches and hand grasping at different wrist positions.

To integrate all components together, hierarchical control comprising three-level controllers is proposed as the overall control scheme for the exoskeleton hand. In the high-level control, user defined motion intention based on forearm EMG signals is used as control input where the kinematic estimation of the hand is computed based on the established relationship. Finite state machine controller is designed in the transition layer between high level and low-level control to govern and join the fingers and wrist controls together before any movement is executed by the low-level control using the classical control approach, the PID controller. Technically, the high-level controller is used to predict the finger and wrist joint angles and provides continuous isometric grip pattern. Therefore, employing the FSM controller as the mid-level control will limit the predictions to a discrete set of grip patterns. It is a compromise that was made for the purposes of demonstrating and analysing the overall control performance. Due to that, the low-level control was tested using the FSM results yielded for the finger pinches only.

7.2 Conclusion

This research has embarked on the modelling and EMG based control of an exoskeleton hand to provide excellent assistance to the stroke survivors in accomplishing simple daily hand functions. Being able to accomplish these basic tasks, which are often less appreciated by healthy individuals, can significantly improve their quality of life. The research starts with the designing method used to produce the exoskeleton hand model in a virtual environment to avoid complex and challenging mathematical computation of the system modelling. Besides, the virtual model can save the development cost and provides a reliable testing platform with the exoskeleton hand.

The design exoskeleton hand is done by following the anatomy and biomechanics of the human hand closely. Anthropometry measurement of the human hand is compared and referred for the measurement of the exoskeleton hand. The simulation diagram of the designed exoskeleton hand shows a satisfactory result with a few joint movement restrictions that can be improved in the future.

In defining user motion intention, the EMG data collected is processed and analysed to produce a functional time domain features that is useful to study the muscle excitation and to establish the relationship between EMG signals, finger pinch/hand grip strength and different wrist positions.

Valuable WL features are produced and proven efficient to be used in estimating the respective joint angles through the implementation of ANN model. The performance of the ANN and ANFIS modelling are compared, and the ANN model is concluded to be superior to the ANFIS model.

The hierarchical control framework employing the results from all stage of research together yielded a viable and effective control approach for controlling the exoskeleton hand. The control design was validated, and its control performances were analysed. Several statistical approaches were used to measure the accuracy of the results obtained in the respective stage such as the one-way ANOVA with Turkey Kramers test, the RMSE and the MSE, the regression value and the standard control response; steady-state error and percentage of overshoot.

Overall, based on all the aforementioned simulation results, it can be concluded that the modelling and EMG based controller for exoskeleton hand is successfully achieved with several limitations. The proposed supervised learning methods are capable in providing joint angle estimations that can be used to continuously predict the isometric grip pattern. The proposed control framework can be easily replicate to integrate and control the fingers and wrist movements of the exoskeleton hand.

7.3 Recommendations for Future Work

Despite all the careful evaluations and efforts that had been done to efficiently model and control the exoskeleton hand, there are a few suggestions for improvement that can be done to improve the control performance of the exoskeleton hand further. The suggestions are as follows:

1. Based on the exoskeleton model scheme, the palm is designed as the body distal to the wrist and is tied to the ground. It is attached to the forearm that is freely moved with a single DOF joint represented as the wrist. The designed structure is due to the amendment made in the scope of this research that only considered the wrist structure to be included after the model is complete. It need to be improvise by changing the forearm to be the distal body to the wrist.

2. The joint finger estimation is done based on the time domain features that are not suitable for non-stationary datasets. Therefore, it is useful to study another type of features like frequency domain or time-frequency domain features.
3. The mid-level control is independently designed between finger pinches and wrist position. Integrating these two controllers would be beneficial for the overall control of the exoskeleton hand.
4. Based on the research conducted, it is difficult to achieve robust control solely using EMG signals. Thus, the use of other sensor fusion together with the EMG signal seems necessary. For example, embedding the force measurement using a mechanical sensor together with the EMG signal as part of control input in predicting the intention of the user might improve the performance and adaptability for the exoskeleton hand control. It is also useful if adaptive control can be designed in case of any interruption in acquiring the EMG signals.
5. Cross-validation to randomly produce the training and testing datasets.
6. The control of the exoskeleton hand was done by assuming that the exoskeleton hand provides 100% assistance, which may not always be true. Analysing the control performance at different assistive percentages would increase the efficiency of the overall control.
7. Feedback sensor for safety. In the development of the exoskeleton hand control scheme, there is no proprioceptive feedback provided to observe the performance of the grasping task that are carried out automatically. In the case of unsuccessful event, the only available feedback is based on user's direct vision to reset or stop the controller. Therefore, including the feedback sensor as part of the control design will increase the safety measures for the users.

REFERENCES

- Amirabdollahian, F., Ates, S., Basteris, A., Cesario, A., Buurke, J., Hermens, H., Hofs, D., Johansson, E., Mountain, G., Nasr, N., Nijenhuis, S., Prange, G., Rahman, N., Sale, P., Schätzlein, F., Van Schooten, B., and Stienen, A. (2014). Design, development and deployment of a hand/wrist exoskeleton for home-based rehabilitation after stroke - SCRIPT project. *Robotica*. <https://doi.org/10.1017/S0263574714002288>
- Armagan, O., Tascioglu, F., and Oner, C. (2003). Electromyographic biofeedback in the treatment of the hemiplegic hand: a placebo-controlled study. *Am J Phys Med Rehabil*, 82. <https://doi.org/10.1097/01.phm.0000091984.72486.e0> LB - Armagan2003
- Ates, S., Haarman, C. J. W., and Stienen, A. H. A. (2017). SCRIPT passive orthosis: design of interactive hand and wrist exoskeleton for rehabilitation at home after stroke. *Autonomous Robots*. <https://doi.org/10.1007/s10514-016-9589-6>
- Ates, S., Leon, B., Basteris, A., Nijenhuis, S., Nasr, N., Sale, P., Cesario, A., Amirabdollahian, F., and Stienen, A. H. A. (2014). Technical evaluation of and clinical experiences with the SCRIPT passive wrist and hand orthosis. In *Proceedings - 2014 7th International Conference on Human System Interactions, HSI 2014*. <https://doi.org/10.1109/HSI.2014.6860472>
- Ates, S., Lobo-Prat, J., Lammertse, P., Kooij, H. van der, and Stienen, A. H. A. (2013). SCRIPT Passive Orthosis: Design and technical evaluation of the wrist and hand orthosis for rehabilitation training at home. In *2013 IEEE 13th International Conference on Rehabilitation Robotics (ICORR)* (pp. 1–6). <https://doi.org/10.1109/ICORR.2013.6650401>
- Ates, S., Mora-Moreno, I., Wessels, M., and Stienen, A. H. A. (2015). Combined active wrist and hand orthosis for home use: Lessons learned. In *2015 IEEE International Conference on Rehabilitation Robotics (ICORR)* (pp. 398–403). <https://doi.org/10.1109/ICORR.2015.7281232>
- Baker, M. D., McDonough, M. K., McMullin, E. M., Swift, M., and BuSha, B. F. (2011). Orthotic Hand-Assistive Exoskeleton. In *2011 IEEE 37th Annual Northeast Bioengineering Conference (NEBEC)* (pp. 1–2). <https://doi.org/10.1109/NEBC.2011.5778523>
- Barr, A. E., Barbe, M. F., and Clark, B. D. (2004). Work-related musculoskeletal disorders of the hand and wrist: epidemiology, pathophysiology, and sensorimotor changes. *The Journal of Orthopaedic and Sports Physical Therapy*, 34(10), 610–627. <https://doi.org/10.2519/jospt.2004.34.10.610>
- Bertani, R., Melegari, C., De Cola, M. C., Bramanti, A., Bramanti, P., and Calabrò, R. S. (2017). Effects of robot-assisted upper limb rehabilitation in stroke patients: a systematic review with meta-analysis. *Neurological Sciences*, 38(9), 1561–1569. <https://doi.org/10.1007/s10072-017-2995-5>
- Bionik Labs. (2010a). InMotion HAND. Retrieved November 26, 2018, from <https://www.bioniklabs.com/products/inmotion-hand>
- Bionik Labs. (2010b). InMotion WRIST. Retrieved November 26, 2018, from <https://www.bioniklabs.com/products/inmotion-wrist>
- Bioservo Technologies. (2015). Carbonhand. Retrieved November 26, 2018, from <https://www.bioservo.com/healthcare/carbonhand>

- Broadened Horizons; (2010). PowerGrip assisted grasp orthosis.
- Brokaw, E. B., Black, I., Holley, R. J., and Lum, P. S. (2011). Hand Spring Operated Movement Enhancer (HandSOME): A portable, passive hand Exoskeleton for stroke rehabilitation. *IEEE Transactions on Neural Systems and Rehabilitation Engineering*, 19(4), 391–399. <https://doi.org/10.1109/TNSRE.2011.2157705>
- Buchanan, T. S., Lloyd, D. G., Manal, K., and Besier, T. F. (2004). Neuromusculoskeletal modeling: Estimation of muscle forces and joint moments and movements from measurements of neural command. *Journal of Applied Biomechanics*. <https://doi.org/10.1123/jab.20.4.367>
- Bundhoo, V., Haslam, E., Birch, B., and Park, E. J. (2009). A shape memory alloy-based tendon-driven actuation system for biomimetic artificial fingers, part I: design and evaluation. *Robotica*. <https://doi.org/10.1017/S026357470800458X>
- Cakit, E., Durgun, B., Cetik, O., and Yoldas, O. (2014). A survey of hand anthropometry and biomechanical measurements of dentistry students in Turkey. *Human Factors and Ergonomics In Manufacturing*. <https://doi.org/10.1002/hfm.20401>
- Carolei, A., Sacco, S., Santis, F. De, and Marini, C. (2002). Epidemiology of stroke. *Clinical and Experimental Hypertension*, 24(7–8), 479–483. <https://doi.org/10.1081/CEH-120015323>
- Cempini, M., De Rossi, S. M. M., Lenzi, T., Vitiello, N., and Carrozza, M. C. (2013). Self-alignment mechanisms for assistive wearable robots: A kinetostatic compatibility method. *IEEE Transactions on Robotics*. <https://doi.org/10.1109/TRO.2012.2226381>
- Cesqui, B., Tropea, P., Micera, S., and Krebs, H. I. (2013). EMG-based pattern recognition approach in post stroke robot-aided rehabilitation: a feasibility study. *Journal of NeuroEngineering and Rehabilitation*, 10(1 LB-Cesqui2013), 1–15. <https://doi.org/10.1186/1743-0003-10-75>
- Chen, C. H., and Naidu, D. S. (2011). Fusion of fuzzy logic and PD control for a five-fingered smart prosthetic hand. In *Fuzzy Systems (FUZZ), 2011 IEEE International Conference on* (pp. 2108–2115). <https://doi.org/10.1109/FUZZY.2011.6007645>
- Chen, M., Ho, S. K., Zhou, H. F., Pang, P. M. K., Hu, X. L., Ng, D. T. W., and Tong, K. Y. (2009). Interactive rehabilitation robot for hand function training. In *2009 IEEE International Conference on Rehabilitation Robotics* (pp. 777–780). <https://doi.org/10.1109/ICORR.2009.5209564>
- Chiu, S. L. (1994). Fuzzy model identification based on cluster estimation. *Journal of Intelligent Fuzzy Systems*, 2, 267–278.
- Daiya Industry. (2013). Power assist glove RE. Retrieved November 26, 2018, from <http://www.daiyak.co.jp/product/detail/342>
- DiCicco, M., Lucas, L., and Matsuoka, Y. (2004). Comparison of control strategies for an EMG controlled orthotic exoskeleton for the hand. <https://doi.org/10.1109/robot.2004.1308056>
- Engeberg, E. D. (2013). Human Model Reference Adaptive Control of a Prosthetic Hand. *Journal of Intelligent & Robotic Systems*, 72(1 LB-Engeberg2013), 41–56. <https://doi.org/10.1007/s10846-013-9815-9>

- Esmaeili, M., Gamage, K., Tan, E., and Campolo, D. (2011). Ergonomic considerations for anthropomorphic wrist exoskeletons: A simulation study on the effects of joint misalignment. In *IEEE International Conference on Intelligent Robots and Systems*. <https://doi.org/10.1109/IROS.2011.6048737>
- Exoskeleton Report. (2018). Commercial exoskeletons catalog. Retrieved November 26, 2018, from <https://exoskeletonreport.com/product-tag/hand/>
- Farzad, M., Asgari, A., Dashab, F., Layeghi, F., Karimlou, M., Hosseini, S. A., and Rassafiani, M. (2015). Does Disability Correlate With Impairment After Hand Injury? *Clinical Orthopaedics and Related Research*®, 473(11), 3470–3476. <https://doi.org/10.1007/s11999-015-4228-7>
- Fedák, V., Ďurovský, F., and Róbert, Ľ. (2014). Analysis of robotic system motion in SimMechanics and MATLAB GUI environment. *InTechopen*. <https://doi.org/10.5772/58371>
- Fleischer, C., Kondak, K., Wege, A., and Kossyk, I. (2009). Research on Exoskeletons at the TU Berlin. In T. Kröger & F. M. Wahl (Eds.), *Advances in Robotics Research: Theory, Implementation, Application* (pp. 335–346). Berlin, Heidelberg: Springer Berlin Heidelberg. https://doi.org/10.1007/978-3-642-01213-6_30 LB - Fleischer2009
- Franck, J. A., Smeets, R. J., and Seelen, H. (2017). Changes in arm-hand function and arm-hand skill performance in patients after stroke during and after rehabilitation. *PloS One.*, 12(6), e0179453. Retrieved from <https://doi.org/10.1371/journal.pone.0179453>
- General Electric Company. (1969). *Hardiman I prototype project*. Retrieved from <https://apps.dtic.mil/dtic/tr/fulltext/u2/701359.pdf>
- Gilardi, G., Haslam, E., Bundhoo, V., and Park, E. J. (2010). A shape memory alloy based tendon-driven actuation system for biomimetic artificial fingers, part II: modelling and control. *Robotica*, 28(5), 675–687. <https://doi.org/DOI: 10.1017/S0263574709990324>
- Gopura, R. A. R. C., Bandara, D. S. V., Kiguchi, K., and Mann, G. K. I. (2016). Developments in hardware systems of active upper-limb exoskeleton robots: A review. *Robotics and Autonomous Systems*. <https://doi.org/10.1016/j.robot.2015.10.001>
- Gopura, R. A. R. C., and Kiguchi, K. (2008). EMG-based control of an exoskeleton robot for human forearm and wrist motion assist. In *Robotics and Automation, 2008. ICRA 2008. IEEE International Conference on* (pp. 731–736). <https://doi.org/10.1109/ROBOT.2008.4543292>
- Gopura, R. A. R. C., Kiguchi, K., and Bandara, D. S. V. (2011). A brief review on upper extremity robotic exoskeleton systems. *2011 6th International Conference on Industrial and Information Systems, ICIIS 2011 - Conference Proceedings*, 8502, 346–351. <https://doi.org/10.1109/ICIINFS.2011.6038092>
- Hahne, J. M., Bießmann, F., Jiang, N., Rehbaum, H., Farina, D., Meinecke, F. C., Muller, K. R., and Parra, L. C. (2014). Linear and nonlinear regression techniques for simultaneous and proportional myoelectric control. *IEEE Transactions on Neural Systems and Rehabilitation Engineering*. <https://doi.org/10.1109/TNSRE.2014.2305520>
- Halaki, M., and Gi, K. (2012). Normalization of EMG signals: to normalize or not to normalize and what to normalize to? In *Computational Intelligence in Electromyography Analysis - A Perspective on Current Applications and Future Challenges*. <https://doi.org/10.5772/49957>

- Harlaar, J., Prevo, A. J., v.d. Zwan, A. J., and Vogelaar, T. W. (2016). EMG analysis during voluntary movements in spastic patients compared to normal values and the effect of cooling. *Clinical Neurophysiology*, 61(3), S220. [https://doi.org/10.1016/0013-4694\(85\)90834-X](https://doi.org/10.1016/0013-4694(85)90834-X)
- Hasegawa, Y., Tokita, J., Kamibayashi, K., and Sankai, Y. (2011). Evaluation of fingertip force accuracy in different support conditions of exoskeleton. In *Robotics and Automation (ICRA), 2011 IEEE International Conference on* (pp. 680–685). <https://doi.org/10.1109/ICRA.2011.5980512>
- Heo, P., Gu, G. M., Lee, S. J., Rhee, K., and Kim, J. (2012). Current hand exoskeleton technologies for rehabilitation and assistive engineering. *International Journal of Precision Engineering and Manufacturing*, 13(5), 807–824. <https://doi.org/10.1007/s12541-012-0107-2>
- Ho, N. S. K., Tong, K. Y., Hu, X. L., Fung, K. L., Wei, X. J., Rong, W., and Susanto, E. A. (2011). An EMG-driven exoskeleton hand robotic training device on chronic stroke subjects: Task training system for stroke rehabilitation. In *2011 IEEE International Conference on Rehabilitation Robotics* (pp. 1–5). <https://doi.org/10.1109/ICORR.2011.5975340>
- Hu, X. L., Tong, K. Y., Song, R., Zheng, X. J., Lui, K. H., Leung, W. W. F., Ng, S., and Au-Yeung, S. S. Y. (2009). Quantitative evaluation of motor functional recovery process in chronic stroke patients during robot-assisted wrist training. *Journal of Electromyography and Kinesiology*. <https://doi.org/10.1016/j.jelekin.2008.04.002>
- Huo, W., Huang, J., Wang, Y., and Wu, J. (2010). Control of a rehabilitation robotic exoskeleton based on intentional reaching direction. In *2010 International Symposium on Micro-NanoMechatronics and Human Science: From Micro and Nano Scale Systems to Robotics and Mechatronics Systems, MHS 2010, Micro-Nano GCOE 2010, Bio-Manipulation 2010*. <https://doi.org/10.1109/MHS.2010.5669522>
- Huo, W., Huang, J., Xu, W., Mohammed, S., and Amirat, Y. (2015). Control of upper-limb power-assist exoskeleton using a human-robot interface based on motion intention recognition. *IEEE Transactions on Automation Science and Engineering*. <https://doi.org/10.1109/TASE.2015.2466634>
- Iqbal, J., Khan, H., Tsagarakis, N. G., and Caldwell, D. G. (2014). A novel exoskeleton robotic system for hand rehabilitation - Conceptualization to prototyping. *Biocybernetics and Biomedical Engineering*, 34(2), 79–89. <https://doi.org/10.1016/j.bbe.2014.01.003>
- Iqbal, J., Tsagarakis, N. G., and Caldwell, D. G. (2010). A human hand compatible optimised exoskeleton system. In *Robotics and Biomimetics (ROBIO), 2010 IEEE International Conference on* (pp. 685–690). <https://doi.org/10.1109/ROBIO.2010.5723409>
- Iqbal, J., Tsagarakis, N. G., and Caldwell, D. G. (2011). A multi-DOF robotic exoskeleton interface for hand motion assistance. *Proceedings of the Annual International Conference of the IEEE Engineering in Medicine and Biology Society, EMBS*, 1575–1578. <https://doi.org/10.1109/IEMBS.2011.6090458>
- Iqbal, J., Tsagarakis, N. G., Fiorilla, A. E., and Caldwell, D. G. (2010). A portable rehabilitation device for the Hand. In *2010 Annual International Conference of the IEEE Engineering in Medicine and Biology* (pp. 3694–3697). <https://doi.org/10.1109/IEMBS.2010.5627448>
- Jang, J.-S. (1993). ANFIS: adaptive-network-based fuzzy inference system. *IEEE Transactions on Systems, Man, and Cybernetics*, 23(3), 665–685. <https://doi.org/10.1109/21.256541>

- Jarrasse, N., and Morel, G. (2012). Connecting a human limb to an exoskeleton. *IEEE Transactions on Robotics*, 28(3), 697–709. <https://doi.org/10.1109/TRO.2011.2178151>
- Jee, S. C., Lee, Y. S., Lee, J. H., Park, S., Jin, B., and Yun, M. H. (2016). Anthropometric classification of human hand shapes in Korean population. In *Proceedings of the Human Factors and Ergonomics Society*. <https://doi.org/10.1177/1541931213601281>
- Johnson, W., Onuma, O., Owolabi, M., and Sachdev, S. (2016). Stroke: A global response is needed. *World Health Organization. Bulletin of the World Health Organization*, 94 (9), 634-634,634A.
- Kadowaki, Y., Noritsugu, T., Takaiwa, M., Sasaki, D., and Kato, M. (2011). Development of soft power-assist glove and control based on human intent. *Journal of Robotics and Mechatronics*, Vol. 23, N.
- Kang, J., Meng, W., Abraham, A., and Liu, H. (2014). An adaptive PID neural network for complex nonlinear system control. *Neurocomputing*, 135, 79–85. <https://doi.org/http://dx.doi.org/10.1016/j.neucom.2013.03.065>
- Khezri, M., and Jahed, M. (2011). A Neuro-Fuzzy Inference System for sEMG-Based Identification of Hand Motion Commands. *IEEE Transactions on Industrial Electronics*, 58(5), 1952–1960. <https://doi.org/10.1109/TIE.2010.2053334>
- Khushaba, R. N., Al-Ani, A., and Al-Jumaily, A. (2010). Orthogonal Fuzzy Neighborhood Discriminant Analysis for Multifunction Myoelectric Hand Control. *IEEE Transactions on Biomedical Engineering*, 57(6), 1410–1419. <https://doi.org/10.1109/TBME.2009.2039480>
- Khushaba, R. N., and Kodagoda, S. (2012). Electromyogram (EMG) feature reduction using Mutual Components Analysis for multifunction prosthetic fingers control. In *Control Automation Robotics & Vision (ICARCV), 2012 12th International Conference on* (pp. 1534–1539). <https://doi.org/10.1109/ICARCV.2012.6485374>
- Khushaba, R. N., Kodagoda, S., Liu, D., and Dissanayake, G. (2011). Electromyogram (EMG) based fingers movement recognition using Neighborhood Preserving Analysis with QR-decomposition. In *Proceedings of the 2011 7th International Conference on Intelligent Sensors, Sensor Networks and Information Processing, ISSNIP 2011*. <https://doi.org/10.1109/ISSNIP.2011.6146512>
- Khushaba, R. N., Kodagoda, S., Takruri, M., and Dissanayake, G. (2012). Toward improved control of prosthetic fingers using surface electromyogram (EMG) signals. *Expert Systems with Applications*, 39(12), 10731–10738. <https://doi.org/http://dx.doi.org/10.1016/j.eswa.2012.02.192>
- Kiguchi, K. (2007). Active exoskeletons for upper-limb motion assist. *International Journal of Humanoid Robotics*, 04(03), 607–624. <https://doi.org/10.1142/S0219843607001175>
- Kline, T., Kamper, D., and Schmit, B. (2005). Control system for pneumatically controlled glove to assist in grasp activities. In *9th International Conference on Rehabilitation Robotics, 2005. ICORR 2005*. (pp. 78–81). <https://doi.org/10.1109/ICORR.2005.1501056>
- Koeneman EJ Wolf SL, Herring DE, Koeneman JB, S. R. S. (2004). A pneumatic muscle hand therapy device. *Conf Proc IEEE EngMed BiolSoc*.
- Kong, Y. K., and Kim, D. M. (2015). The relationship between hand anthropometrics, total grip

- strength and individual finger force for various handle shapes. *International Journal of Occupational Safety and Ergonomics*. <https://doi.org/10.1080/10803548.2015.1029726>
- Konrad, P. (2006). *The ABC of EMG: A Practical Introduction to Kinesiological Electromyography*.
- Lalitharatne, S. W. H. M. T. D. (2014). *A Study of Controlling Upper-Limb Exoskeletons Using EMG and EEG signals*. Department of Science and Advanced Technology, Saga University.
- Lambercy, O., Schröder, D., Zwicker, S., and Gassert, R. (2013). Design of a thumb exoskeleton for hand rehabilitation. In *Proceedings of the 7th International Convention on Rehabilitation Engineering and Assistive Technology* (p. 41:1--41:4). Kaki Bukit TechPark II, Singapore: Singapore Therapeutic, Assistive & Rehabilitative Technologies (START) Centre. Retrieved from <http://dl.acm.org/citation.cfm?id=2567429.2567477>
- Lee, K. S., and Jung, M. C. (2014). Flexion and extension angles of resting fingers and wrist. *International Journal of Occupational Safety and Ergonomics*. <https://doi.org/10.1080/10803548.2014.11077038>
- Lenny Lucas and Yoky Matsuoka, M. D. (2004). An EMG-Controlled Hand Exoskeleton for Natural Pinching. *Journal of Robotics and Mechatronics, Vol.16 No.*
- Li, J., Zhang, Z., Tao, C., and Ji, R. (2017). A number synthesis method of the self-adapting upper-limb rehabilitation exoskeletons. *International Journal of Advanced Robotic Systems, 14(3)*, 1729881417710796. <https://doi.org/10.1177/1729881417710796>
- Luca, C. J. De. (1979). Physiology and Mathematics of Myoelectric Signals. *IEEE Transactions on Biomedical Engineering, BME-26(6)*, 313–325. <https://doi.org/10.1109/TBME.1979.326534>
- Marinov, B. (2015). Daiya Industry Pneumatic Power Assist Glove. Retrieved November 26, 2018, from <https://exoskeletonreport.com/2015/12/daiya-industry-pneumatic-power-assist-glove/>
- Martinez, L. A., Olaloye, O. O., Talarico, M. V, Shah, S. M., Arends, R. J., and BuSha, B. F. (2010). A power-assisted exoskeleton optimized for pinching and grasping motions. In *Proceedings of the 2010 IEEE 36th Annual Northeast Bioengineering Conference (NEBEC)* (pp. 1–2). <https://doi.org/10.1109/NEBC.2010.5458232>
- McLain, T. M. (2010). *The use of factor analysis in the development of hand sizes for glove design*.
- Meng, Q., Meng, Q., Yu, H., and Wei, X. (2017). A survey on sEMG control strategies of wearable hand exoskeleton for rehabilitation. In *2017 2nd Asia-Pacific Conference on Intelligent Robot Systems, ACIRS 2017*. <https://doi.org/10.1109/ACIRS.2017.7986086>
- Meng, W., Liu, Q., Zhou, Z., and Ai, Q. (2014). Active interaction control applied to a lower limb rehabilitation robot by using EMG recognition and impedance model. *Industrial Robot: An International Journal, 41(5)*, 465–479. <https://doi.org/doi:10.1108/IR-04-2014-0327>
- Miranda-Linares, D., Alrezage, G., and Tokhi, M. O. (2015). Control of lower limb exoskeleton for elderly assistance on basic mobility tasks. In *2015 19th International Conference on System Theory, Control and Computing, ICSTCC 2015 - Joint Conference SINTES 19, SACCS 15, SIMSIS 19*. <https://doi.org/10.1109/ICSTCC.2015.7321333>

- Mohamad, A. J., Sidek, S. N., Mohideen, A. J. H., Ibrahim, M. T., and Ali, K. (2012). Development of EMG measurement system to control mobile robot using frontalis and zygomaticus major muscles. In *Biomedical Engineering and Sciences (IECBES), 2012 IEEE EMBS Conference on* (pp. 1009–1013). <https://doi.org/10.1109/IECBES.2012.6498126>
- Mohideen, A. J. H., and Sidek, S. N. (2011). Development of EMG circuit to study the relationship between flexor digitorum superficialis muscle activity and hand grip strength. In *Mechatronics (ICOM), 2011 4th International Conference On* (pp. 1–7). <https://doi.org/10.1109/ICOM.2011.5937200>
- Moore, K. I., Dalley, A. F., and Agur, A. M. R. (2014). *Clinically oriented anatomy: upper limb* (7th Editio). Lippincott Williams & Wilkins.
- Muceli, S., and Farina, D. (2012). Simultaneous and proportional estimation of hand kinematics from EMG during mirrored movements at multiple degrees-of-freedom. *IEEE Transactions on Neural Systems and Rehabilitation Engineering*, 20(3), 371–378. <https://doi.org/10.1109/TNSRE.2011.2178039>
- Mulas, M., Folgheraiter, M., and Gini, G. (2005). An EMG-controlled exoskeleton for hand rehabilitation. *Proceedings of the 2005 IEEE 9th International Conference on Rehabilitation Robotics, 2005*, 371–374. <https://doi.org/10.1109/ICORR.2005.1501122>
- Myomo Inc. (2015). The MyoPro orthosis. Retrieved November 26, 2018, from <https://myomo.com/what-is-a-myopro-orthosis/>
- MyoMo Inc, and Compliance Solutions Ltd. (2017). *MyoPro user manual: sections for all MyoPro 2 devices*. Retrieved from <http://myomo.com/wp-content/uploads/2017/12/MyoPro-2-Motion-G-Full-Manual.pdf>
- Nag, A., Nag, P. K., and Desai, H. (2003). Hand anthropometry of Indian women. *Indian Journal of Medical Research*. <https://doi.org/10.1016/j.biotechadv.2011.08.021>. Secreted
- Ngeo, J. G., Tamei, T., and Shibata, T. (2014). Continuous and simultaneous estimation of finger kinematics using inputs from an EMG-to-muscle activation model. *Journal of NeuroEngineering and Rehabilitation*. <https://doi.org/10.1186/1743-0003-11-122>
- Ngeo, J., Tamei, T., and Shibata, T. (2012). Continuous estimation of finger joint angles using muscle activation inputs from surface EMG signals. In *Proceedings of the Annual International Conference of the IEEE Engineering in Medicine and Biology Society, EMBS*. <https://doi.org/10.1109/EMBC.2012.6346535>
- Ngeo, J., Tamei, T., Shibata, T., Orlando, M. F. F., Behera, L., Saxena, A., and Dutta, A. (2013). Control of an optimal finger exoskeleton based on continuous joint angle estimation from EMG signals. In *Proceedings of the Annual International Conference of the IEEE Engineering in Medicine and Biology Society, EMBS*. <https://doi.org/10.1109/EMBC.2013.6609506>
- NHS Healthcare Trust. (2014). Stroke: Information for patients, their carers, families and friends. Buckinghamshire Healthcare NHS Trust. Retrieved from <http://www.uhs.nhs.uk>
- Noritsugu, T., Takaiwa, M., and Sasaki, D. (2008). Power Assist Wear Driven with Pneumatic Rubber Artificial Muscles. In *2008 15th International Conference on Mechatronics and Machine Vision in Practice* (pp. 539–544). <https://doi.org/10.1109/MMVIP.2008.4749589>

- Novak, D., and Riener, R. (2015). A survey of sensor fusion methods in wearable robotics. In *Robotics and Autonomous Systems*. <https://doi.org/10.1016/j.robot.2014.08.012>
- Peerdeman, B., Boerey, D., Kallenbergy, L., Stramigioli, S., and Misra, S. (2010). A biomechanical model for the development of myoelectric hand prosthesis control systems. In *2010 Annual International Conference of the IEEE Engineering in Medicine and Biology* (pp. 519–523). <https://doi.org/10.1109/IEMBS.2010.5626085>
- Pezent, E., Rose, C. G., Deshpande, A. D., and O'Malley, M. K. (2017). Design and characterization of the OpenWrist: A robotic wrist exoskeleton for coordinated hand-wrist rehabilitation. In *2017 International Conference on Rehabilitation Robotics (ICORR)* (pp. 720–725). <https://doi.org/10.1109/ICORR.2017.8009333>
- Phinyomark, A., Phukpattaranont, P., and Limsakul, C. (2012). Feature reduction and selection for EMG signal classification. *Expert Systems with Applications*. <https://doi.org/10.1016/j.eswa.2012.01.102>
- Phinyomark, A., Quaine, F., Charbonnier, S., Serviere, C., Tarpin-Bernard, F., and Laurillau, Y. (2013). EMG feature evaluation for improving myoelectric pattern recognition robustness. *Expert Systems with Applications*. <https://doi.org/10.1016/j.eswa.2013.02.023>
- Phinyomark, A., Quaine, F., Charbonnier, S., Serviere, C., Tarpin-Bernard, F., and Laurillau, Y. (2014). Feature extraction of the first difference of EMG time series for EMG pattern recognition. *Computer Methods and Programs in Biomedicine*. <https://doi.org/10.1016/j.cmpb.2014.06.013>
- Pons, J., Ceres, R., and Calderón, L. (2008). *Introduction to Wearable Robotics*. <https://doi.org/10.1002/9780470987667.ch1>
- Poole, J. L., Santhanam, D. D., and Latham, A. L. (2013). Hand impairment and activity limitations in four chronic diseases. *Journal of Hand Therapy*, 26(3), 232–237. <https://doi.org/https://doi.org/10.1016/j.jht.2013.03.002>
- Raghavan, P. (2007). The nature of hand motor impairment after stroke and its treatment. *Current Treatment Options in Cardiovascular Medicine*, 9(3), 221–228. <https://doi.org/10.1007/s11936-007-0016-3>
- Raghavan, P. (2015). Upper Limb Motor Impairment After Stroke. *Physical Medicine and Rehabilitation Clinics of North America*, 26(4), 599–610. <https://doi.org/https://doi.org/10.1016/j.pmr.2015.06.008>
- Rehab-Robotics. (2015). Hand of hope. Retrieved November 26, 2018, from <http://www.rehab-robotics.com/hoh/index.html>
- Rose, C. G., Sergi, F., Yun, Y., Madden, K., Deshpande, A. D., and O'Malley, M. K. (2015). Characterization of a hand-wrist exoskeleton, READAPT, via kinematic analysis of redundant pointing tasks. In *IEEE International Conference on Rehabilitation Robotics*. <https://doi.org/10.1109/ICORR.2015.7281200>
- Rotella, M. F., Reuther, K. E., Hofmann, C. L., Hage, E. B., and BuSha, B. F. (2009). An orthotic hand-assistive exoskeleton for actuated pinch and grasp. In *2009 IEEE 35th Annual Northeast Bioengineering Conference* (pp. 1–2). <https://doi.org/10.1109/NEBC.2009.4967693>
- Sasaki, D., Noritsugu, T., and Takaiwa, M. (2005). Development of Active Support Splint driven

- by Pneumatic Soft Actuator (ASSIST). In *Proceedings of the 2005 IEEE International Conference on Robotics and Automation* (pp. 520–525). <https://doi.org/10.1109/ROBOT.2005.1570171>
- Shields Main, J. A., Peterson, S. W. and Strauss, A. M., B. L. (1997). An anthropomorphic hand exoskeleton to prevent astronaut hand fatigue during extravehicular activities. *Proc. of The IEEE Transactions on Systems, Man and Cybernetics, Part A: Systems and Humans*,.
- Shrirao, N. A., Reddy, N. P., and Kosuri, D. R. (2009). Neural network committees for finger joint angle estimation from surface EMG signals. *BioMedical Engineering Online*. <https://doi.org/10.1186/1475-925X-8-2>
- Sidek, S. N., and Mohideen, A. J. H. (2012). Mapping of EMG signal to hand grip force at varying wrist angles. In *Biomedical Engineering and Sciences (IECBES), 2012 IEEE EMBS Conference on* (pp. 648–653). <https://doi.org/10.1109/IECBES.2012.6498069>
- Song, R., Tong, K. Y., Hu, X. L., and Zheng, X. J. (2007). Myoelectrically Controlled Robotic System That Provide Voluntary Mechanical Help for Persons after Stroke. In *2007 IEEE 10th International Conference on Rehabilitation Robotics* (pp. 246–249). <https://doi.org/10.1109/ICORR.2007.4428434>
- Suresh, N., Li, X., Zhou, P., and Rymer, W. Z. (2011). Examination of motor unit control properties in stroke survivors using surface EMG decomposition: A preliminary report. In *2011 Annual International Conference of the IEEE Engineering in Medicine and Biology Society* (pp. 8243–8246). <https://doi.org/10.1109/IEMBS.2011.6092032>
- Swanson, A. B., Göran-Hagert, C., and de Groot Swanson, G. (1987). Evaluation of impairment in the upper extremity. *The Journal of Hand Surgery*, 12(5, Part 2), 896–926. [https://doi.org/https://doi.org/10.1016/S0363-5023\(87\)80257-5](https://doi.org/https://doi.org/10.1016/S0363-5023(87)80257-5)
- Takahashi CD Le V, Motiwala RR, Cramer SC, D.-Y. L. (2008). Robot-based handmotor therapy after stroke. *Brain*.
- The Festo Group. (2012). ExoHand: new areas fo action for man and machine. Retrieved November 26, 2018, from <https://www.festo.com/group/en/cms/10233.htm>
- The Stroke Association. (2018a). Physical effects of stroke. England and Wales. Retrieved from <http://http/https://www.stroke.org.uk>
- The Stroke Association. (2018b). State of nation: stroke statistic. England, United Kingdom: The Stroke Association. Retrieved from <http://www.stroke.org.uk>
- Tong, K. Y., Ho, S. K., Pang, P. M. K., Hu, X. L., Tam, W. K., Fung, K. L., Wei, X. J., Chen, P. N., and Chen, M. (2010). An intention driven hand functions task training robotic system. *2010 Annual International Conference of the IEEE Engineering in Medicine and Biology Society, EMBC'10*, 3406–3409. <https://doi.org/10.1109/IEMBS.2010.5627930>
- Trybus, M., Lorkowski, J., Brongel, L., and Hřadki, W. (2006). Causes and consequences of hand injuries. *The American Journal of Surgery*, 192(1), 52–57. <https://doi.org/https://doi.org/10.1016/j.amjsurg.2005.10.055>
- Tucker, M. R., Olivier, J., Pagel, A., Bleuler, H., Bouri, M., Lamercy, O., Del Millán, J. R., Riener, R., Vallery, H., and Gassert, R. (2015). Control strategies for active lower extremity prosthetics and orthotics: A review. *Journal of NeuroEngineering and Rehabilitation*.

<https://doi.org/10.1186/1743-0003-12-1>

- Tyromotion. (2018). AMADEO: the hand therapy world champion. Retrieved November 26, 2018, from <https://tyromotion.com/en/produkte/amadeo/>
- Varol, H. A., Sup, F., and Goldfarb*, M. (2010). Multiclass real-time intent recognition of a powered lower limb prosthesis. *IEEE Transactions on Biomedical Engineering*, 57(3), 542–551. <https://doi.org/10.1109/TBME.2009.2034734>
- Viteckova, S., Kutilek, P., de Boisboissel, G., Krupicka, R., Galajdova, A., Kauler, J., Lhotska, L., and Szabo, Z. (2018). Empowering lower limbs exoskeletons: state-of-the-art. *Robotica*, 36(11), 1743–1756. <https://doi.org/DOI: 10.1017/S0263574718000693>
- Wang, F., Shastri, M., Jones, C. L., Gupta, V., Osswald, C., Xuan, K., Kamper, D. G., Sarkar, N., Kang, X., Kamper, D. G., and Sarkar, N. (2011). Design and control of an actuated thumb exoskeleton for hand rehabilitation following stroke. *Proceedings - IEEE International Conference on Robotics and Automation*, 3688–3693. <https://doi.org/10.1109/ICRA.2011.5980099>
- Wang, S., Li, J., and Zheng, R. (2010). A Resistance Compensation Control Algorithm for a Cable-Driven Hand Exoskeleton for Motor Function Rehabilitation. In H. Liu, H. Ding, Z. Xiong, & X. Zhu (Eds.), *Intelligent Robotics and Applications: Third International Conference, ICIRA 2010, Shanghai, China, November 10-12, 2010. Proceedings, Part II* (pp. 398–404). Berlin, Heidelberg: Springer Berlin Heidelberg. https://doi.org/10.1007/978-3-642-16587-0_37 LB - Wang2010
- Wege, a., and Zimmermann, a. (2007). Electromyography sensor based control for a hand exoskeleton, 1470–1475. <https://doi.org/10.1109/ROBIO.2007.4522381>
- Wei, W., Guo, S., Zhang, F., Guo, J., Ji, Y., and Wang, Y. (2013). A novel upper limb rehabilitation system with hand exoskeleton mechanism. In *2013 IEEE International Conference on Mechatronics and Automation* (pp. 285–290). <https://doi.org/10.1109/ICMA.2013.6617932>
- Worden, K., Anderson, S. R., Baldacchino, T., Jacobs, W. R., and Rowson, J. (2018). Simultaneous force regression and movement classification of fingers via surface EMG within a unified bayesian framework. *Frontiers in Bioengineering and Biotechnology*. <https://doi.org/10.3389/fbioe.2018.00013>
- Worsnopp, T. T., Peshkin, M. a., Colgate, J. E., and Kamper, D. G. (2007). An actuated finger exoskeleton for hand rehabilitation following stroke. *2007 IEEE 10th International Conference on Rehabilitation Robotics, ICORR'07*, 00(c), 896–901. <https://doi.org/10.1109/ICORR.2007.4428530>
- Xu, J., Haith, A. M., and Krakauer, J. W. (2015). Motor control of the hand before and after stroke. In K. K., C. L., & B. N. (Eds.), *Clinical Systems Neuroscience*. Springer, Tokyo. https://doi.org/https://doi.org/10.1007/978-4-431-55037-2_14
- Yamada, Y., Morizono, T., Sato, S., Shimohira, T., Umetani, Y., Yoshida, T., and Aoki, S. (2001). Proposal of a SkilMate finger for EVA gloves. In *Robotics and Automation, 2001. Proceedings 2001 ICRA. IEEE International Conference on* (Vol. 2, pp. 1406–1412 vol.2). <https://doi.org/10.1109/ROBOT.2001.932807>
- Yang, J., Xie, H., and Shi, J. (2016). A novel motion-coupling design for a jointless tendon-driven

finger exoskeleton for rehabilitation. *Mechanism and Machine Theory*.
<https://doi.org/10.1016/j.mechmachtheory.2015.12.010>

Yasuhisa, H., Yasuyuki, M., Kosuke, W., and Yoshiyuki, S. (2008). Five-fingered assistive hand with mechanical compliance of human finger. In *Robotics and Automation, 2008. ICRA 2008. IEEE International Conference on* (pp. 718–724).
<https://doi.org/10.1109/ROBOT.2008.4543290>

Yu, W., Rosen, J., and Li, X. (2011). PID admittance control for an upper limb exoskeleton. In *Proceedings of the 2011 American Control Conference* (pp. 1124–1129).
<https://doi.org/10.1109/ACC.2011.5991147>

Zardoshti-Kermani, M., Wheeler, B. C., Badie, K., and Hashemi, R. M. (1995). EMG feature evaluation for movement control of upper extremity prostheses. *IEEE Trans Rehabil Eng*, 3.
<https://doi.org/10.1109/86.481972> LB - Zardoshti-Kermani1995

Appendix A: The commercially available exoskeleton hand

Characteristics	Assistive Device(s)		
			
Device Name	MyoPro	Daiya Glove	Carbonhand (or also known as SEM Glove)
Company	MyoMo Inc (2015)	Daiya Industry (2013)	Bioservo Technologies (2015)
Functions	Powered orthosis that work as a mobile assistive device.	A pneumatic power assist glove that employed the soft exoskeleton technology.	A soft powered glove use to assist individuals with weaken hand strength.
Basic Features	Portable and lightweight arm brace, a powered elbow orthosis with surface electromyography (EMG) sensors, a static or manually set multi-articulating wrist (MAW), and a powered 3-jaw-chuck grasp.	It consists a glove with three fingers compartment (with pink, ring and middle finger merged together), sensors, and a controller that link compressed gas canister.	A lightweight glove with sensors, a pouch with a controller and batteries and a connection system.
Supported Movement	Elbow flexion/extension, wrist flexion/extension and supination/pronation, and hand grasping.	Support bending and stretching of fingers.	Cover full degrees of freedom for the hand.
Approximate Cost	\$13,400 or \$ 150 per 1 hour session.	250, 000 yen	£4730 or €6000

Characteristics	Rehabilitation Device(s)			
				
Device Name	AMADEO	Hand of Hope	InMotion Hand	InMotion WRIST
Company	Tyromotion (2018)	Rehab-Robotics (2015)	Bionik Labs (2010a)	Bionik Labs (2010b)
Functions	Rehabilitation device using powered end effector exoskeleton.	Neuromuscular rehabilitation of the hand and forearm with biofeedback system.	Rehabilitation device that provides intensive sensorimotor grasp and release hand therapy.	Rehabilitation device that provides intensive sensorimotor wrist and forearm therapy
Basic Features	Adjustable hand-arm support, electrically driven mechanism, integrated biofeedback, a control and operating unit (all-in-one PC).	Hand brace with two surface sensors attached to the extensor and flexor muscle of the arm associated with real-time interactive games.	Contoured finger and thumb grips with adjustable-length forearm rest.	Robotic arm with 3 active degrees-of-freedom. Adjustable-height robot and workstation.
Supported Movement	Assistive and interactive therapies for flexion and extension movements of the finger and thumb.	Full range of motion for fingers, hand opening and grasping.	Grasp and release exercises combined with reaching movements	Wrist abduction/adduction, wrist flexion/extension Forearm pronation/supination Wrist and forearm combination
Approximate Cost	Overall cost is not stated. \$ 300 per 1-hour session.	€ 20, 000	Not stated	\$ 10, 000 +

Characteristics	Augmentative Device (s)		
			
Device Name	ExoHand	Ironhand	RoboGlove
Company	The Festo Group (2012)	Bioservo Technologies	General Motors and NASA
Functions	An augmentative exoskeleton that works as a master-slave system to tele-operate a robotic hand.	A soft powered glove for professional use that reduce fatigue and injury due to repetitive tasks. It employed soft extra muscle technology that can augment the user's finger force.	A force multiplying and motor assisted glove designed to help reducing the grasping force needed by the factory workers; either for extended time or for repetitive work.
Basic Features	Consists of eight double-action pneumatic actuators, potentiometer and pressure sensors which provide force amplification and force feedback to the overall system.	Consists of a glove that covers all fingers, equipped with sensors and servomotor, and a power unit.	Consists of a glove that covers all fingers, equipped with actuators and artificial tendons that mimic the muscles of the human hand.
Supported Movement	Covers full degrees of freedom for the hand and provide diverse techniques for grasping and objects handling.	Covers full degrees of freedom for the hand.	Covers full degrees of freedom for the hand.
Approximate Cost	Not stated.	Not stated.	Not stated.

Appendix B: Documentation for EMG data collection



Department of Automatic Control and Systems Engineering
Amy Johnson Building
The University of Sheffield
Portobello Street
Sheffield S1 3JD

03 May 2016

Dear participants

As part of the research requirements for doctoral program at The University of Sheffield (TUOS), I am conducting a research for the purpose of investigating the inter-relation between forearm electromyogram (EMG) signals hand grip force and wrist angles. This will feed into design of assistive exoskeleton hand control. The electromyogram is extracted from forearm muscles using surface electrodes thus non-invasive.

I would welcome your participation (participants either male or female aged between 30 to 40 years old) is entirely voluntary, and you may withdraw from this study at any time. The promise of strict confidentiality is assured in both the collection and reporting of the data. Any findings obtained in connection with this study will be presented in such a way that no individual will be identifiable. By completing the attached consent form, you will be granting me permission to publish aggregated results in my dissertation, in peer reviewed journals, and at professional conferences.

Hopefully, the results from this research will enhance the technology in communication between human and machine and assist the control development of exoskeleton hand in ways that would benefit and assist stroke survivors and others. Should you have any questions about this study, please contact me at nabas1@sheffield.ac.uk. Thank you in advance for your time and willingness to participate in this study.

Sincerely,

~~Norafizah~~ Abas
PhD Candidate
E-mail: nabas1@sheffield.ac.uk

Title of Research Project: Development of Exoskeleton Hand Controller Based on Forearm Electromyogram Signal

Name of Researcher: Norafizah Abas

Participant Identification Number for this project:

Please initial box

1. I confirm that I have read and understand the information letter dated 03 May 2016 explaining the above research project and I have had the opportunity to ask questions about the project.
2. I understand that my participation is voluntary and that I am free to withdraw at any time without giving any reason and without there being any negative consequences. In addition, should I not wish to proceed with any particular procedure or procedures in any of the experiment, I am free to decline.
3. I understand that my responses will be kept strictly confidential. I give permission for the researcher to have access to my anonymised responses. I understand that my name will not be linked with the research material, and I will not be identified or identifiable in the report or reports that result from the research.
4. I agree for the data collected from me to be used in future research.
5. I agree to take part in the above research project.

Name of Participant

Date

Signature

Norafizah Abas

Date

Signature

PhD Candidate

Department of Automatic Control and Systems Engineering

Amy Johnson Building

The University of Sheffield

Portobello Street

Sheffield S1 3JD

E-mail: nabas1@sheffield.ac.uk

Appendix C: Time domain features without normalisation for finger movements

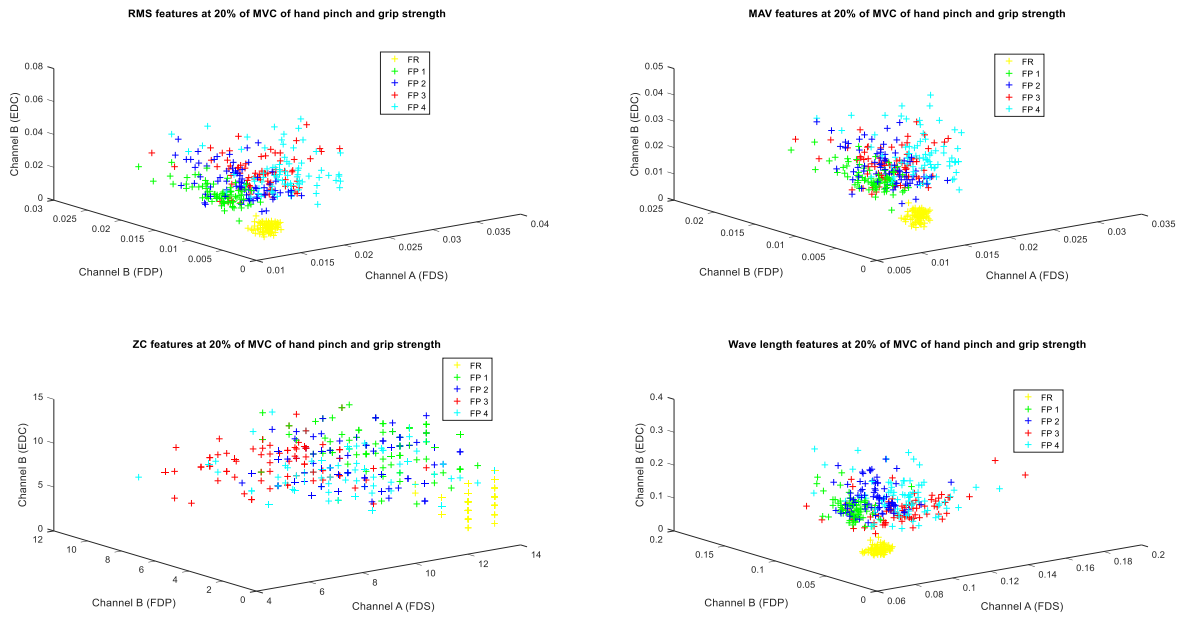


Figure C.1: Features extracted (from FDS, FDP and EDC muscles) at 20% of MVC finger pinch strength for four medial fingers

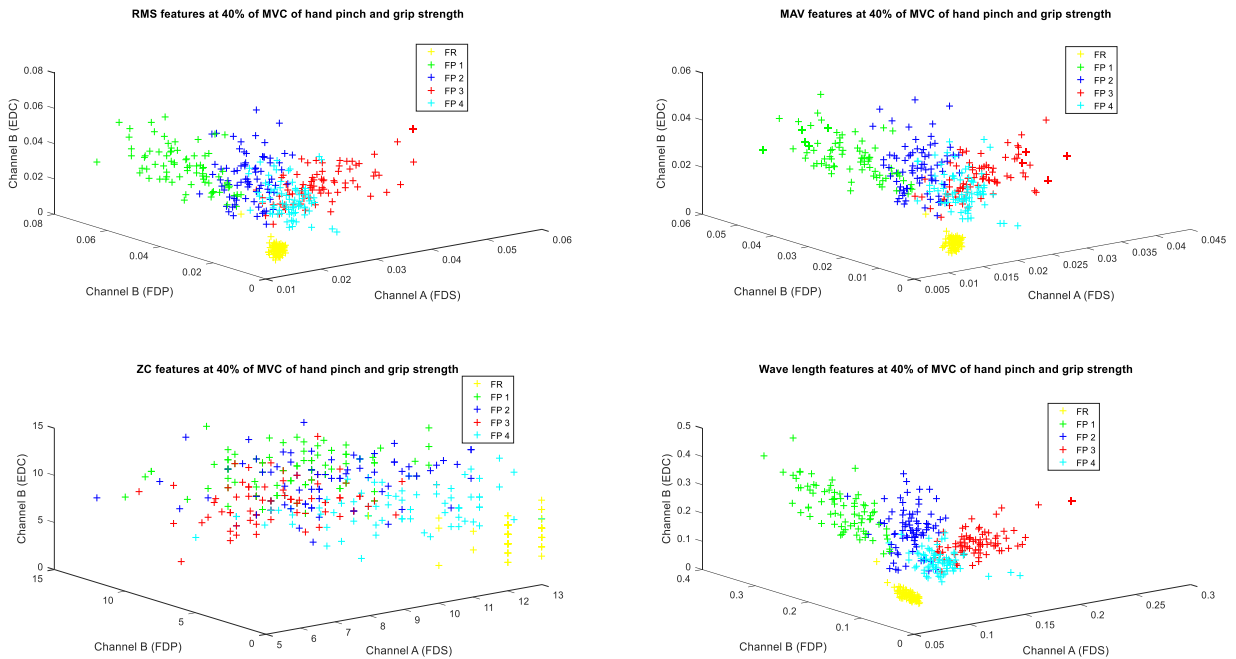


Figure C.2: Features extracted (from FDS, FDP and EDC muscles) at 40% of MVC finger pinch strength for four medial fingers

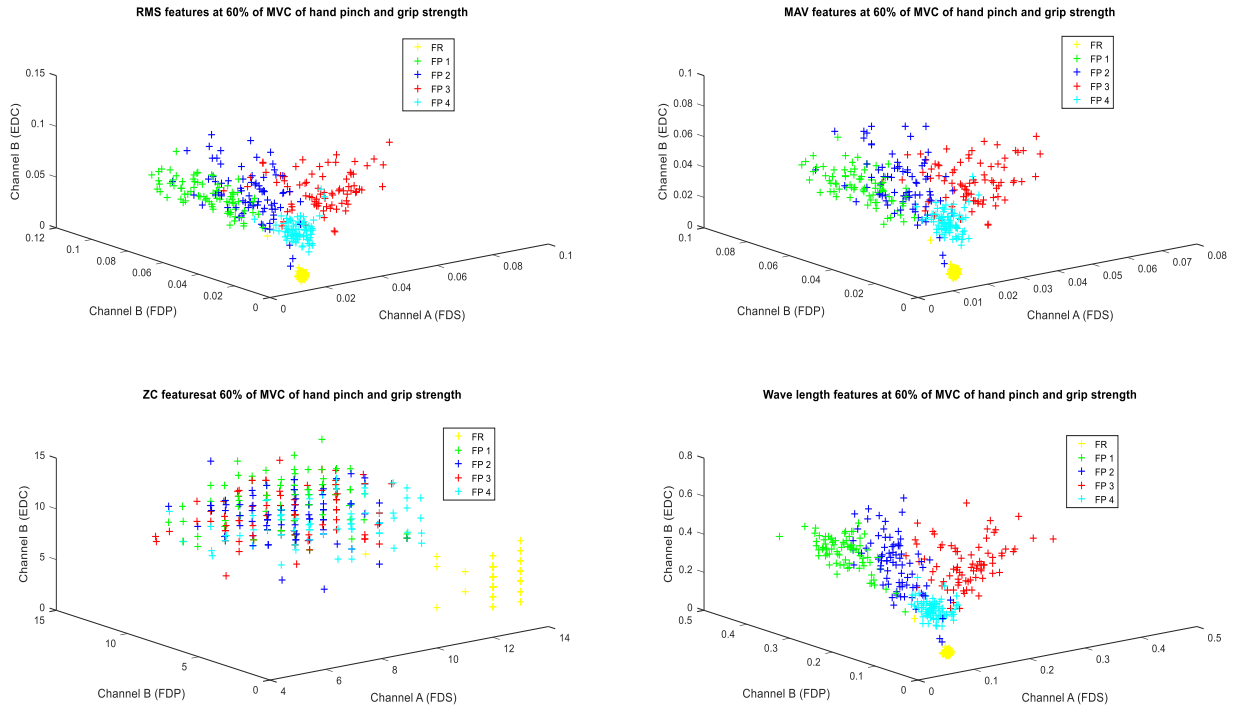


Figure C.3: Features extracted (from FDS, FDP and EDC muscles) at 60% of MVC finger pinch strength for four medial fingers

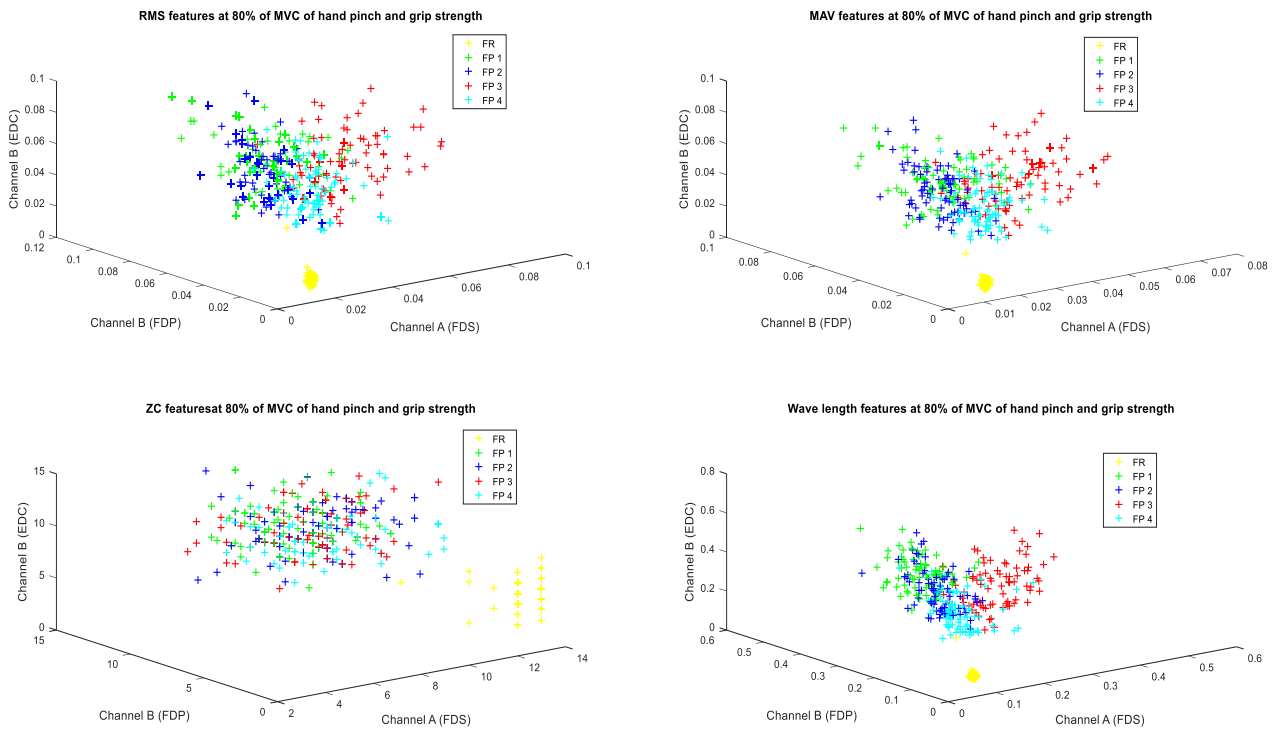


Figure C.4: Features extracted (from FDS, FDP and EDC muscles) at 80% of MVC finger pinch strength for four medial fingers

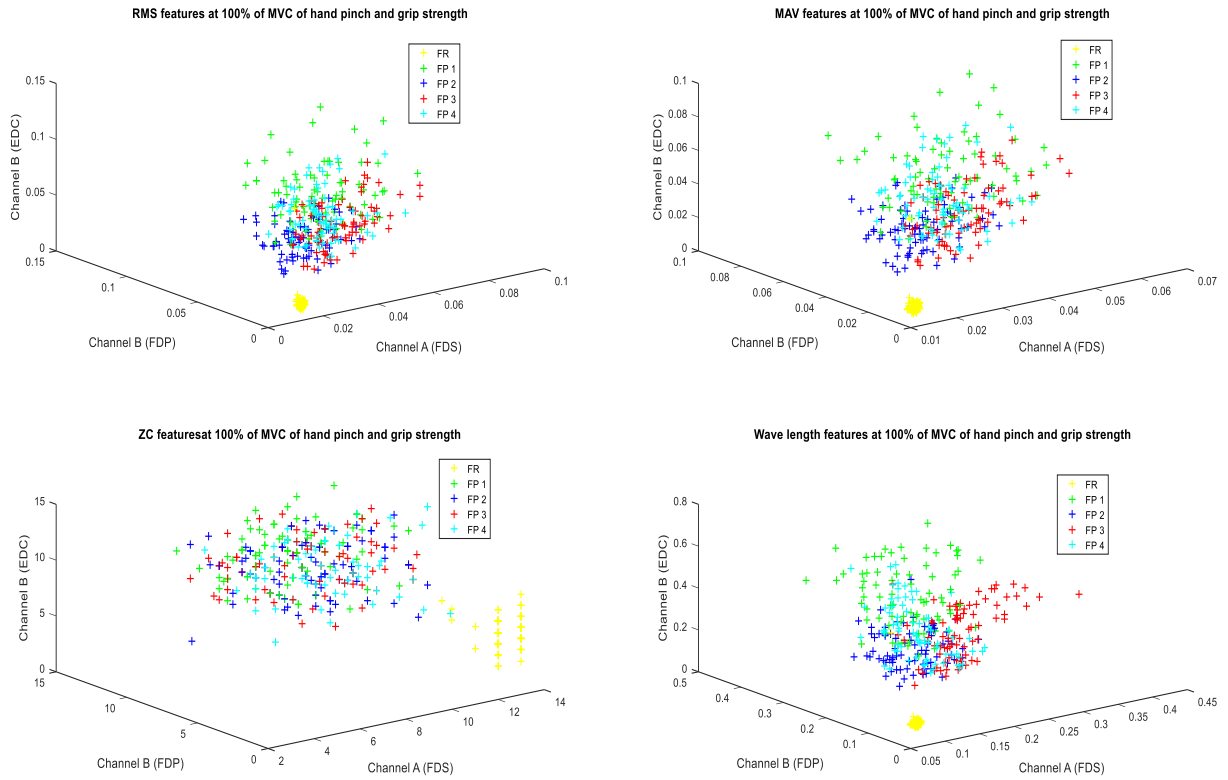


Figure C.5: Features extracted (from FDS, FDP and EDC muscles) at 100% of MVC finger pinch strength for four medial fingers

Appendix D: Time domain features with normalisation for finger movements

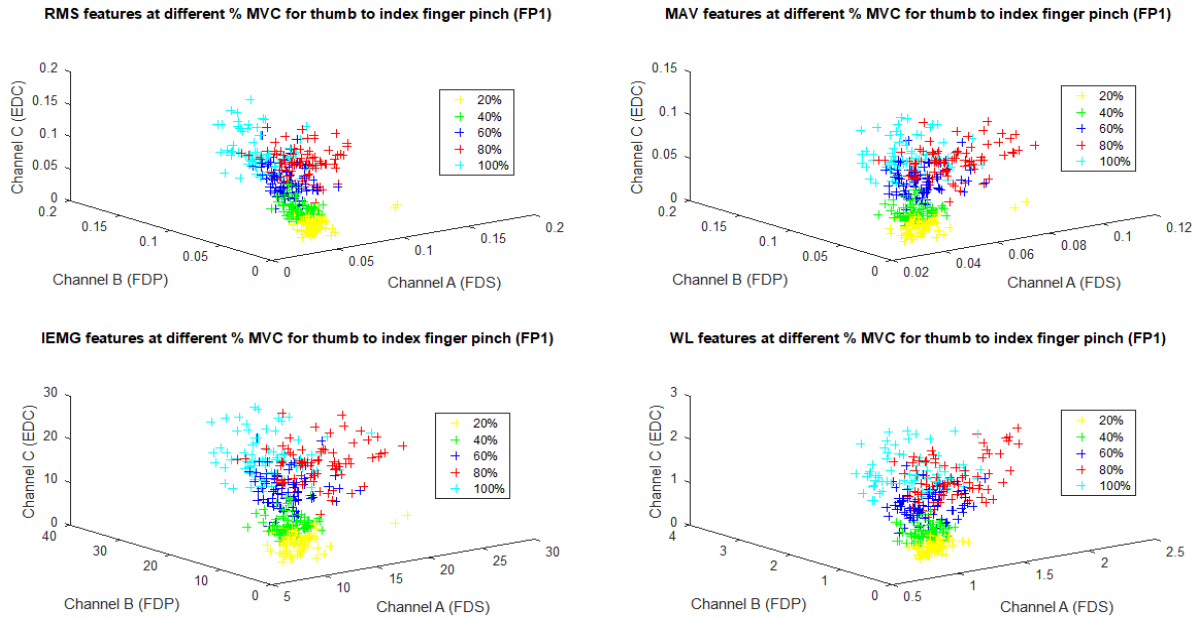


Figure D.1: Extracted features from FDS, FDP and EDC muscles based on normalised EMG at different % of MVC (from 20 to 100%) for index to thumb finger pinch (FP1)

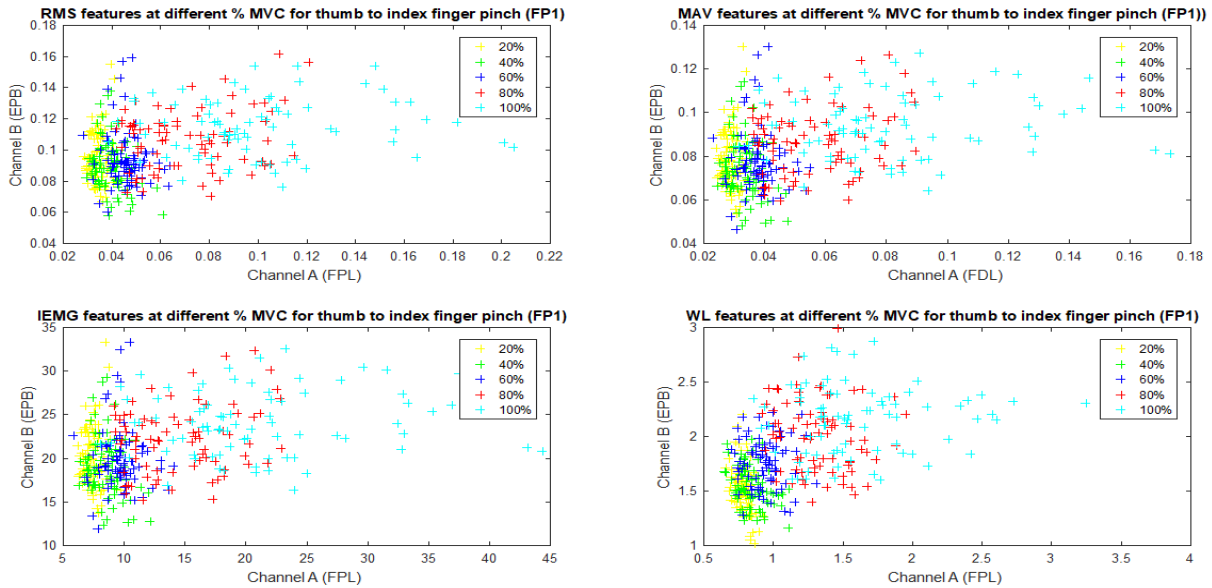


Figure D.2: Extracted features from FPL and EPB muscles based on normalised EMG at different % of MVC (from 20 to 100%) for index to thumb finger pinch (FP1). The FPL and EPB muscles are contributed to the thumb movement

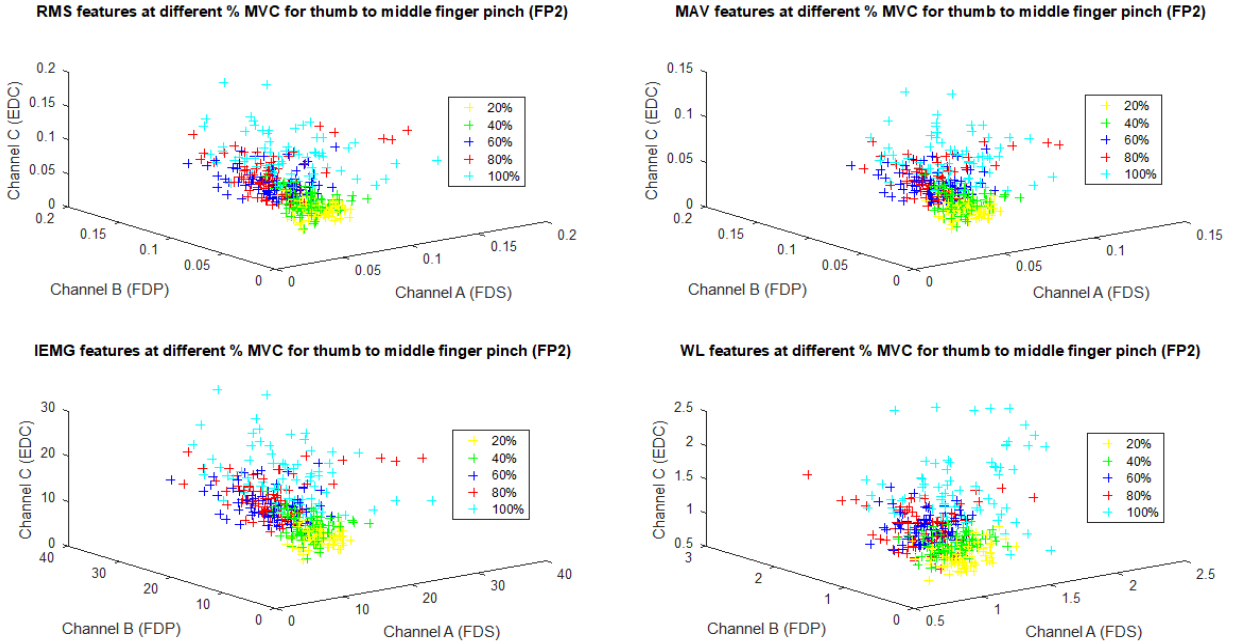


Figure D.3: Extracted features from FDS, FDP and EDC muscles based on normalised EMG at different % of MVC (from 20 to 100%) for middle to thumb finger pinch (FP2)

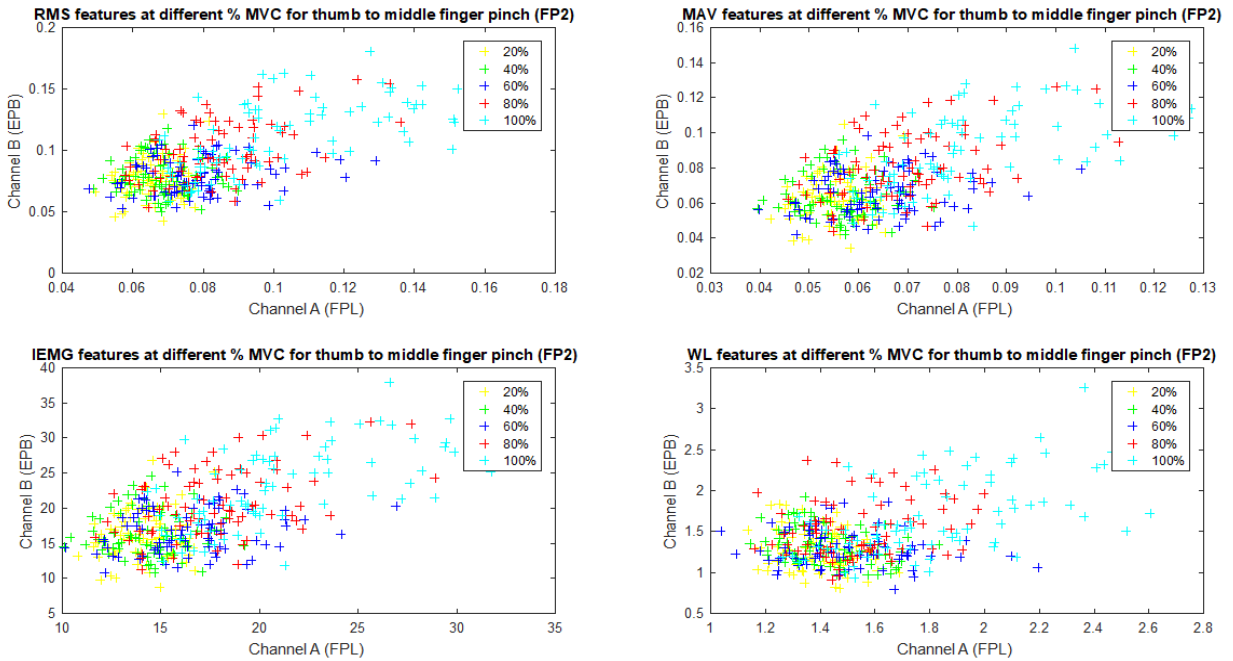


Figure D.4: Extracted features from FPL and EPB muscles based on normalised EMG at different % of MVC (from 20 to 100%) for middle to thumb finger pinch (FP2). The FPL and EPB muscles are contributed to the thumb movement

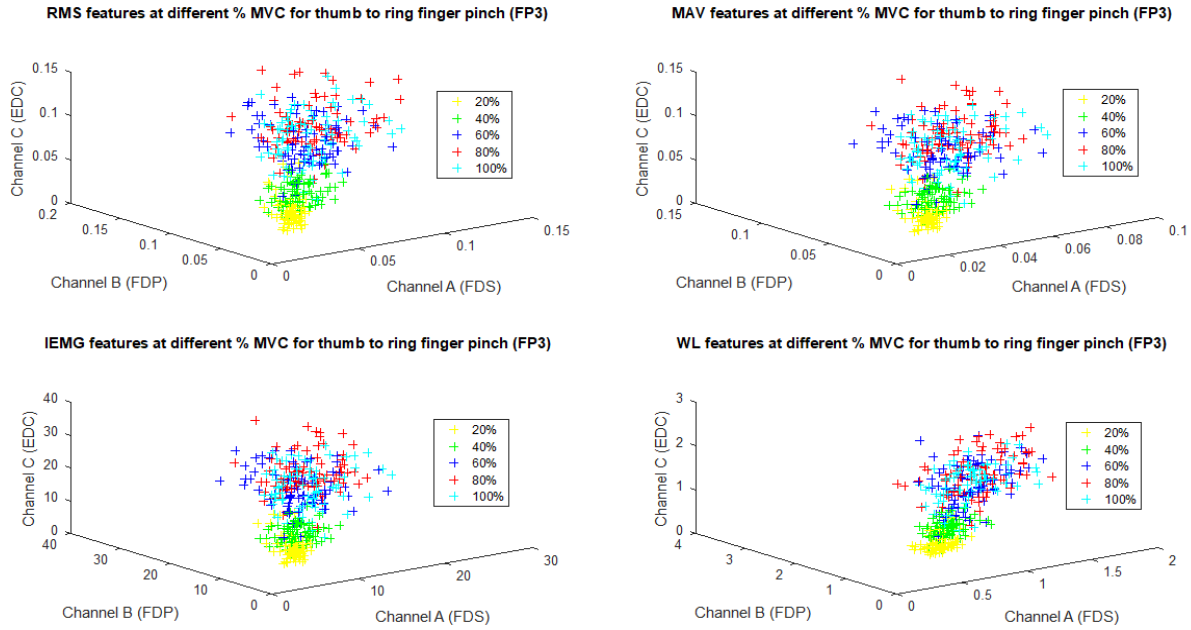


Figure D.5: Extracted features from FDS, FDP and EDC muscles based on normalised EMG at different % of MVC (from 20 to 100%) for ring to thumb finger pinch (FP3)

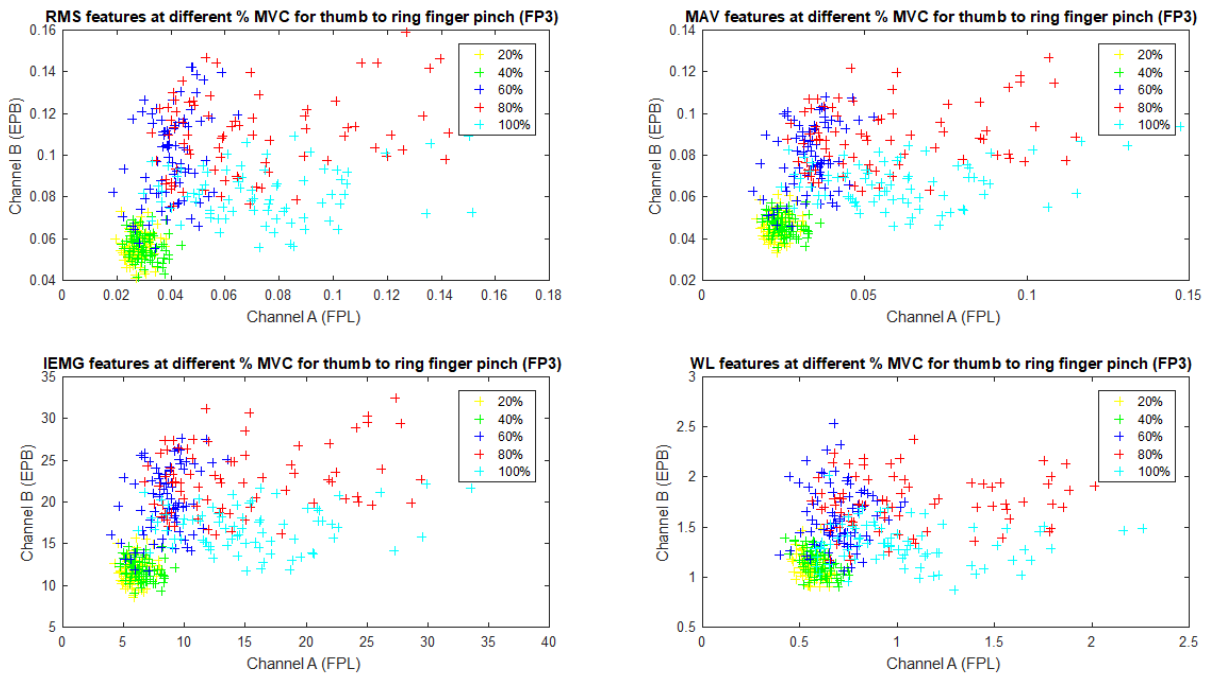


Figure D.6: Extracted features from FPL and EPB muscles based on normalised EMG at different % of MVC (from 20 to 100%) for ring to thumb finger pinch (FP3). The FPL and EPB muscles are contributed to the thumb movement

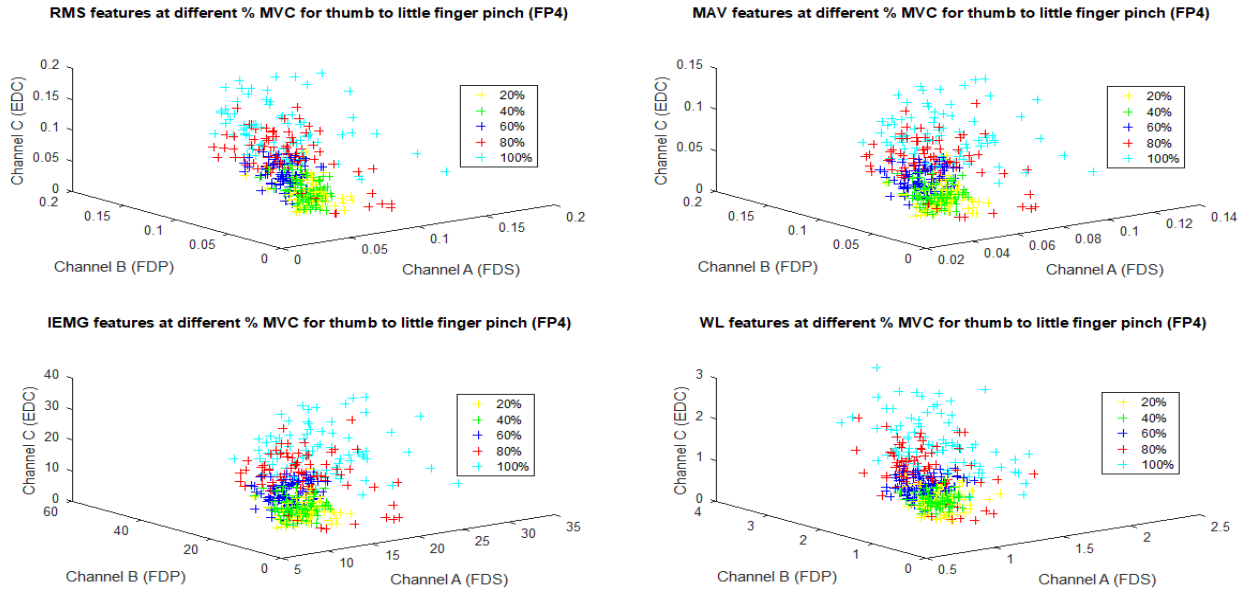


Figure D.7: Extracted features from FDS, FDP and EDC muscles based on normalised EMG at different % of MVC (from 20 to 100%) for middle to thumb finger pinch (FP4). Each of the MVC percentage of normalised EMG is corresponding to the same MVC percentage of finger pinch strength

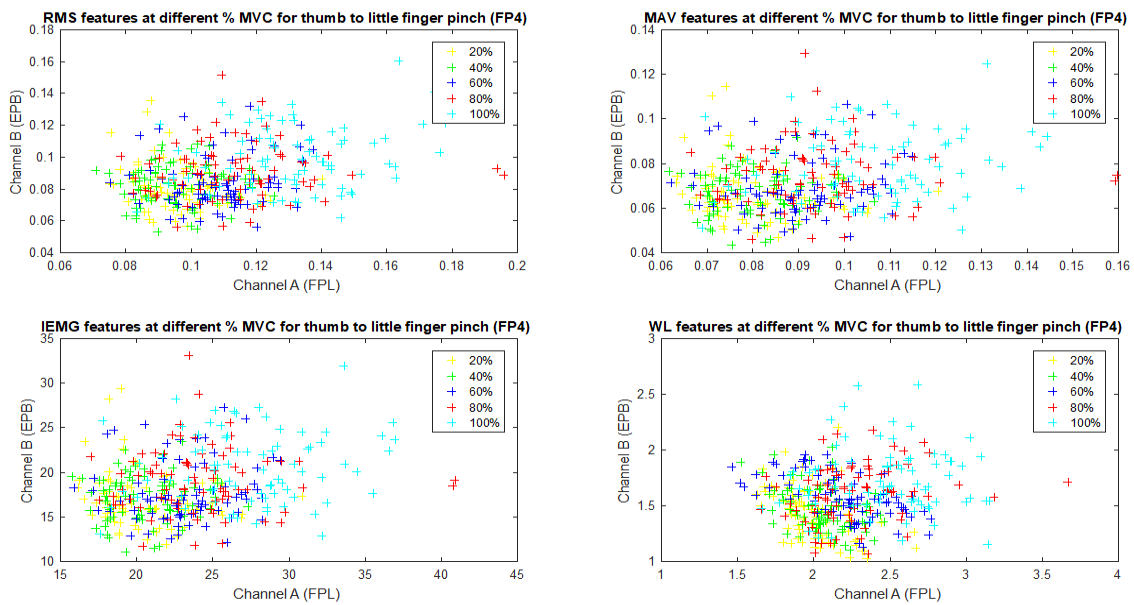


Figure D.8: Extracted features from FPL and EPB muscles based on normalised EMG at different % of MVC (from 20 to 100%) for pinky to thumb finger pinch (FP4). The FPL and EPB muscles are contributed to the thumb movement

Appendix E: The standard deviation computed for the features contributed to the finger movement

Task/Motion	Feature	Muscles	Standard deviation values				
			20% of MVC	40% of MVC	60% of MVC	80% of MVC	100% of MVC
Index to thumb pinch (FP1)	RMS	FDS	0.0115	0.0062	0.0139	0.0197	0.0187
		FDP	0.0047	0.0092	0.0213	0.0204	0.0229
		EDC	0.0076	0.0107	0.0139	0.0156	0.0207
		FPL	0.0032	0.0060	0.0066	0.0207	0.0368
		EPB	0.0165	0.0165	0.0181	0.0194	0.0182
	MAV	FDS	0.0074	0.0052	0.0095	0.0144	0.0126
		FDP	0.0039	0.0072	0.0171	0.0170	0.0184
		EDC	0.0063	0.0078	0.0104	0.0123	0.0132
		FPL	0.0027	0.0050	0.0058	0.0153	0.0302
		EPB	0.0137	0.0135	0.0143	0.0151	0.0145
	IEMG	FDS	1.9009	1.3236	2.4298	3.6853	3.2184
		FDP	0.9890	1.8378	4.3677	4.3563	4.7075
		EDC	1.6203	2.0040	2.6676	3.1512	3.3872
		FPL	0.6793	1.2706	1.4800	3.9162	7.7377
		EPB	3.5056	3.4676	3.6596	3.8666	3.7036
	WL	FDS	0.0841	0.1002	0.1818	0.2846	0.2821
		FDP	0.0412	0.1333	0.3260	0.3779	0.4293
		EDC	0.1080	0.1227	0.1959	0.2718	0.3126
		FPL	0.0542	0.1047	0.1292	0.2369	0.5166
		EPB	0.2269	0.1888	0.2234	0.3330	0.3068
Middle to thumb pinch (FP2)	RMS	FDS	0.0091	0.0101	0.0159	0.0252	0.0246
		FDP	0.0090	0.0111	0.0200	0.0294	0.0320
		EDC	0.0091	0.0121	0.0130	0.0148	0.0231
		FPL	0.0069	0.0087	0.0154	0.0162	0.0258
		EPB	0.0161	0.0149	0.0147	0.0239	0.0287
	MAV	FDS	0.0071	0.0077	0.0119	0.0192	0.0185
		FDP	0.0075	0.0089	0.0166	0.0233	0.0266
		EDC	0.0067	0.0085	0.0100	0.0100	0.0172
		FPL	0.0058	0.0075	0.0116	0.0130	0.0193
		EPB	0.0132	0.0123	0.0123	0.0191	0.0228
	IEMG	FDS	1.8250	1.9749	3.0393	4.9260	4.7476
		FDP	1.9132	2.2746	4.2600	5.9703	6.8085
		EDC	1.7202	2.1676	2.5483	2.5584	4.4001
		FPL	1.4930	1.9093	2.9594	3.3289	4.9462
		EPB	3.3757	3.1557	3.1477	4.8895	5.8478
	WL	FDS	0.1442	0.1456	0.1569	0.2096	0.3567
		FDP	0.1021	0.1344	0.2121	0.3871	0.4195
		EDC	0.1354	0.1248	0.1728	0.1950	0.3644
		FPL	0.1147	0.1491	0.2125	0.1978	0.3210
		EPB	0.2459	0.2248	0.2172	0.3369	0.4751

Ring to thumb pinch (FP3)	RMS	FDS	0.0072	0.0118	0.0220	0.0211	0.0212
		FDP	0.0142	0.0105	0.0280	0.0195	0.0223
		EDC	0.0091	0.0111	0.0184	0.0212	0.0218
		FPL	0.0039	0.0046	0.0087	0.0325	0.0303
		EPB	0.0069	0.0063	0.0216	0.0198	0.0140
	MAV	FDS	0.0051	0.0078	0.0159	0.0135	0.0143
		FDP	0.0111	0.0084	0.0225	0.0169	0.0177
		EDC	0.0067	0.0089	0.0152	0.0173	0.0168
		FPL	0.0031	0.0039	0.0072	0.0257	0.0242
		EPB	0.0061	0.0050	0.0161	0.0160	0.0105
	IEMG	FDS	1.2963	1.9928	4.0616	3.4631	3.6512
		FDP	2.8531	2.1411	5.7603	4.3180	4.5383
		EDC	1.7265	2.2873	3.9001	4.4165	4.2915
		FPL	0.7976	1.0059	1.8337	6.5775	6.2014
		EPB	1.5529	1.2924	4.1122	4.0973	2.6843
	WL	FDS	0.1010	0.1125	0.3148	0.2784	0.2464
		FDP	0.1279	0.1295	0.5273	0.4909	0.3505
		EDC	0.1277	0.1360	0.2852	0.3460	0.3070
		FPL	0.0505	0.0681	0.1250	0.4060	0.3686
		EPB	0.1182	0.1228	0.3041	0.2737	0.2025
Pinky to thumb pinch (FP4)	RMS	FDS	0.0087	0.0076	0.0091	0.0171	0.0225
		FDP	0.0130	0.0089	0.0146	0.0301	0.0358
		EDC	0.0152	0.0163	0.0144	0.0307	0.0289
		FPL	0.0127	0.0119	0.0135	0.0205	0.0209
		EPB	0.0143	0.0125	0.0162	0.0170	0.0198
	MAV	FDS	0.0066	0.0061	0.0072	0.0131	0.0170
		FDP	0.0094	0.0074	0.0115	0.0239	0.0303
		EDC	0.0106	0.0110	0.0106	0.0224	0.0208
		FPL	0.0111	0.0096	0.0118	0.0164	0.0174
		EPB	0.0120	0.0100	0.0130	0.0143	0.0155
	IEMG	FDS	1.6870	1.5582	1.8425	3.3516	4.3475
		FDP	2.4160	1.8845	2.9350	6.1216	7.7495
		EDC	2.7197	2.8119	2.7108	5.7441	5.3296
		FPL	2.8343	2.4678	3.0190	4.1962	4.4567
		EPB	3.0817	2.5504	3.3324	3.6652	3.9655
	WL	FDS	0.1192	0.0899	0.1377	0.1967	0.2480
		FDP	0.2317	0.1074	0.2005	0.4907	0.7308
		EDC	0.1881	0.1484	0.1689	0.4005	0.4329
		FPL	0.2073	0.1984	0.2995	0.3355	0.3572
		EPB	0.2400	0.1986	0.1943	0.2577	0.2943

Appendix F: Time domain features without normalisation for wrist movements

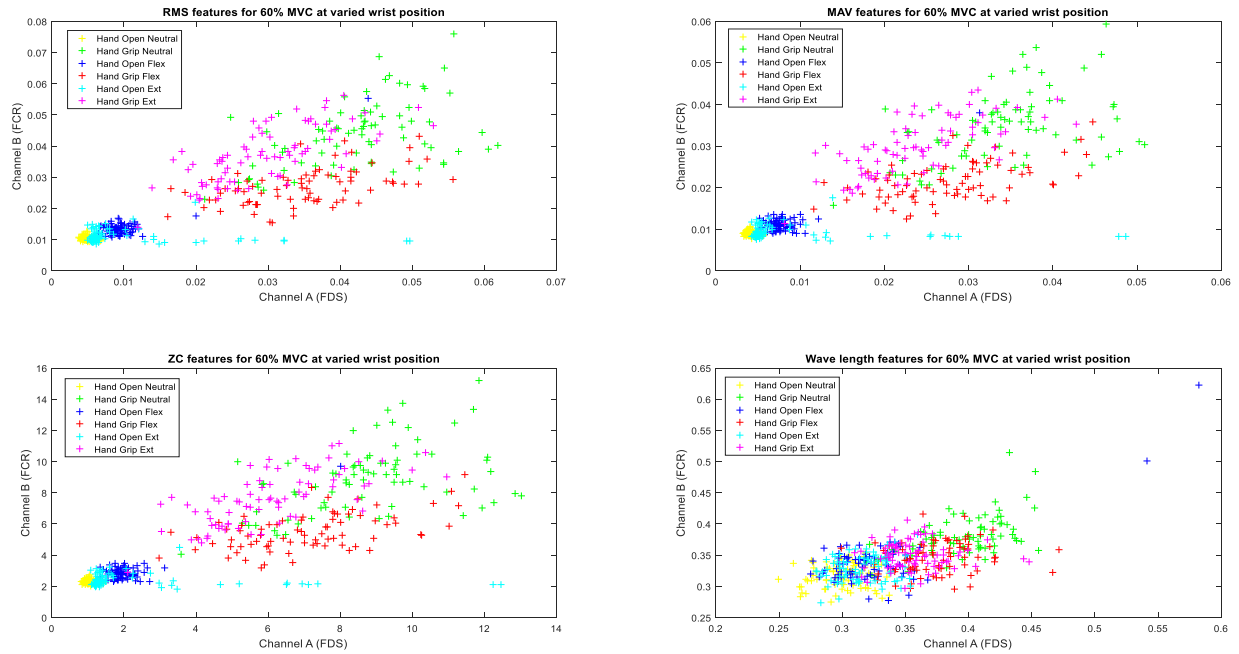


Figure F.1: Features extracted from flexor muscles (FDS and FCR muscles) at 60% of MVC finger pinch strength for various wrist positions

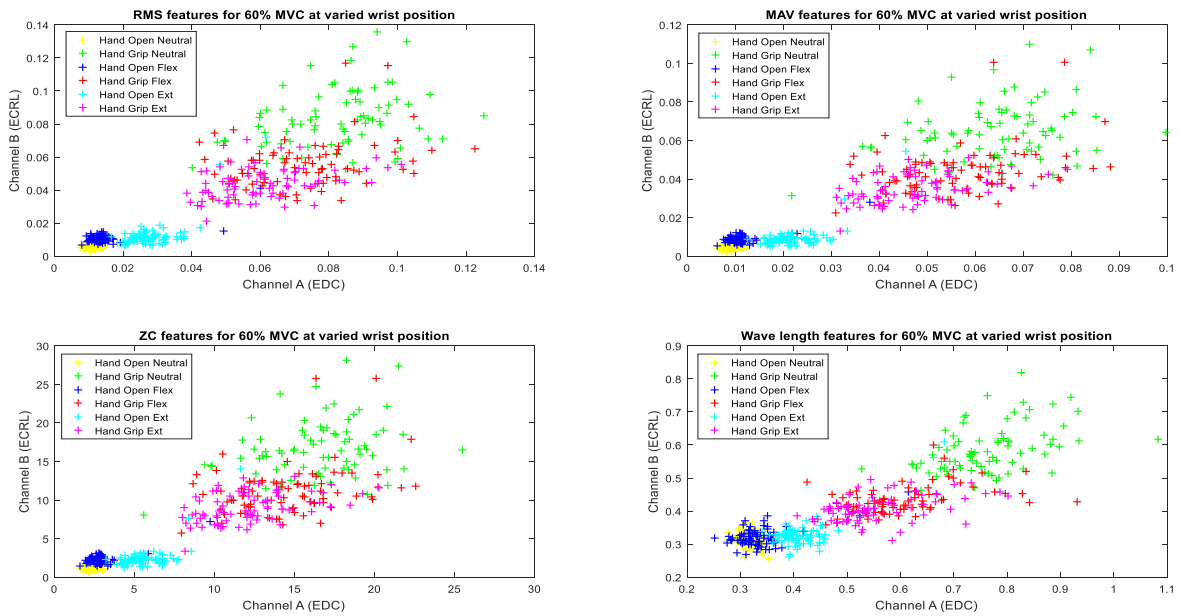


Figure F.2: Features extracted from extensor muscles (EDC and ECRL muscles) at 60% of MVC finger pinch strength for various wrist positions

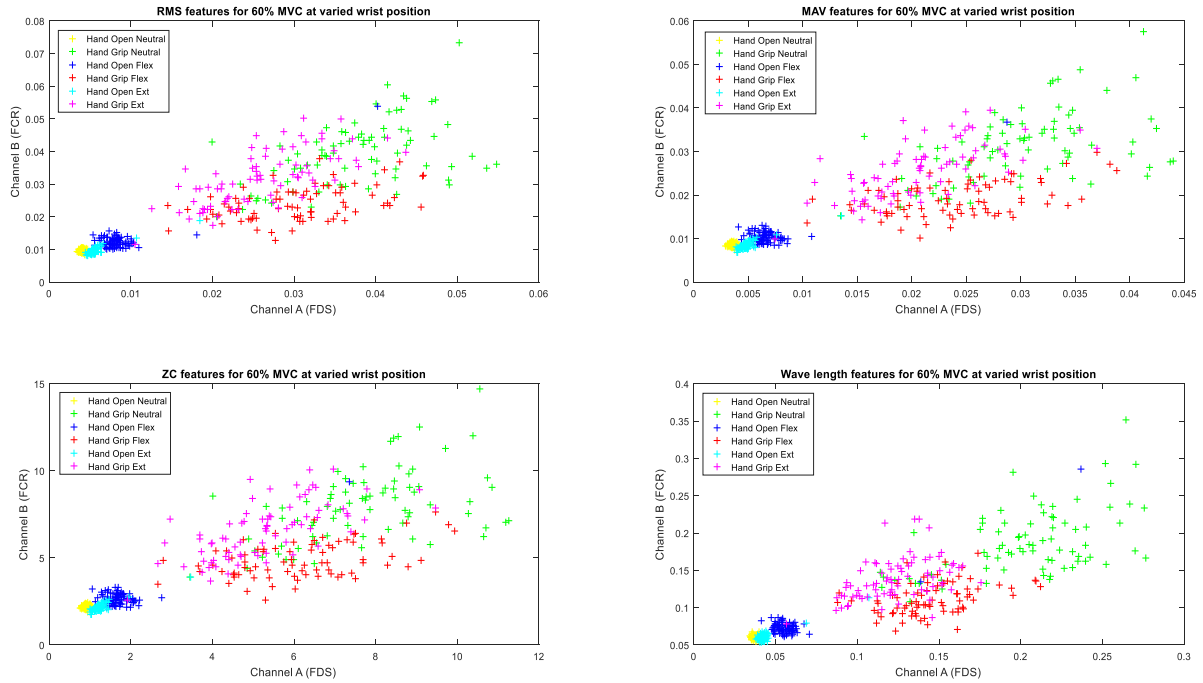


Figure F.3: Features extracted from flexor muscles (FDS and FCR muscles) at 60% of MVC finger pinch strength for various wrist positions (with filter)

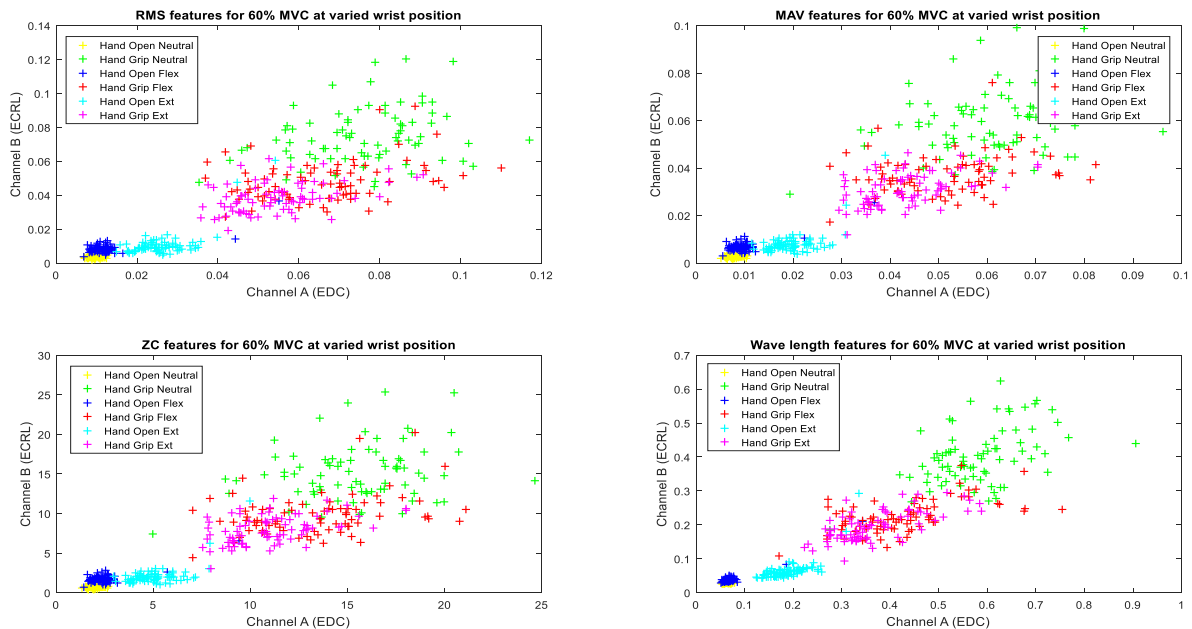


Figure F.4: Features extracted from extensor muscles (EDC and ECRL muscles) at 60% of MVC finger pinch strength for various wrist positions (with filter)

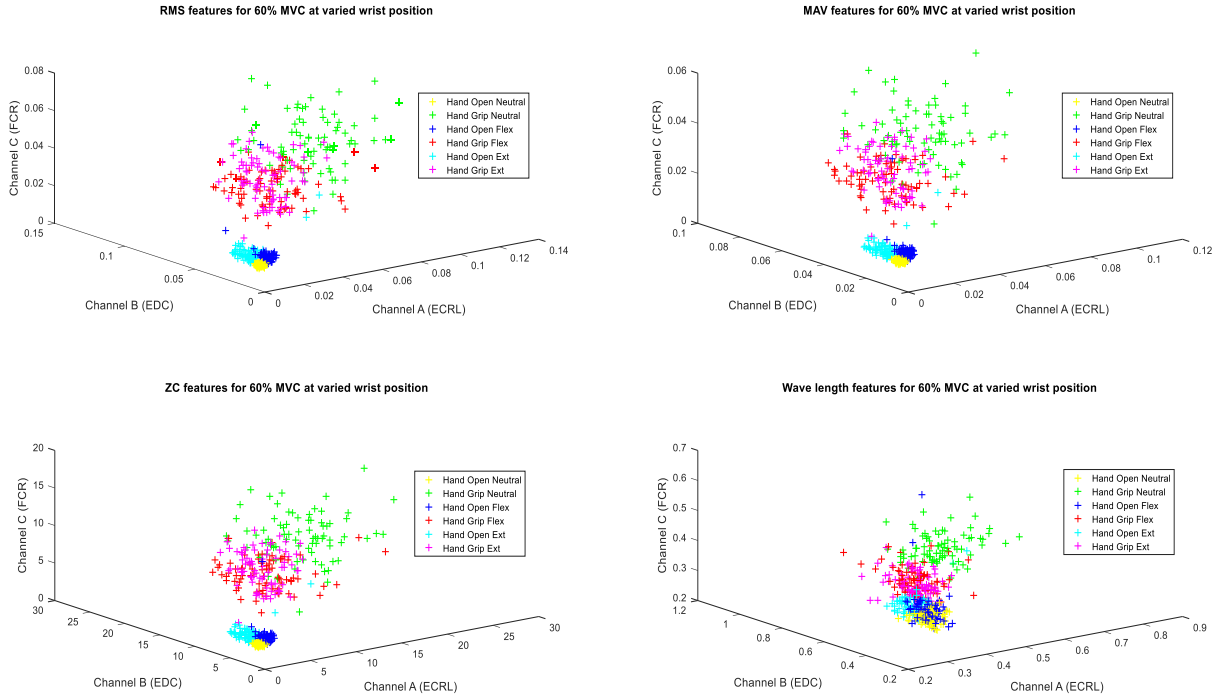


Figure F.5: Features extracted (from EDC, ECRL and FCR muscles) at 60% of MVC finger pinch strength for various wrist positions (without filter)

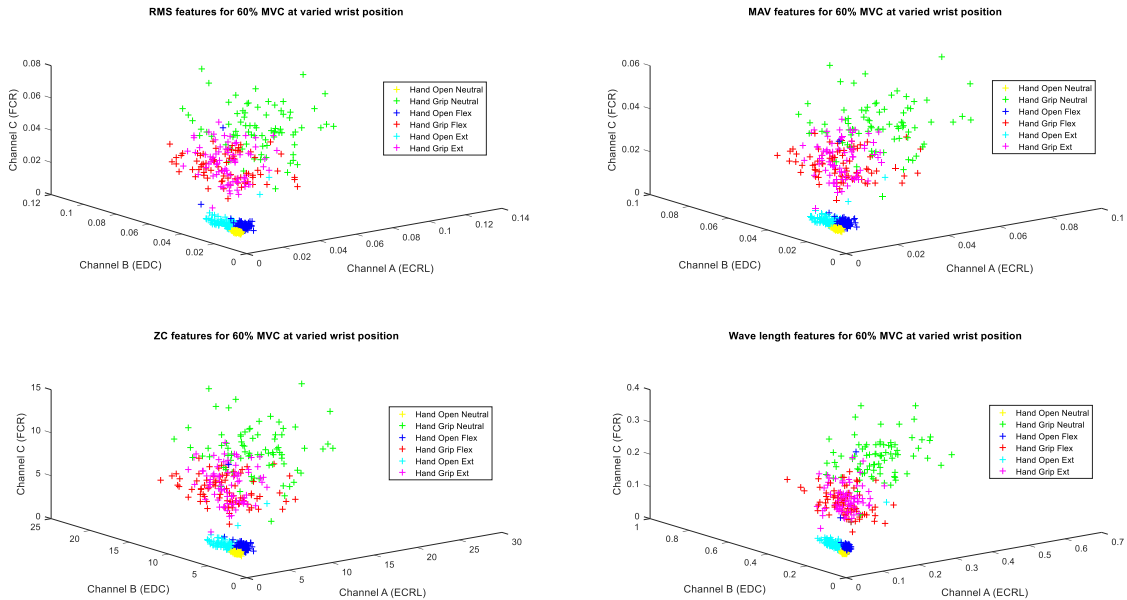


Figure F.6: Features extracted (from EDC, ECRL and FCR muscles) at 60% of MVC finger pinch strength for various wrist positions (with filter)

Appendix G: Time domain features with normalisation for wrist movements

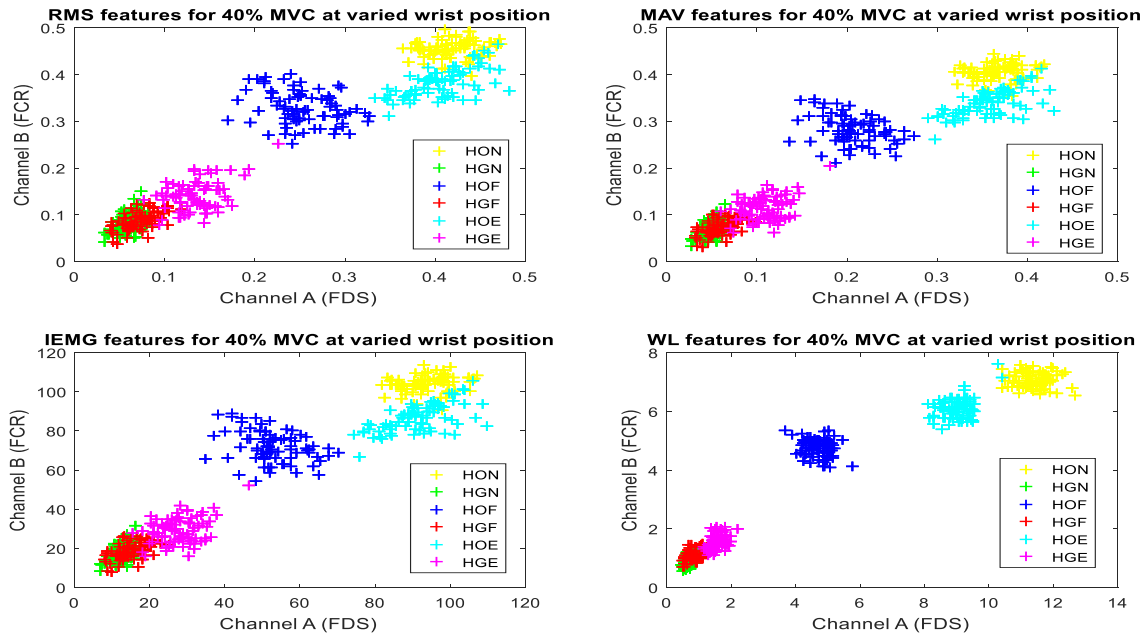


Figure G.1: Features extracted from flexion muscles (FDS and FCR muscles) at 40% of MVC for handgrip strength at wrist positions with prismatic power grip (adducted thumb)

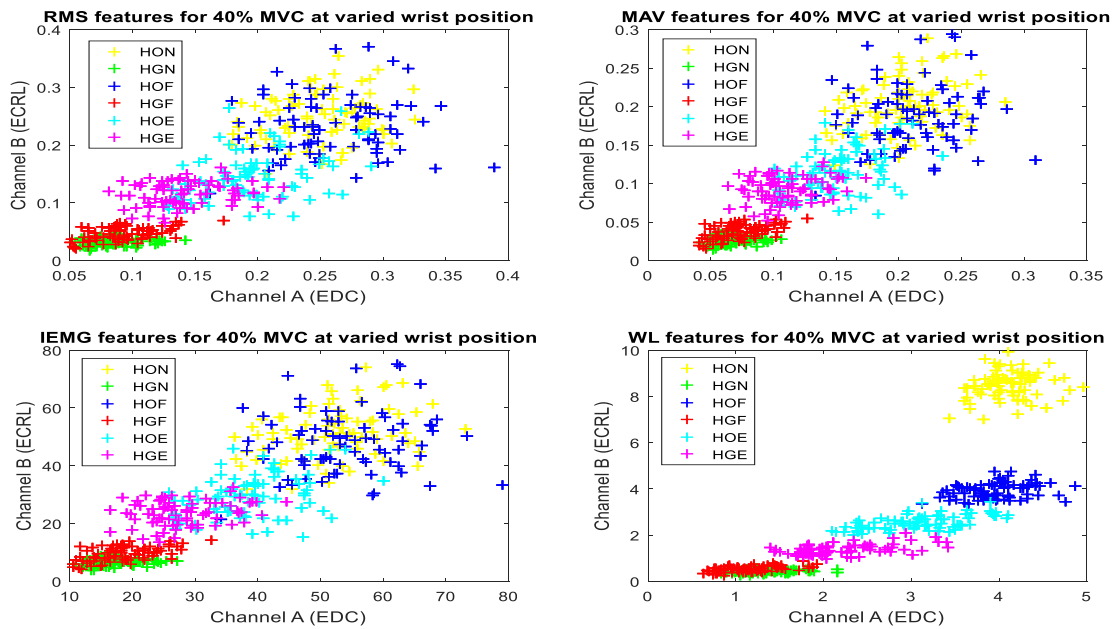


Figure G.2: Features extracted from extension muscles (EDC and ECRL muscles) at 40% of MVC for handgrip strength at wrist positions with prismatic power grip (adducted thumb)

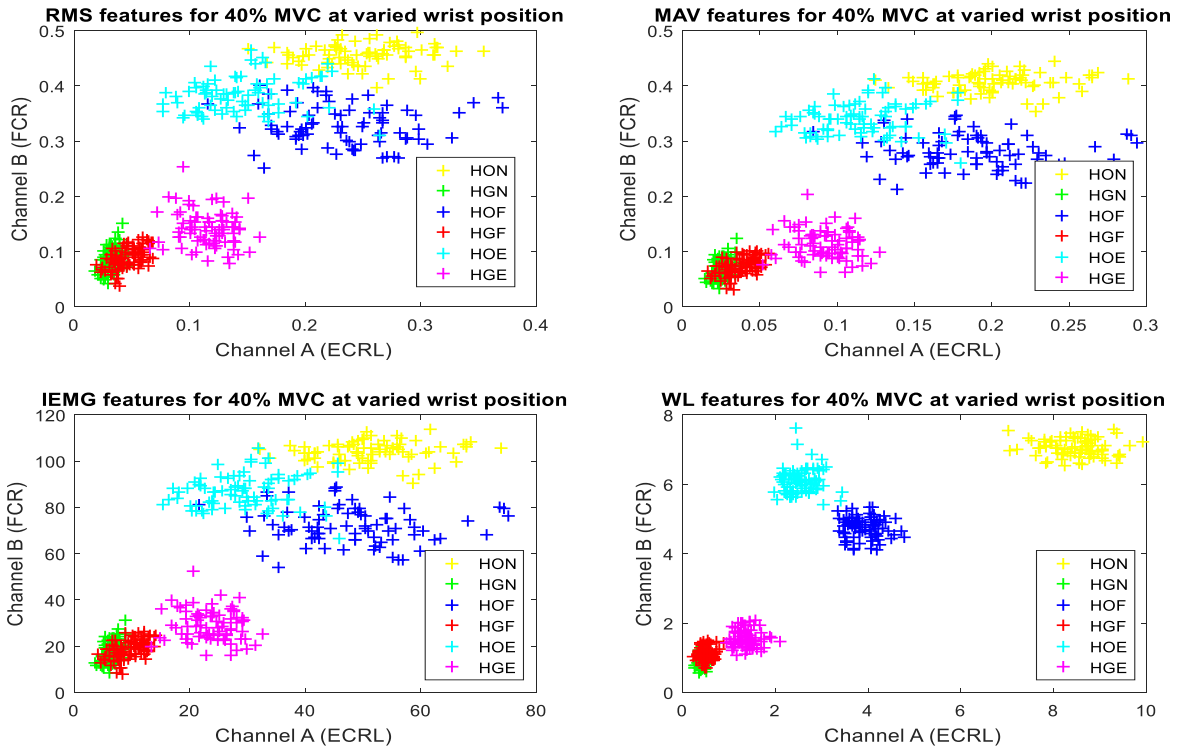


Figure G.3: Features extracted from flexion-extension muscles (ECRL and FCR muscles) at 40% of MVC for handgrip strength at wrist positions with prismatic power grip (adducted thumb)

Appendix H: Validation of finger joint angle estimations based on ANN model

Table H.1: Performance index for joint finger estimation using the ANN.

Finger Joint	Features & % MVC	Neural Network			Results			
		Input	Hidden layer	Output	Training		Testing	
					MSE	Regression	MSE	Regression
MCP	Wave length for 20%	3	25	1	22.198	0.910	21.775	0.917
PIP		3	25	1	26.085	0.909	24.470	0.906
DIP		3	10	1	3.529	0.894	3.842	0.883
MCP	Wave length for 40%	3	20	1	12.486	0.949	14.316	0.950
PIP		3	15	1	13.925	0.953	13.447	0.954
DIP		3	10	1	1.909	0.945	1.703	0.951
MCP	Wave length for 60%	3	15	1	8.851	0.966	6.704	0.971
PIP		3	15	1	8.628	0.972	6.889	0.977
DIP		3	10	1	1.302	0.962	1.018	0.974
MCP	Wave length for 80%	3	15	1	7.824	0.970	3.391	0.988
PIP		3	15	1	9.12	0.968	8.471	0.972
DIP		3	10	1	1.55	0.955	1.88	0.943
MCP	Wave length for 100%	3	20	1	8.780	0.966	5.663	0.977
PIP		3	15	1	12.053	0.961	10.325	0.962
DIP		3	10	1	1.569	0.945	1.430	0.955

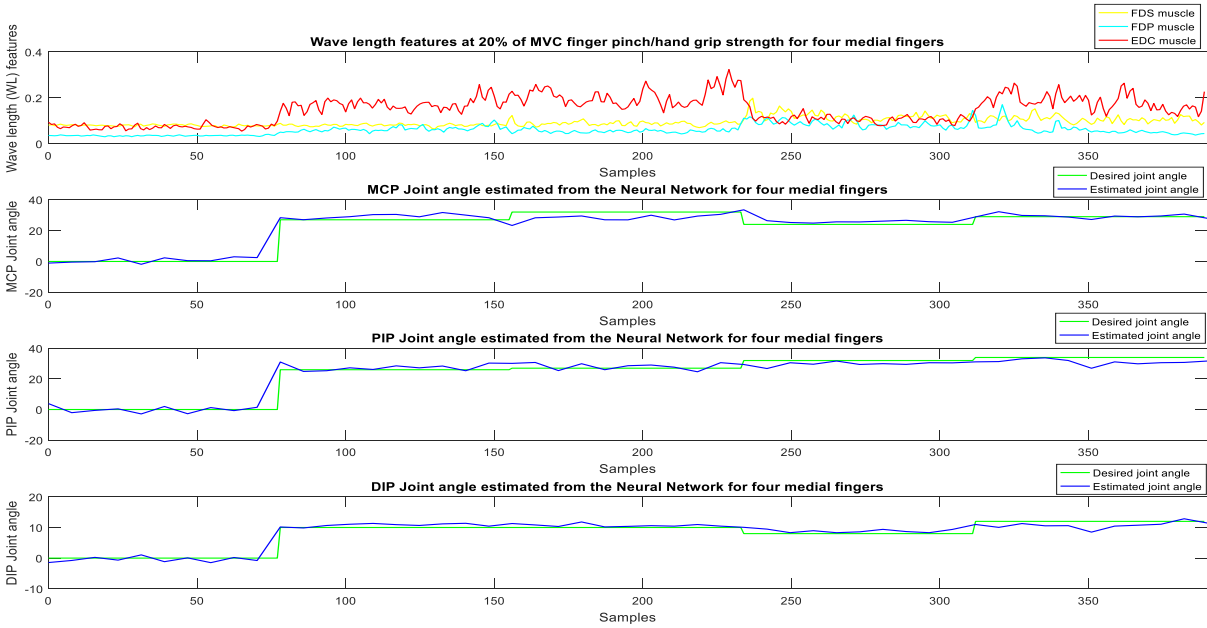


Figure H.1: Joint angle estimated from the Neural Network for four medial fingers based on wavelength features at 20% MVC for different finger pinches (FR, FP1, FP2, FP3, & FP4)

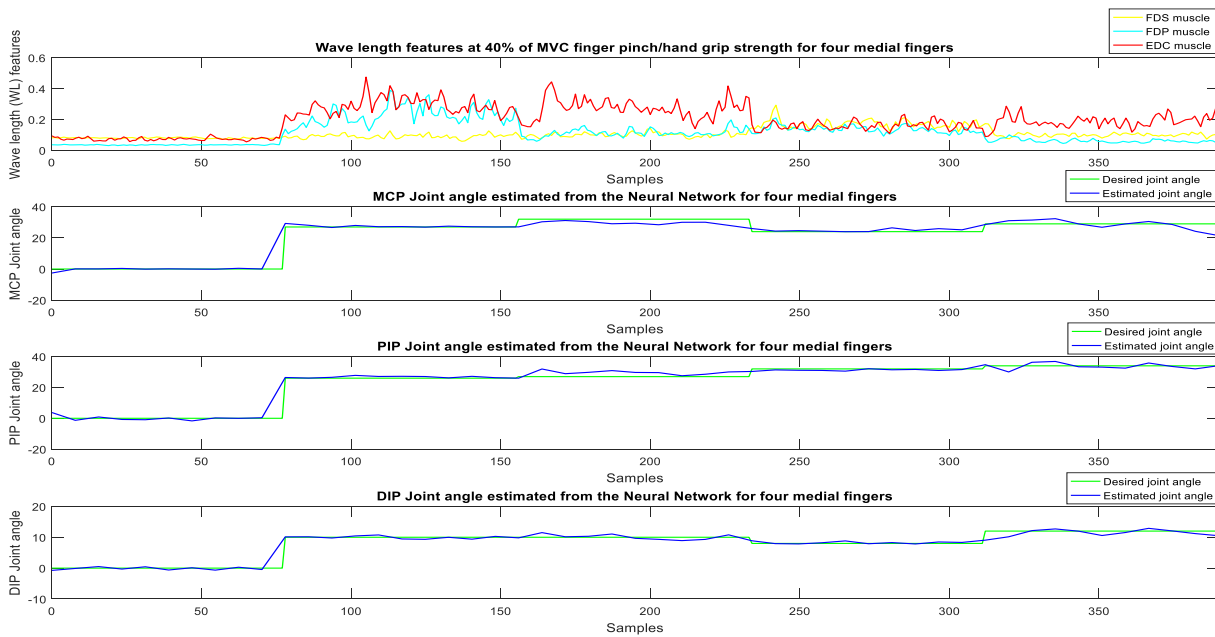


Figure H.2: Joint angle estimated from the Neural Network for four medial fingers based on wavelength features at 40% MVC for different finger pinches (FR, FP1, FP2, FP3, & FP4)

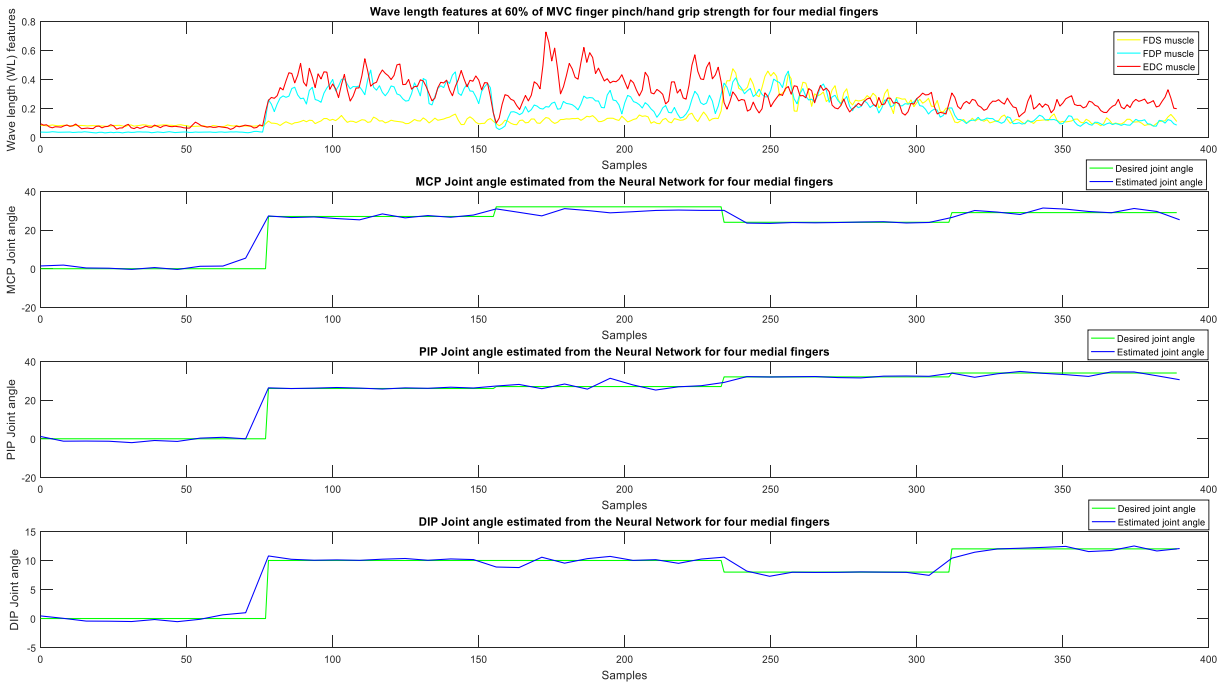


Figure H.3: Joint angle estimated from the Neural Network for four medial fingers based on wavelength features at 60% MVC for different finger pinches (FR, FP1, FP2, FP3, & FP4)

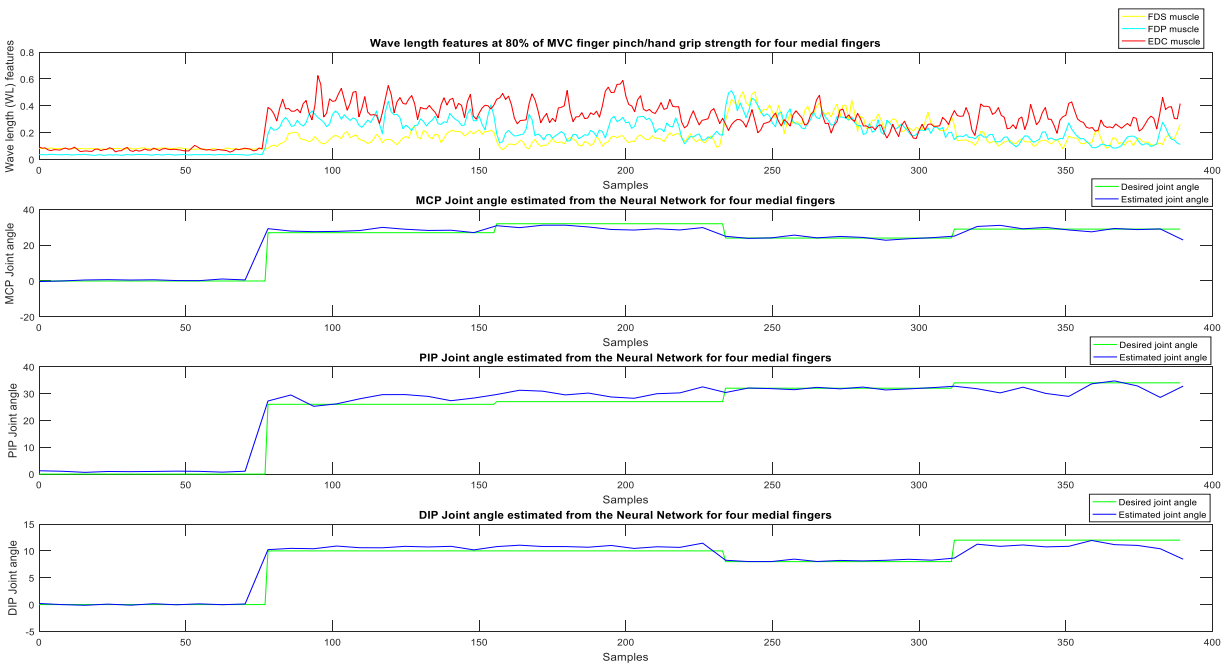


Figure H.4: Joint angle estimated from the Neural Network for four medial fingers based on wavelength features at 80% MVC for different finger pinches (FR, FP1, FP2, FP3, & FP4)

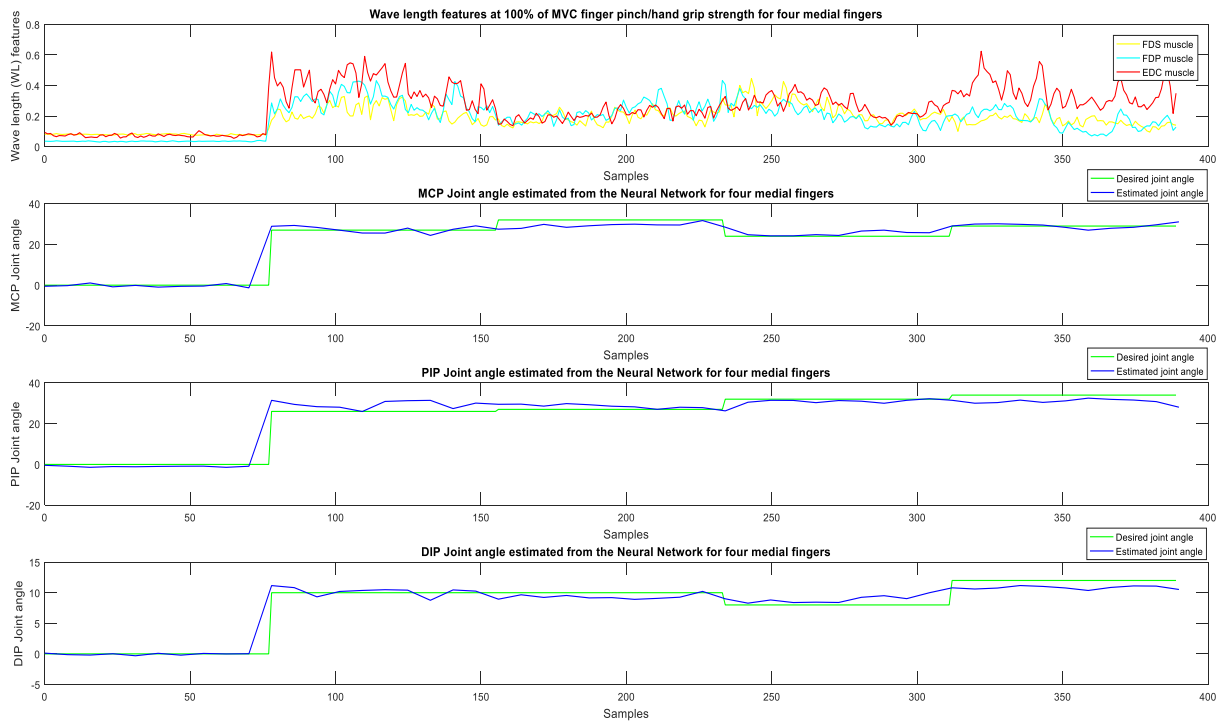


Figure H.5: Joint angle estimated from the Neural Network for four medial fingers based on wavelength features at 100% MVC for different finger pinches (FR, FP1, FP2, FP3, & FP4)

Appendix I: Validation of finger joint angle estimations based on ANFIS model

Table I.1: Performance index for joint finger estimation using the ANFIS

Joint	FE methods & % MVC	Results							
		Grid Partition				Clustering			
		MAE	MSE	RMSE	Correlation	MAE	MSE	RMSE	Correlation
MCP	Wave length for 20%	3.9833	26.5224	5.1500	0.9113	2.5152	11.1402	3.3377	0.9596
PIP		3.4462	21.7194	4.6604	0.9371	3.0527	15.1898	3.8974	0.9509
DIP		1.3626	3.1855	1.7848	0.9167	1.1125	1.9365	1.3916	0.9450
MCP	Wave length for 40%	4.0123	27.3700	5.2316	0.9094	2.4282	12.5302	3.5398	0.9632
PIP		3.1467	22.9175	4.7872	0.9293	2.2381	13.2285	3.6371	0.9645
DIP		1.4067	4.3216	2.0788	0.8864	0.9289	1.9025	1.3793	0.9501
MCP	Wave length for 60%	3.5627	23.5748	4.8554	0.9168	2.5912	13.0490	3.6123	0.9659
PIP		3.2527	22.3284	4.7253	0.9259	3.1136	16.8805	4.1086	0.9587
DIP		1.3703	4.2457	2.0605	0.8816	1.1403	2.2305	1.4935	0.9523
MCP	Wave length for 80%	3.3476	18.1560	4.2610	0.9409	2.0426	6.7332	2.5948	0.9815
PIP		3.5682	21.5475	4.6419	0.9347	3.4551	16.1666	4.0208	0.9554
DIP		1.2533	3.2517	1.8032	0.9146	0.7883	1.0737	1.0362	0.9701
MCP	Wave length for 100%	2.7961	14.3170	3.7838	0.9489	2.3147	11.4363	3.3818	0.9638
PIP		3.8038	22.9109	4.7865	0.9365	3.6279	21.9981	4.6902	0.9489
DIP		1.2159	2.8101	1.6763	0.9215	0.9094	1.7301	1.3153	0.9510

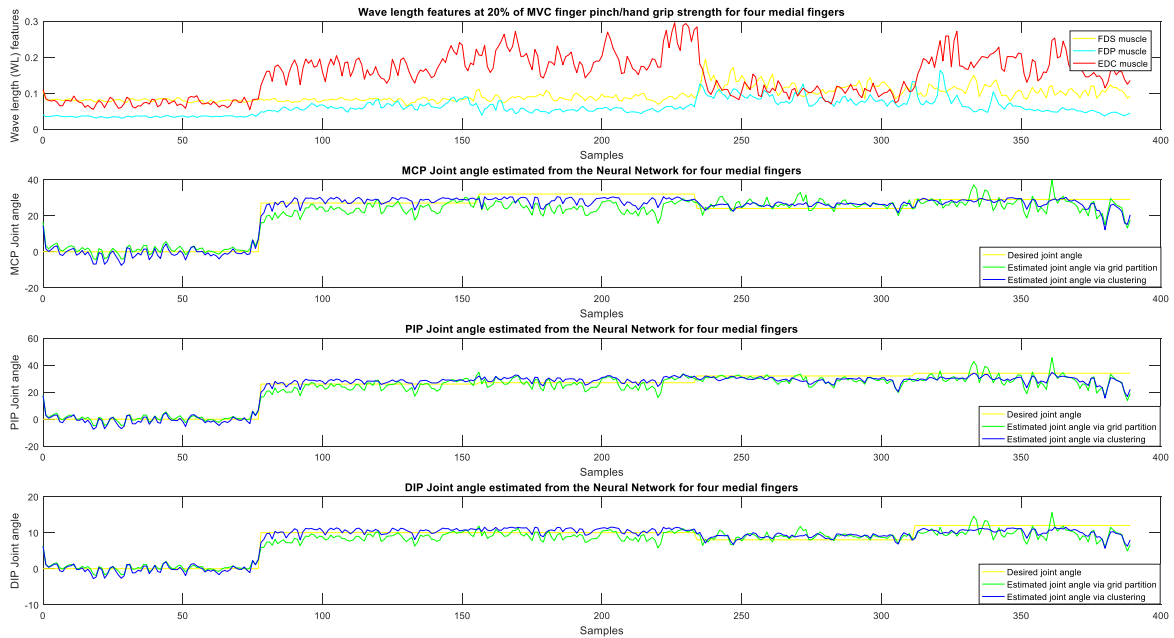


Figure I.1: Joint angle estimated from the Adaptive Neuro-Fuzzy Inference System (ANFIS) for four medial fingers based on wavelength features at 20% MVC for different finger pinches (FR, FP1, FP2, FP3, & FP4)

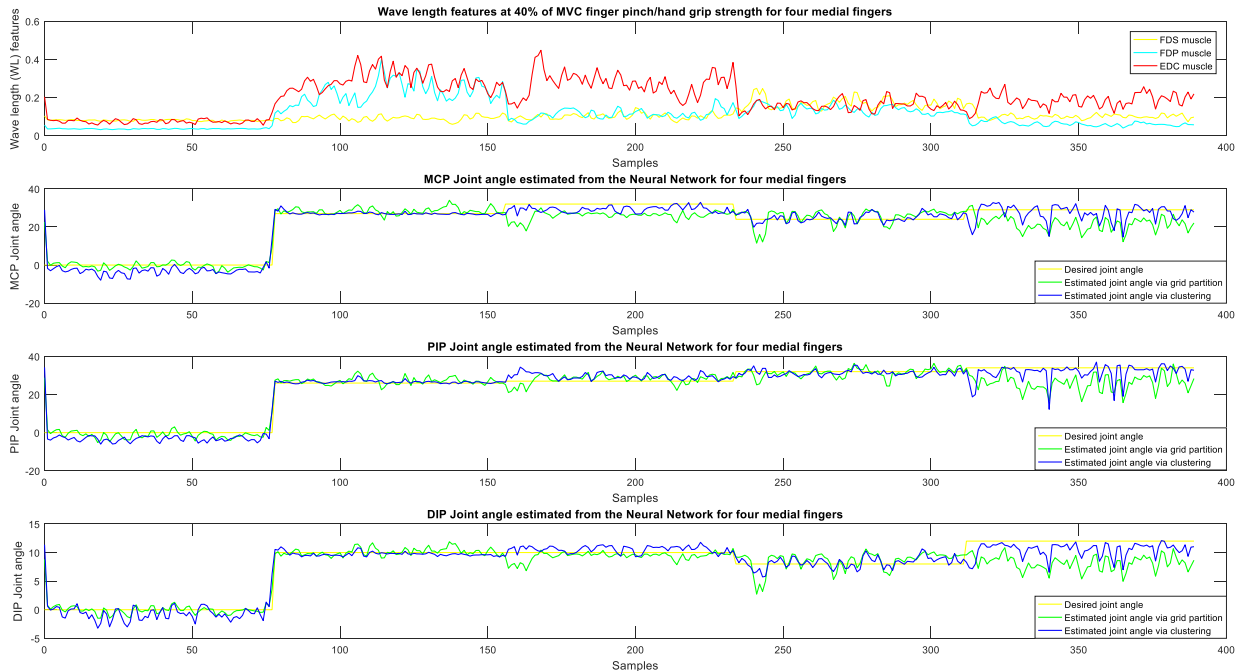


Figure I.2: Joint angle estimated from the Adaptive Neuro-Fuzzy Inference System (ANFIS) for four medial fingers based on wavelength features at 40% MVC for different finger pinches (FR, FP1, FP2, FP3, & FP4)

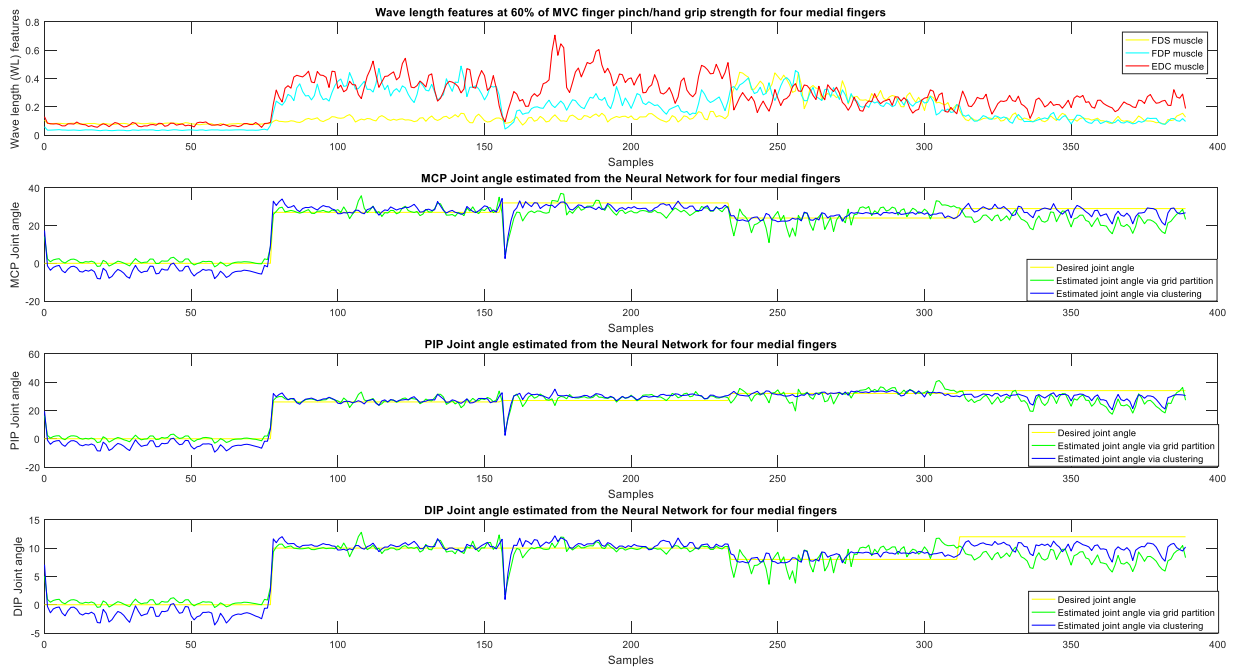


Figure I.3: Joint angle estimated from the Adaptive Neuro-Fuzzy Inference System (ANFIS) for four medial fingers based on wavelength features at 60% MVC for different finger pinches (FR, FP1, FP2, FP3, & FP4)

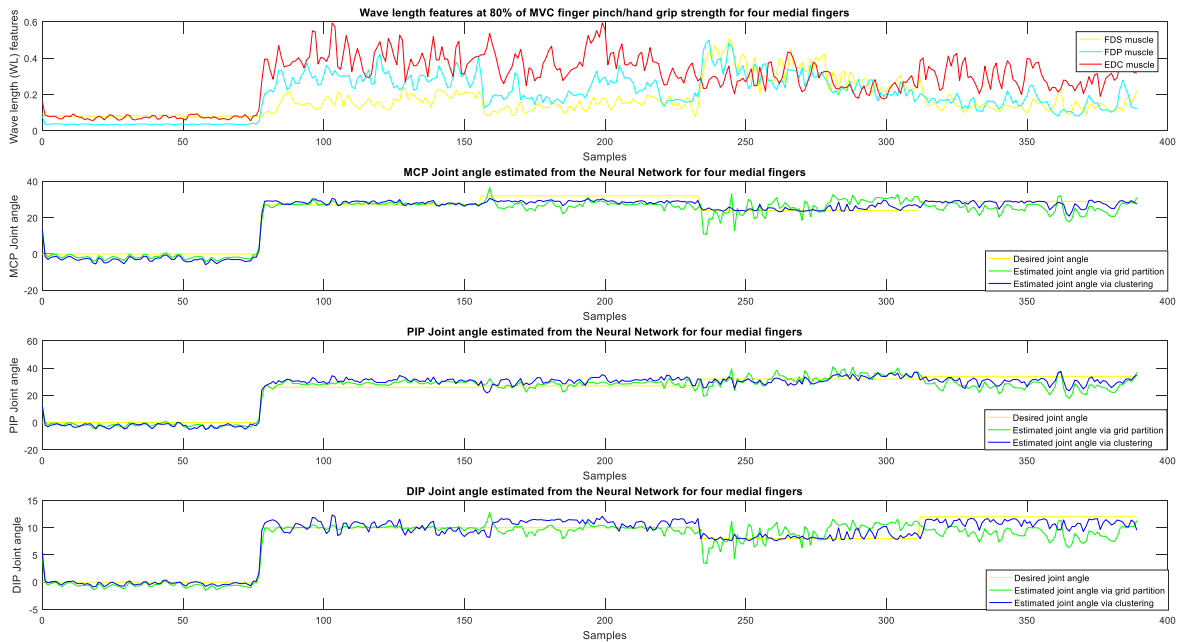


Figure I.4: Joint angle estimated from the Adaptive Neuro-Fuzzy Inference System (ANFIS) for four medial fingers based on wavelength features at 80% MVC for different finger pinches (FR, FP1, FP2, FP3, & FP4)

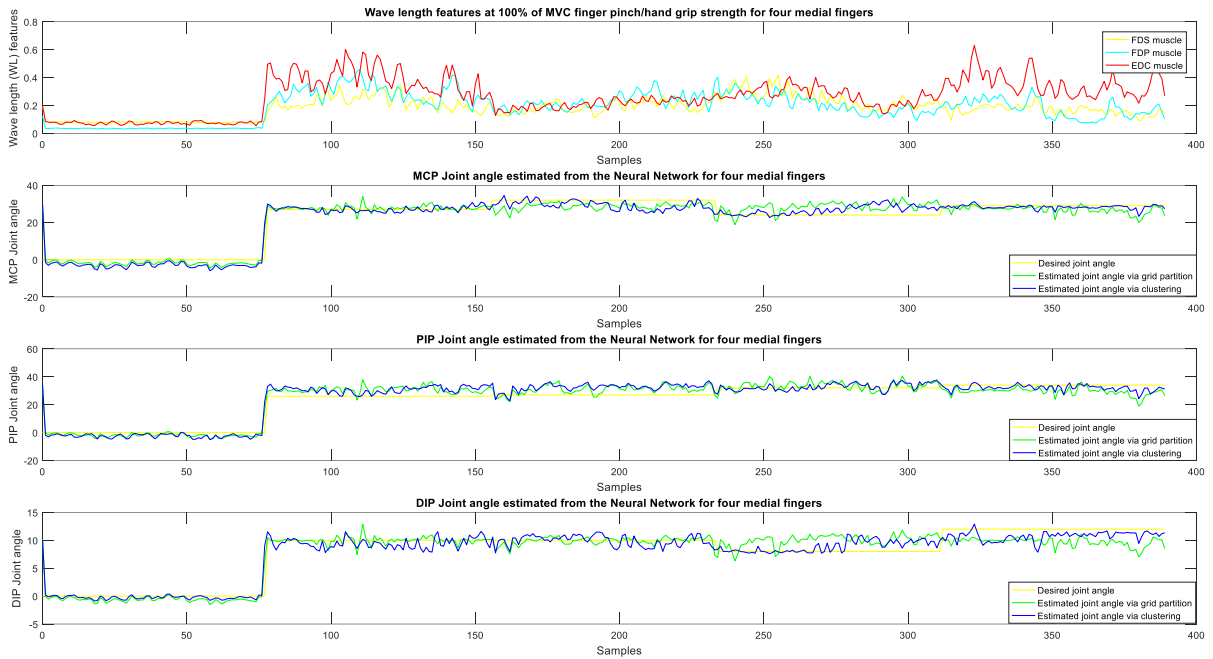


Figure I.5: Joint angle estimated from the Adaptive Neuro-Fuzzy Inference System (ANFIS) for four medial fingers based on wavelength features at 100% MVC for different finger pinches (FR, FP1, FP2, FP3, & FP4)

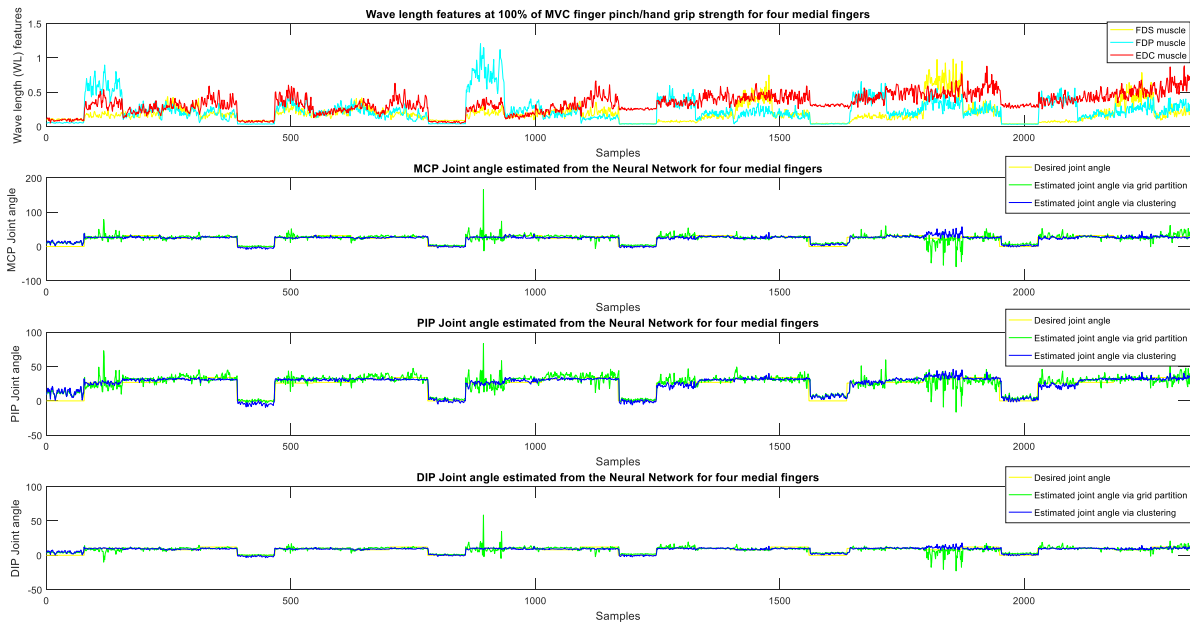


Figure I.6: Joint angle estimated from the Adaptive Neuro-Fuzzy Inference System (ANFIS) for four medial fingers based on wavelength features at 60% MVC for different finger pinches (FR, FP1, FP2, FP3, & FP4)